Fracture mechanics approach to optimize inspection planning of offshore welds for wind turbines

Ruiz Munoz, Gustavo Adolfo

Link to article, DOI:
10.11581/DTU:00000031

Publication date:
2018

Document Version
Publisher's PDF, also known as Version of record

The Technical University of Denmark

PhD dissertation

Fracture mechanics approach to optimize inspection planning of offshore welds for wind turbines

Author: *Gustavo-Adolfo Ruiz-Muñoz*

Supervised by
Professor Mathias Stolpe
Professor John Dalsgaard Sørensen
Professor Christian Frithiof Niordson
Senior Researcher Martin Alexander Eder
M.Sc. Civil Engineer Thomas Østergaard

February 1, 2018

Preface

This research has been part of my life for more than three years. During this time, I have continuously faced work and personal issues that have challenged my integrity and character. Fortunately, I have received support from many different people. It is impossible to show my gratitude to every person in a brief note, but I would like to acknowledge the help of those people who encouraged my ideas during the toughest moments of this research.

From an academic perspective, I want to thank Martin Alexander Eder for all our productive discussions. His great support has definitely enhanced the quality of this work. Additionally, I would like to express my gratitude to Mathias Stolpe for guiding me through different bureaucratic tasks and helping me to make corrections on the manuscripts. Finally, I want to thank John Dalsgaard Sørensen for his wise advises in the probabilistic field.

Apart from the above contributions, the ideas given by Thomas Østergaard and Christian Niordson have also had a positive impact in this research. I also appreciate all the support provided by Rachel Meyer and Karina Isabel Culqui.

From a personal level, I would like to thank all of my family, friends and ex-friends. Their different contributions in my life have indirectly shaped the ideas and the necessary attitude to write this work.

Abstract

In the present work, fracture mechanics-based concepts are introduced into a fatigue life prediction framework used to optimise inspection planning of offshore welds for wind turbines. Offshore welds are typically subject to fatigue loading conditions in corrosive environments which can lead to accelerated crack growth, detrimentally affecting the structural integrity. The offshore wind industry commonly applies inspection/repair procedures in conjunction with corrosion protection systems in order to prolong the lifetime of offshore welds. The research conducted through this work addresses three important issues in the offshore wind industry, namely, the optimal inspection interval, cost of maintenance as well as the impact of protection system failure on the maintenance planning. This thesis is grossly divided into three different studies which encompass a stress-based fatigue approach, a fracture mechanics-based fatigue approach and a probability theory-based approach. Aforementioned fields are incorporated into inspection planning simulations, all of which are shown to provide meaningful predictions for the industry. Furthermore, the current research entails innovative approaches and methods used to simulate fatigue crack propagation in welded steel components with the following common characteristics: the Multiple-Site Damage and Residual Stresses. The research results presented herein show a strong dependency of the maintenance planning on the prevailing environmental conditions. Moreover, the parametric studies conducted suggest that the total maintenance costs can significantly vary depending on the adopted inspection planning strategy. The research results presented in this thesis can aid the development of cost effective solutions in the off-shore maintenance framework.

Nomenclature

Notation	Meaning
$a, \Delta a$	Crack length and crack growth.
a_f	Crack size limit before failure.
A	Area.
A_n	Amplitude of the higher order terms.
C	Paris Law parameter.
C_A, C_B	Parameters for the bilinear Paris Law.
C_f	Cost of failure.
C_W	Annual cost of a wind turbine failure.
C_P,C_V	Cost of the technicians and cost of the vessel.
C_U,C_{GW}	Cost of the ultrasonic equipment and the repair equipment.
C_O	Cost of logistics and data analysis.
C_{TOTAL}, C_I, C_R	Total cost, cost of inspection and cost of repair.
C_0	Material constant related to crack closure effects.
d	Distance between the crack tip and a boundary.
d_{LEFM}	Distance of the Application Limit of LEFM.
D, D_f	Damage and damage limit to failure.
E	Young's Modulus.
f	Loading frequency.
f_{eq}	Equivalent Crack Opening Factor.
f_{ij}	Dimensionless function.
F	Crack velocity factor.
g	Limit state function.
g_{ij}	Dimensionless function.
G	Gravity force.
i, j, n	Integer indexes.
J	J-Integral.
k	Constant related to the Stress Intensity Factor.
K, K^{max}	Stress Intensity Factor (SIF) and maximum SIF.
K_{eq}	Equivalent SIF.
K_A, K_B	SIF.
ΔK_{eq}	Equivalent SIF range.
K_C	Maximum SIF before fatigue failure.
ΔK_{th}	SIF threshold.
K_{eq}^{max}, K_{eq}^{min}	Maximum and minimum equivalent SIF.

Notation	Meaning
K_I, K_{II}, K_{III}	SIF for mode-I, mode-II and mode-III.
$K_{I,RS}$, $K_{II,RS}$	Residual stress SIF (RSFI) for mode-I and mode-II.
K_I^{max}, K_{II}^{max}	Maximum SIF of the periodic load for mode-I and -II.
K_I^{min}, K_{II}^{min}	Minimum SIF of the periodic load for mode-I and -II.
ΔK_{TP}	Transition point in between the two linear stages of the Paris Law.
$K_{op,eq}$	Opening equivalent SIF.
$\Delta K_{eff,eq}$	Effective equivalent SIF range.
m	Paris Law parameter.
m_A, m_B	Parameters for the bilinear Paris Law.
M	Moment.
n_j	Normal Vector.
N	Number of cycles.
ΔN	Load cycle increment.
p, q	Material crack growth parameters.
P	External load.
P_{accum,T_n}	Accumulated probability of a failure at year T_n.
$P_f(t)$	Probability of a failure event for a time interval t.
$P_{t,n}$	Annual probability of failure.
P_{d,T_n}	Probability to repair a crack at year T_n.
r	Distance from the crack tip.
r_0	Notch radius.
$r_{O'}$	Plastic zone radius.
$r_{O\varepsilon}$	Plastic zone radius for plane strain conditions.
$r_{O\sigma}$	Plastic zone radius for plane stress conditions.
R	Stress ratio.
s	Standard Deviation.
S	Stress.
ΔS	Stress range.
S_{max}	Maximum nominal stress.
$S^{(1)}, S^{(2)}$	Load and auxiliary load.
t, t_{lim}	Time and limit of time for the fatigue analysis.
t_h	Thickness of the specimen.
T_{Ins}	Inspection interval.
T_n	Year of inspection.
t_{TEP}	Period of time a system is environmentally protected.
u_i	Displacement vector.
u_1, u_2	Normalized and uncorrelated variables.

Notation	Meaning
$\mathbf{u}$	Vector of the normalized and uncorrelated variables.
x, y	Cartesian axis reference.
v, w	Wind and wave velocity.
W	Strain energy density.
α	Crack opening parameter.
$\boldsymbol{\alpha}$	Unitarian vector.
β	Reliability index.
β_{accum}	Accumulated reliability index.
β_t	Annual reliability index.
β_{RS}	RS orientation.
γ	Material constant related to crack closure effects.
Γ	Contour.
δ_{ij}	Kronecker delta.
ε_{ij}	Strain distribution.
θ	Circumferential coordinate reference.
θ_0	Crack propagation direction.
μ	Mean.
ν	Poisson's ratio.
σ_A,σ_B	Tensional stresses.
$\sigma_{\theta\theta}$	Tangential stress around the crack tip.
σ_R	Residual Stress (RS).
σ_o σ_{ys}	Flow stress and yield stress.
σ_{ij}	Stress distribution.
σ_{22}	Stress applied to the crack.
$\sigma_{external}$	External stress loading.
σ_{c_xx}	Stress value after extrapolation.
Φ	Acceleration factor.

Abbreviations

Notation	Meaning
API	American Petroleum Institute.
BIE	Boundary Integral Equation.
EAC	Environmental Assisted Cracking.
EPFM	Elasto-Pastic Fracture Mechanics.
FE	Finite Element.
FEM	Finite Element Method.
FORM	First Order Reliability Methods.
FM	Fracture Mechanics.
FZ	Fusion Zone.
HAZ	Heat Affected Zone.
HCF	High Cycle Fatigue.
ISO	International Organization for Standardization.
LEFM	Linear Elastic Fracture Mechanics.
MCS	Maximum Circumferential Stress.
MIG	Metal Inert Gas.
MTS	Maximum Tangential Stress.
MSD	Multiple Site Damage.
PENS	Probabilistic Effective Notch Stress.
PFM	Probabilistic Fracture Mechanics.
PoD	Probability of Detection.
PZL	Plastic Zone Link-Up.
RS	Residual Stresses.
RSIF	Residual Stress Intensity Factor.
SB	Stress-Based.
SC	Stress Concentration.
SIF	Stress Intensity Factor.
SORM	Second Order Reliability Methods
TP	Transition Piece.
TEP	Transitional Environmental Protection.
TIG	Tungsten Inert Gas.
TMFEA	Thermo-Mechanical Finite Element Analysis.

Contents

1 Introduction

The offshore wind industry has constantly grown since the first offshore wind farm in 1991. Three main designs are commonly found depending on the foundation design: floating wind turbines, jacket wind turbines and monopile wind turbines. The monopile wind turbine is an offshore structure divided into five main components Fig. 1a:

- The blades: Structures that rotate around the nacelle due to the effects of the wind.
- The nacelle: Its main purpose is to transform the kinematic energy into electricity.
- The tower: Conical structure which is joined to the transition piece. It supports the nacelle and the blades.
- Transition Piece (TP): Cylindrical component in between the tower and the monopile. It is partially immersed and includes the boat landing platform, ladders and the entrance to the wind turbine.
- The monopile: Cylindrical structure immersed into the sea.

Each component of the wind turbine is manufactured onshore and the final assembly is done offshore. Firstly, the monopile is embedded into the seabed by hydraulic ram drivers. Secondly, the transition piece is attached to the top of the monopile. Finally, the tower, nacelle and blades are added to the structure.

Once these five components of the wind turbine are mounted, an export cable carries electric power from the nacelle to the offshore substation. The export cable crosses the monopile through one groove. The groove includes a film to isolate the water inside the monopile with the sea water.

During the installation process, a grouting connection made of concrete is placed in between the transition piece and the monopile, Fig 1b. However, concrete requires time to cure before it can serve as a structural support. Engineers found a solution by installing a component, named bracket, that temporary supports the TP while the concrete cures.

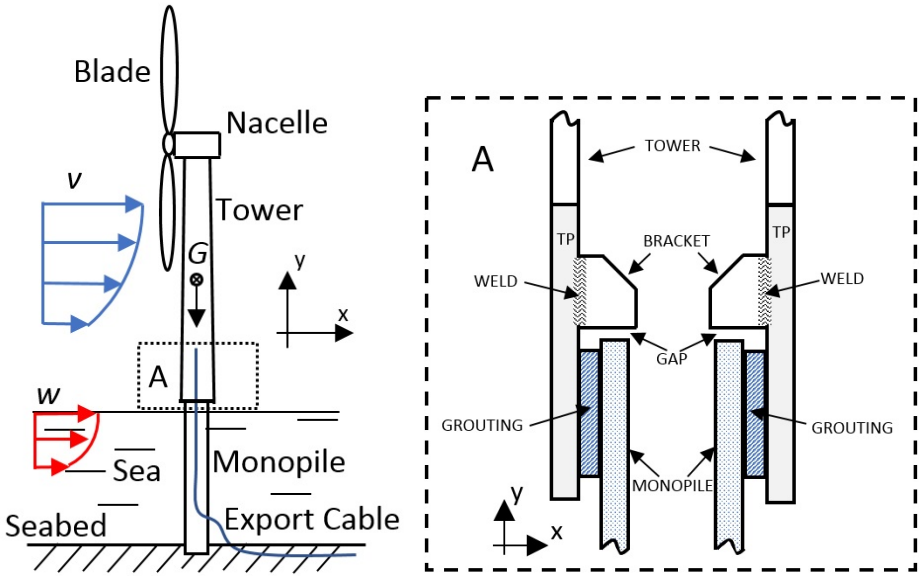

(a) (b)

Figure 1: Illustration of: (a) An offshore wind turbine with foundation type 'monopile'. The parameter v represents the wind velocity and w the wave velocity [1]; (b) Section A of the wind turbine that illustrates the assembly of the tower, the Transition Piece (TP) and the monopile.

The bracket is a steel structure welded to the transition piece. There are 12 brackets in each wind turbine, Fig. 2a. Each pair of brackets is supported by a hydraulic jack as shown in Fig. 2b. After the grouting connection cures, the hydraulic jack is removed. At that moment, the brackets are no longer structurally relevant and the force is solely transferred via the grouted joint.

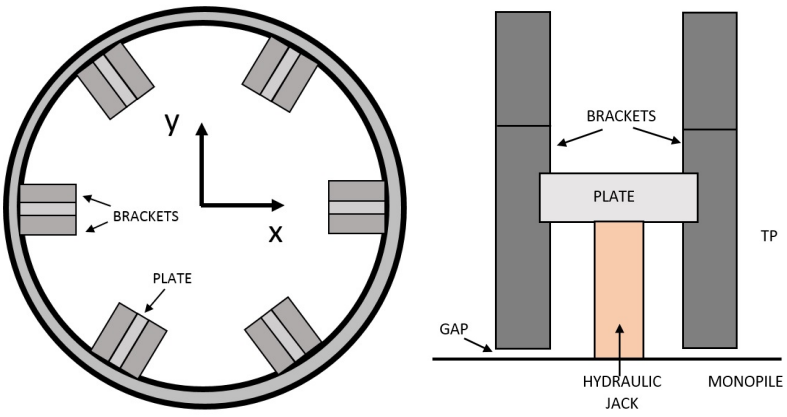

(a) (b)

Figure 2: Illustration of: (a) The 12 brackets and 6 plates around the TP; (b) The brackets, hydraulic pump and plate during the curing process of the grouting connection.

In some wind farm projects, the grouting connection has satisfactorily supported the wind turbines for few years of operation. However, the dynamic response of the structure during the shutdown of some wind turbines has damaged the grouting connection. Two main consequences appear due to this failure:

- Some brackets re-established contact with the mono-pile head.
- The displacement of the structure has moved the export cable.

The contact between the monopile and the bracket suggests that some brackets became load bearing elements. The grouting connection may still be structurally relevant, but it is currently unknown how much load is supported by either the grouting or the bracket piece.

Additionally, the displacement of the export cable has damaged the film inside the groove of the monopile. Consequently, water can flow through the groove. As the tie changes, sea water with high concentration of air dissolved flows inside the monopile and some brackets may be temporally immersed. This process created a corrosive environment inside the TP, Fig. 3.

Figure 3: Photograph of the bracket inside the wind turbine, Fig. 1b. The bracket is subject to severe corrosion. Photograp from Ørsted®.

The permanent bracket support and the highly corrosive environment introduce a structural and environmental situation that the foundation was not designed for. The question raised is what type of maintenance can result in being cost effective to the structure.

1.1 Previous studies

The situation presented in Fig. 3 introduces some doubts in whether the wind turbine may fail and what type of maintenance is required to prevent failure. Since a wind turbine is dynamically loaded, components of the wind turbine are typically subject to a vast number of cyclic stresses. If the amplitude of those stresses is sufficiently high, the structural components may fail due to fatigue.

Fatigue is the main cause of failure in offshore structures because it may introduce cracks that can compromise the integrity of each component. Increasing the amplitude of the load signal as well as introducing an aggressive environment accelerates the fatigue damage.

Previous structural studies of brackets were done by Ørsted® engineers and external consultants. Those researches assumed the worst structural and environmental conditions, i.e. complete failure of grouting connection and

free corrosion conditions. Engineers found several Stress Concentration (SC) locations inside the bracket and around the weld that connects the bracket to the TP. The SC locations are spots where crack propagation is more likely to occur.

The studies done in the industry predicted a lifetime shorter than the actual performance of the structure. Additionally, the fatigue studies were incomplete and lacking any detailed plan to inspect.

1.2 The fatigue and maintenance challenge

The wind turbine lifetime estimated in previous studies is conservative. Additionally, there is room for improvement in plans to mitigate failures due to fatigue. Therefore, there is a strong motivation to further investigate about these two topics.

It is important to state that both fatigue and maintenance assessments are closely related. If the fatigue analysis does not lead to results that can compromise the integrity of the foundation, maintenance might not be necessary. On the other hand, if failure is predicted during the operational time of a wind turbine, the preferred option is an effective maintenance coherent with a cost or reliability-based approach.

An analysis that combines a realistic lifetime estimation and effective maintenance planning for bracket connections includes several challenges. Firstly, a life estimation assessment should be performed using better techniques than in previous studies. Secondly, effective inspection planning should use techniques that would optimize the inspection and repair intervals. An optimal inspection-repair activity is performed when during inspections, cracks are detected and on the limit for repair. Those cracks expose a serious structural risk and can be repaired on time.

In an ideal scenario, fatigue analysis would accurately determine if the brackets fail during the operational time. The fatigue analysis would predict the crack propagation and determine the inspection interval. Inspections would confirm the existence of the crack predicted in the fatigue model, and technicians would repair it. All these activities would be performed using a cost-effective approach, i.e. performing the inspections and repairs necessary to assure the lowest global cost.

This ideal scenario is extremely complex. First, there are many uncertainties in geometries, environmental loading and material characteristics. In addition, there are no fatigue models that perfectly predict crack propagation

and failure of a welded structure. Finally, inspections and repair techniques depend on several other factors such as human expertise or equipment.

All the limitations mentioned present the tasks of fatigue and maintenance assessment as extremely difficult. However, from the 90's, there has been a strong development of maintenance strategies of offshore structures. The American Bureau of Shipping [2], the Det Norsk Veritas (DNV) [3] and the American Petroleum Institute (API) [4] have published documents and developed softwares that deal with maintenance of offshore structures based on a probabilistic risk analysis. They proposed different guidelines for offshore components but they are not fully optimized in terms of costs.

The current research proposes a method of approaching the optimum maintenance period of offshore welds from a conservative perspective and under variable environmental conditions.

1.3 Objective of this research

The objective of this research is to shed some light on the fatigue analysis and inspection planning of offshore welds for wind turbines subject to fatigue loading. The 3D case in Fig. 3 has served as an inspiration to the topic. The dissertation is divided into five core studies:

(i) Common fatigue life assessment methods in industry for offshore welds: This research compares the most common methods used in industry to estimate the life of a welded structure subject to cyclic loading and different environmental conditions.

(ii) The fracture mechanics approach for fatigue analysis of offshore welds: The fatigue analysis from a fracture mechanics perspective is presented. This study includes concepts related to offshore welds such as corrosion, multiple flaws and residual stresses.

(iii) Probabilistic fatigue analysis: The current research introduces the terms probabilities of failure and reliability curves. Different reliability methods are illustrated.

(iv) Risk-Based Inspection Planning for Offshore welds from a fracture mechanics perspective: This work describes the concepts behind the maintenance plan from a probabilistic fracture mechanics method. This section presents a case and describes a cost effective approach to maintenance.

Additionally, the current research includes the following manuscripts:

(i) Manuscript A: Ruiz-Muñoz GA. Method to Analyse Multiple Site Damage Fatigue before and after Crack Coalescence. Eng Fract Mech 2017; In press

(ii) Manuscript B: Ruiz-Muñoz GA, Eder MA. A conservative approach for Mode I-II fatigue analysis under residual stresses: The RSIF Proportionality Conjecture. Submitted to Fatigue Fract Eng M.

(iii) Manuscript C: Ruiz-Muñoz GA. The effects of multiple-site damage and corrosion on the structural reliability of a thin plate with a hole. International conference on Structural Integrity and Durability, August 15-18, 2017, Dubrovnik, Croatia.

(iv) Manuscript D: Ruiz-Muñoz GA, Sørensen JD. Probabilistic inspection planning of offshore welds subject to the transition from protected to corrosive environment. Submitted to Mar Struct.

2 Common fatigue life assessment methods of offshore welds in industry

The fatigue life assessment of an offshore weld is commonly done in industry through procedures addressed in standards, e.g. BS7910 [5] or DNVGL-RP-C203 [6]. However, it is necessary to understand the structural and material characteristics of a weld component to correctly apply concepts from standards.

2.1 Introduction to fatigue

Fatigue is the phenomenon that occurs when a material irreversibly deforms due to cycling loading. If the load ranges are sufficiently high, this phenomenon will continue until the structure fails. The deformations expected during the fatigue process are separated into two stages. The early stage includes micro-structural deformations in the form of voids. In the later stage, few of those voids become cracks that propagate through the structure until failure occurs. However, some structures may already include geometrical crack shape defects prior to the fatigue process and present situations where the first stage is negligible. A weld is one of these components, and its role in many fatigue studies is crucial.

There are three types of fatigue analysis:

- The Low Cycle Fatigue, $N \lesssim 10^4$ cycles
- The High Cycle Fatigue (HCF), 10^4 cycles $\lesssim N \lesssim 10^8$ cycles.
- The Very High Cycle Fatigue, $N \gtrsim 10^8$ cycles.

Note that N stands for the fatigue cycles a structure is subject to. The present work focuses only on HCF cases, since HCF loads are common in the wind turbines.

2.2 Weld structural characteristics

Welding is one of the most common joining techniques in industry. Welds are generally performed through Tungsten Inert Gas (TIG) or Metal Inert Gas (MIG) methods. The TIG welds consist of melting the base material of the metallic structures. This procedure is done through a gas of ions in

order to protect the welding zone from oxidisation, as shown in Fig. 4a. The MIG technique also includes a shielding gas that protects from oxidisation, but uses a consumable metallic bar that is melted. Melted metal is placed in between two metallic structures to join them once it solidifies, Fig. 4b. [7]

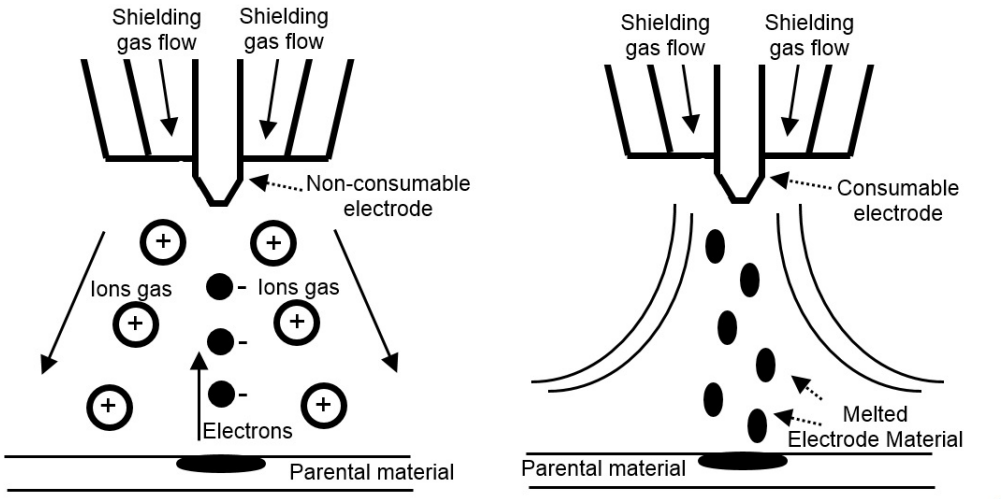

(a) (b)

Figure 4: Illustration of the weld manufacturing: (a) Tungsten inert gas (TIG); (b) Metal inert gas (MIG).

The TIG dressing is a slow and low productivity method and usually is applied only for thin plates [8]. On the other hand, MIG welds are commonly performed in the offshore wind turbine industry. The MIG welded area is commonly divided into four zones, Fig. 5:

- Weld: Molten material from the consumable electrode bar which solidifies after a period of time.
- The Fusion Zone (FZ): Part of the base material of the structure that suffers change of phase during the welding procedure.
- The Heat Affected Zone (HAZ): Base material exposed to high temperatures below the liquids point.
- The parent material: Rest of the material in a welded structure.

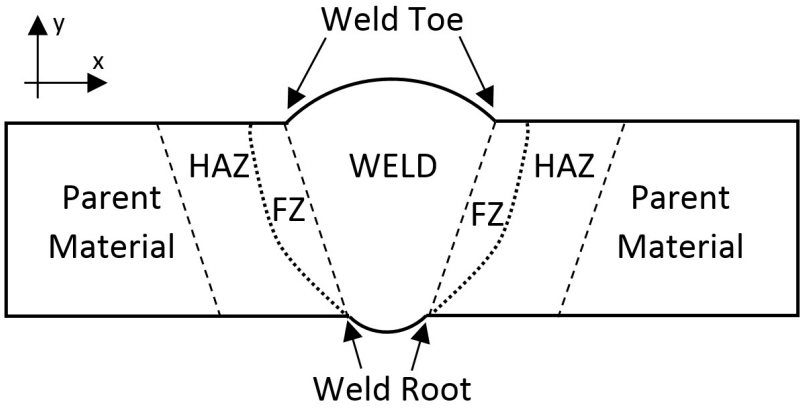

Figure 5: Illustration of the four areas in a weld: the Weld, the Fusion Zone (FZ), the Heat affected Zone (HAZ) and the parent material.

The DNVGL-RP-C203 Standard [6] shows many types of weld connections. However, welds can generally be divided into two mayor groups:

- Fillet welds: The welded material is added onto the surface of two metallic structures to support the contact in between those structures, Fig. 6a.
- Butt welds: The welded material is added to the structure to fulfil a gap in between two metallic structures. Welding techniques can be applied on one side of the structure (Single Penetration Fig. 6b) or on both sides (Double Penetration Fig. 6c).

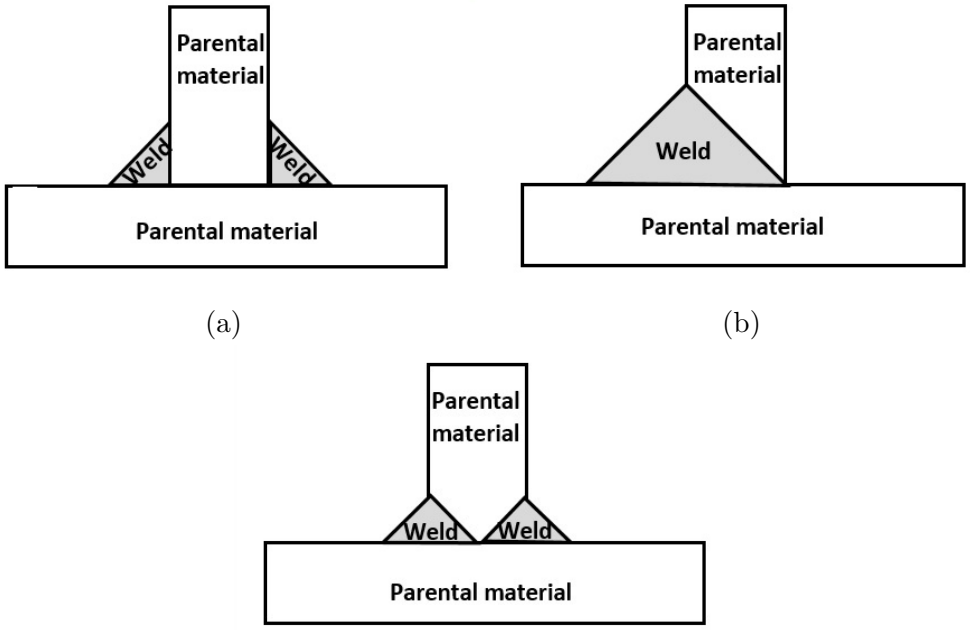

Figure 6: Illustration of the three types of welds:(a) The fillet weld; (b) The single penetration butt weld; (c) The double penetration butt weld.

The weld includes several structural features listed below:

- Weld Geometry: Misalignment between two structural components welded together Fig. 7, weld toe radius or weld root radius are geometric characteristics that clearly influence the fatigue life of a weld. Some of the geometrical peculiarities of the weld, such as the weld toe or root, can be locations of high stress concentrations. [9]

- Weld Residual stresses: These stresses appear during the cooling phase due to contraction of the melt in the FZ and due to thermal expansion/contraction effects in the HAZ. According to Ahmed [9], some locations in the weld include tensional residual stresses, which have a detrimental effect on the fatigue life performance. However, other areas may include compressive residual stresses, which have a positive effect on the fatigue life.

- Imperfections: The weld manufacturing may also include a number of defects listed in the ISO 6520-1:2007 [10]. Examples include lack of penetration, surface roughness and air occlusions, Fig. 7. These defects are responsible for multiple damages and the low fatigue life performance of a weld.

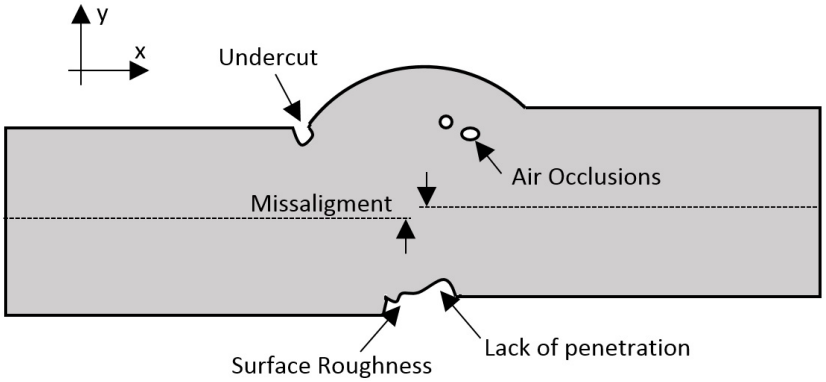

Figure 7: Example of defects found in welds.

2.3 Environmental aspects

The environment usually plays a key role in the integrity of a structure. The moisture, temperature, erosion or periodic water immersions are some of the topics extensively studied to determine the reliability curves of a structural case. All these subjects may have an effect called Environmental Assisted Cracking (EAC). The EAC is a highly complex topic and it strongly influences and exacerbates fatigue life predictions. [11]

Among the EAC causes, corrosion is the most popular. Corrosion is an electrochemical reaction that appears when a structure transfers electrons and ions to the environment that surrounds it. The structure under corrosion would be the equivalent of an anode in an electrochemical cell. The most common mechanisms of localised corrosion are [12] [11]:

- Microbiological: Bacteria can interact with the environment at the steel surface and generate products that can create or accelerate corrosion.
- Corrosion fatigue: It is defined as the fatigue damage acceleration of

a structure in a corrosive environment when compared with an inert environment.

- Stress corrosion cracking: Areas around the crack tip may include high tensile stresses that can develop an electrical potential different to their surroundings.
- Intergranular corrosion: Corrosion caused by the physical and chemical difference between the core and edges of the grains.
- Stray current corrosion: An external source, such as cathodic protection systems in the vicinity, creates an electrical potential that corrodes the steel.
- Crevice corrosion: In a confined space, where there is a difference in oxygen concentration on the steel surface, a driving electrical potential can exist and develop corrosive effects.
- Pitting corrosion: This process starts on an unprotected surface where localised areas are damaged. These spots become pits that act as anodes surrounded by a passive area, which acts as a cathode.
- Galvanic corrosion: Two metals in contact with each other may create driving potential where the less noble metal starts to corrode.

The different types of corrosion are connected to one another. For example, pitting affects crack initiation and, therefore, corrosion fatigue. The synergies between different corrosion aspects that affect crack initiation and propagation explain the difficulties to model EAC. [11]

2.4 The Transitional Environmental Protection process

The corrosive environment has concerned the industry for many years. Methods such as galvanic protection or dehumidifiers are used in order to reduce or eliminate the effects of corrosion in the life of a structure. However, these protection systems may fail during the operational time of an offshore structure. Ruiz and Sørensen [1] define this situation as the Transitional Environmental Protection (TEP) process. In a fatigue study of a structure under the TEP process, calculations should consider variable environmental conditions.

2.5 Common techniques of fatigue life assesment: Constant Amplitude Loading

The weld, environmental and loading characteristics introduce a complex structural system which indicates that the fatigue life estimation is extremely difficult. A method that could combine all these factors and efficiently predict a realistic fatigue performance does not exist. However, there are a number of techniques in industry capable of predicting the life of welds and corroded structures using a conservative approach, i.e. structures are expected to last longer than the fatigue life results.

These techniques are known as the Stress-Based (SB) methods. A SB method estimates the fatigue life of a component from its stress distribution. The SB approach relies on S-N curves for fatigue calculations, Fig. 8, i.e. the results from previous experimental fatigue studies for different structural cases. Each S-N curve corresponds to a weld profile or environmental condition.

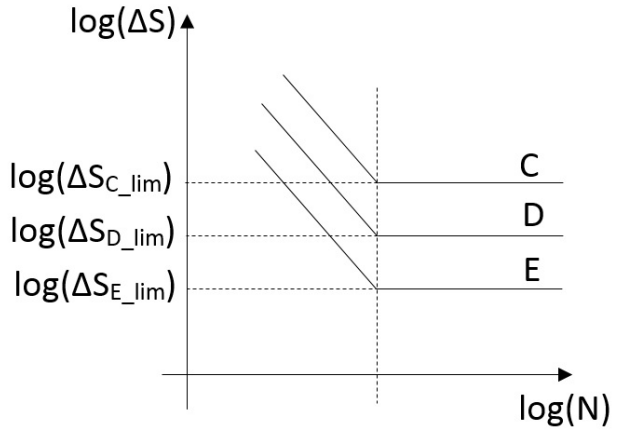

Figure 8: SN curves for different weld profiles. ΔS denotes the stress range and N the number of loading cycles.

2.5.1 The Nominal Stress Approach

The Nominal Stress Approach is the simplest SB technique to evaluate the fatigue life of a weld. The fatigue life assessment of a structural case follows this procedure:

(i) First, the S-N curve that corresponds to the case of study is selected.

(ii) Then, the S-N curve will indicate the number of cycles to failure for the stress range of the case.

This method is extremely efficient since no calculations are needed. However, the main drawback is that the Nominal Stress Approach is limited to a certain range of welded structures or load directions. A real structure may include multi directional stresses or complex welded structures where further advanced methods are required.

2.5.2 The Hot Spot Stress Approach

The Hot Spot Stress approach is a versatile alternative compared to the Notch Stress Approach. Welded structures are modelled through the Finite Element Methods (FEM) and the stresses are calculated. Those locations where the stresses are the highest are called hot spots. At certain distances from those spots, Fig. 9, the surface stresses are retrieved and transformed to an equivalent stress. This procedure is well documented in the standard DNVGL-RP-C203 [6]. The difference between the equivalent stress for a maximum and for a minimum load in a signal is calculated. According to the standard DNVGL-RP-C203 [6], this stress range must be used in a particular S-N curve, named as D-curve, to calculate the fatigue life of a structure.

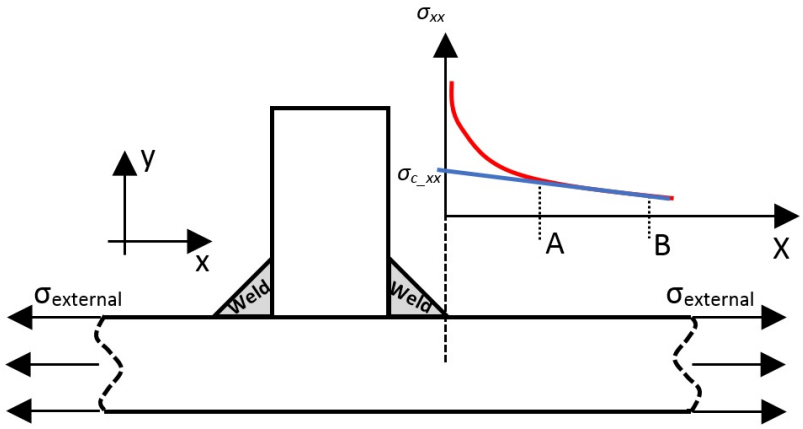

Figure 9: Hot spot stress approach to a fillet weld under tensional cycling stresses $\sigma_{external}$. The curve denoted in blue is the stress distribution of the stress σ_{xx} along the surface of the model. The blue line represents the linear extrapolation from stress values at distance A and B set in the standards. The parameter σ_{c_xx} is the stress extrapolated value for fatigue calculations.

There are two main advantages concerning this method. Firstly, it is a versatile method that can be used to analyse a wide range of welded structures and loading directions. Secondly, detailed modelling of the weld geometry can be omitted in most of the cases.

On the other hand, the hot spot method is not recommended when there are several hot spots in close vicinity to one another, Fig. 10. In those scenarios, the stress surface extrapolation methods described in DNVGL-RP-C203 [6] are no longer valid because of the stress interference between hot spots.

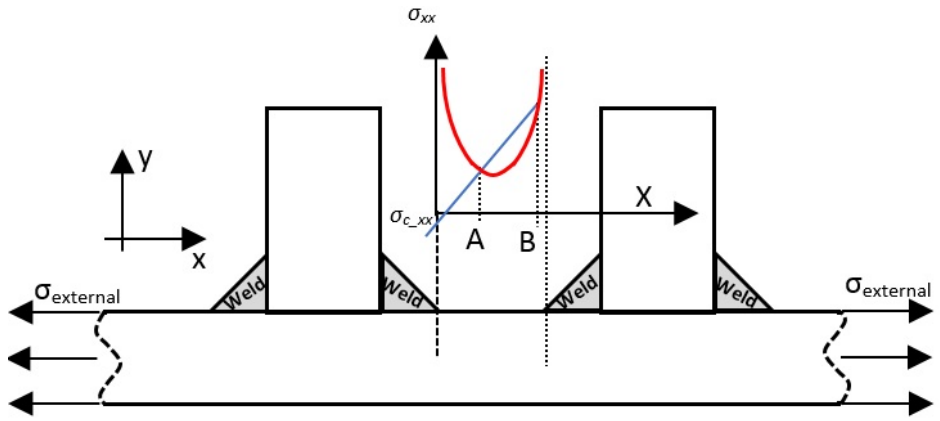

Figure 10: Hot spot methodology when two singularities are in close vicinity to one another. The stress extrapolated value σ_{c_xx} present negative values, leading to inconsistent fatigue life predictions.

2.5.3 The Notch Stress Approach

The notch Stress Approach is a similar method to the Hot Spot Stress Approach. The structure is usually modelled through the FEM, including the weld shape. The weld model must avoid sharp edges that could introduce structural singularities. The weld design includes a toe and a root radius of 1mm according to DNV recommendations [6].

In the Notch Stress Approach, the material is assumed to be linear elastic. The maximum stress of the model is retrieved. This procedure is done for maximum and minimum external load applied in a load cycle. The difference between these two results is a stress range that is later used in a particular S-N from the standards in order to predict the number of cycles to failure.

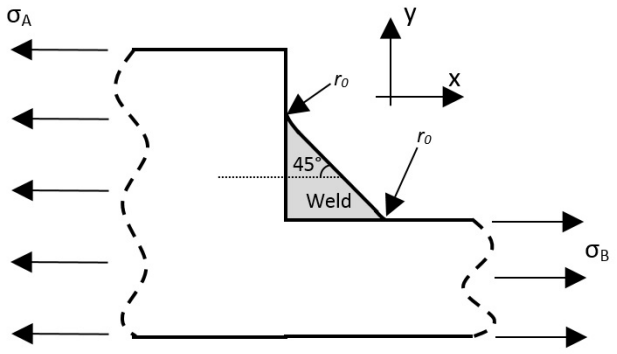

Figure 11: Notch stress approach to a fillet weld. The weld toe radii are defined with a magnitude $r_0 = 1$ mm. The maximum principal stress of this model is retrieved for fatigue life calculations.

2.6 Common techniques of fatigue life assesment: Variable Amplitude Loading

Real structural problems usually include loading signals with variable amplitude. The fatigue life estimations of these cases are normally addressed by combining the techniques used for a constant amplitude loading with the well-known Palmgren-Miner's rule [13]. This rule assumes that the fatigue damage caused by a load signal is the sum of the damages caused by each individual sub-signal that composed it. For a given number of load cycles N, the load is decomposed in k different sub-signals with N_i cycles, where $N = \sum_{i=1}^{k} N_i$. Each load sub-signal is associated with a number of cycles to failure under constant amplitude $N_{i,f}$, where $N_{i,f}$ is calculated as described in Section 2.5. Total damage accumulated in a structure is calculated as

$$D = \sum_{i=1}^{k} \frac{N_i}{N_{i,f}}, \tag{1}$$

where failure occurs whenever the condition $D \geq 1$ is met.

The effects of variable amplitude loading modifies the S-N curves used to calculate $N_{i,f}$. For constant amplitude loading, some DNV S-N curves [6] include a fatigue endurance limit. According to DNV S-N curves [6], if the maximum stress range in a load signal is below the fatigue limit, there is no damage. However, if the load signal includes stress ranges above the original fatigue limit, the S-N curve is modified as shown from Fig.8 to Fig. 12.

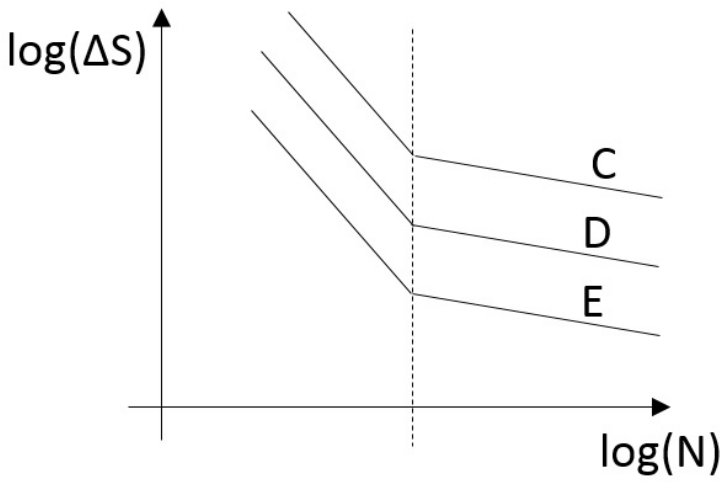

Figure 12: Configuration of S-N curves for variable amplitude loading. The logarithmic results for high cycle stress present tilted straights.

2.7 The Transitional Environmental Protection process for Stress-Based methods

Ruiz and Sørensen [1] propose to include the TEP process in fatigue calculations by assuming the linear accumulated damage model from Palmgren-Miner, Eq. 1. The total damage is the sum of two phases:

- In the first phase, the damage D is calculated and accumulated from S-N curves corresponding to the environmental protection condition, e.g. cathodic protection or air conditions. This phase corresponds to the time prior to the shift in environmental conditions, $t < t_{TEP}$, where t is time and t_{TEP} indicates the time at which the protection system fails.

- In the second phase, the damage D is calculated and accumulated from S-N curves corresponding to the corrosive conditions. This phase corresponds to the period of time after the failure of the protection system, $t \geq t_{TEP}$.

The damage calculations only reach the second phase if the structural case does not fail during the first phase, Fig. 13.

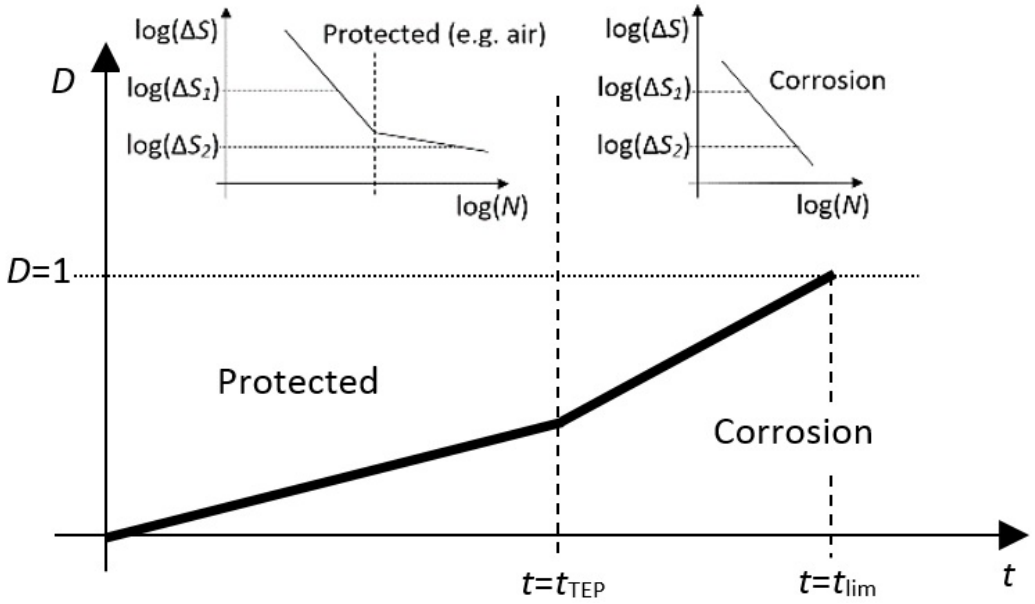

Figure 13: Damage accumulation model for the Transitional Environmental Protection (TEP) process. The structure is subject to stress ranges ΔS_1 and ΔS_2. The S-N curves used to calculate the damage shift from environmentally protected conditions to corrosive conditions at $t = t_{TEP}$.

2.8 Limitations of common existing methods

The methods exposed in this section are the most common techniques for fatigue life estimation in the industry. In general, they present advantages in term of simplicity and computational efficiency. However, they include two major disadvantages:

- These methods can not be used to calculate the real fatigue life behaviour since they lack to consider in detail different features of each weld such as the weld toe radius, porosity, welding internal defects or the residual stress distribution.

- These techniques are stress-based approaches and therefore do not simulate the crack propagation in a structure under fatigue loading. The crack propagation is a key concept for inspection planing [12].

The simplicity of these models leads to a high uncertainty when compared to the real behaviour of structural welds. Therefore, conservative values of the S-N curves are usually considered during the design phase.

On the other hand, the limitations concerning crack propagation lead to seek another method for fatigue life simulation. In this research, that approach will be the Fracture Mechanics (FM) approach.

3 The fracture mechanics approach for fatigue analysis of offshore welds

The fracture mechanics approach for fatigue analysis is the study of the crack development in a structure subject of cycling loads. The main advantage of the fracture mechanics approach, with respect to the SB approach, is that it includes the analysis of the crack length over time, a key concept for inspection planning simulations [12].

3.1 Fracture mechanics principles

The existence of cracks in a component includes stress raisers that can be detrimental for the integrity of a structure. This high concentration of stresses is originated by three types of loading modes, Fig. 14.

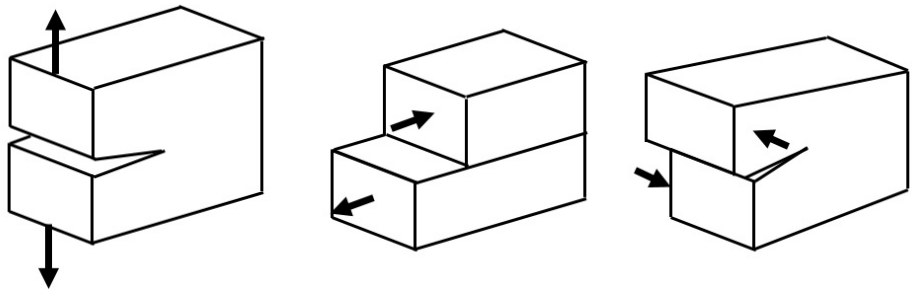

(a) (b) (c)

Figure 14: Three modes of loading in the fracture mecanics studies: (a) Mode-I; (b) Mode-II, (c) Mode-III.

In the FM framework, cracks are often studied under the assumption of the infinitely sharp shape. This condition introduces a structural singularity in the crack tip, where in a linear elastic analysis the stresses increase towards infinite as the distance from the crack tip reduces. [11]

Real structures do not present infinite stress values but instead plastically deform around the crack tip and present finite stress values. Anderson [11] describes the shape of the plastic zone depending on the loading mode, Fig. 15.

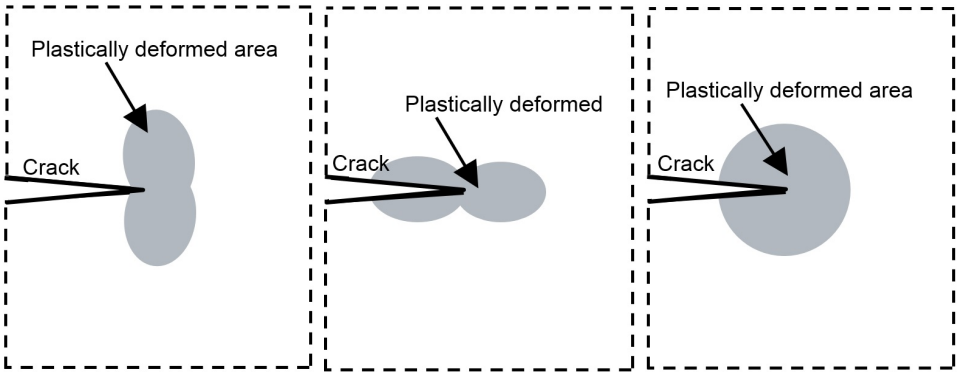

Figure 15: Three plastic areas depending on the mode of load: (a) Mode-I; (b) Mode-II, (c) Mode-III.

The study of the stresses in a plastically deformed area is cumbersome due to the non-linear deformations. However, it is common to simplify the structural problem by assuming the Linear Elastic Fracture Mechanics approach (LEFM).

3.1.1 Introduction to Linear Elastic Fracture Mechanics

Westergaard [14] or Irwin [15] were among the first authors to publish closed-form stress expressions around crack tips for linear elastic isotropic materials. They determined that the stress distribution near the crack tip $\sigma_{i,j}$ for a linear elastic isotropic material is calculated as

$$\sigma_{ij} = \left(\frac{k}{r^{\frac{1}{2}}}\right) f_{ij}(\theta) + \sum_{n=0}^{\infty} A_n r^{\frac{n}{2}} g_{ij}^{(n)}(\theta) \tag{2}$$

where k is a constant, r is the distance from the crack tip, $f_{ij}(\theta)$ and $g_{ij}^{(n)}$ are dimensionless functions of the angular position θ and A_n is the amplitude of the higher order terms.

The first term in Eq. 2, $\left(\frac{k}{r^{\frac{1}{2}}}\right) f_{ij}(\theta)$, is known as the singular term because it approaches infinity when the distance from the crack tip to the stress evaluation point approaches zero, $r \longrightarrow 0$. The second term of Eq. 2, $\sum_{n=0}^{\infty} A_n r^{\frac{n}{2}} g_{ij}^{(n)}(\theta)$, is known as the non-singular part, and it includes the T-stresses. As Anderson[11] explains, the first term in Eq. 2 is leading, and

the stress is proportional to $1/r^{1/2}$ for any given configuration.

The stress distribution around the crack tip follows Eq. 2 as long as the material behaves as elastic. This assumption is known as the Linear Elastic Fracture Mechanics (LEFM) approach, and it is valid when the plastically deformed area is negligible compared to the elastically deformed area, i.e. small scale yielding Fig. 16. The elastic area around the crack tip is also known as the K-dominated region, a zone where stresses are proportional to $1/\sqrt{r}$, where r is the distance from the crack tip. [11]

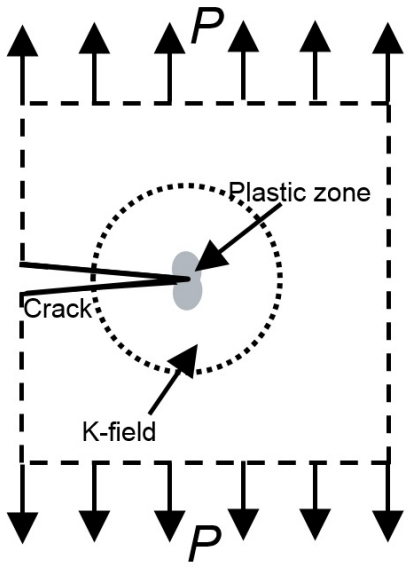

Figure 16: Profile of the plastic zone and K-field for pure mode-I under the assumption of LEFM. [16]

Eq. 2 includes a constant k which is related to the well-known term Stress Intensity Factor(SIF),

$$K = k(2\pi)^{1/2}. \tag{3}$$

The SIF K is vastly studied in the FM framework in order to determine e.g. the fatigue crack propagation [11] or the structural failure due to monotonically increasing loads [17]. There are three different SIF depending on the load direction, mode-I SIF K_I, mode-II SIF K_{II} and mode-III SIF K_{III}, Fig. 14. A common method to calculate the SIF under pure mode-I loading

Fig. 14a is through the prominent J-integral concept proposed by Rice [18],

$$J = \lim_{\Gamma_s \longrightarrow 0} \int_{\Gamma_s} \left(W \delta_{1j} - \sigma_{ij} u_{i,1} \right) n_j d\Gamma \tag{4}$$

where W is the strain energy density denoted as

$$W = \frac{1}{2} \sigma_{ij} \varepsilon_{ij}, \tag{5}$$

δ_{1j} is the Kronecker delta, σ_{ij} and ε_{ij} are the stress and strain tensors, $u_{i,1}$ is the derivative of the displacement vector u_i with respect to the coordinate x_i, $u_{i,1} = \frac{\partial u_i}{\partial x_i}$, n_j is the outward normal vector to the contour Γ_s, Fig. 17, and Γ is the sum of all contours in Fig. 17,

$$\Gamma = \Gamma_0 + \Gamma^+ + \Gamma_s + \Gamma^-. \tag{6}$$

For a homogeneous material under quasi-static, isothermal loading with no body forces, the J-Integral for traction-free crack faces can be written in terms of the integral of an area A as ([19] [20] [21])

$$J = \int_A \left(\sigma_{ij} u_{i,1} - W \delta_{1j} \right) q_{,j} dA \tag{7}$$

where q, j is the derivative of the plateau-type weight function with respect to coordinate x_j,

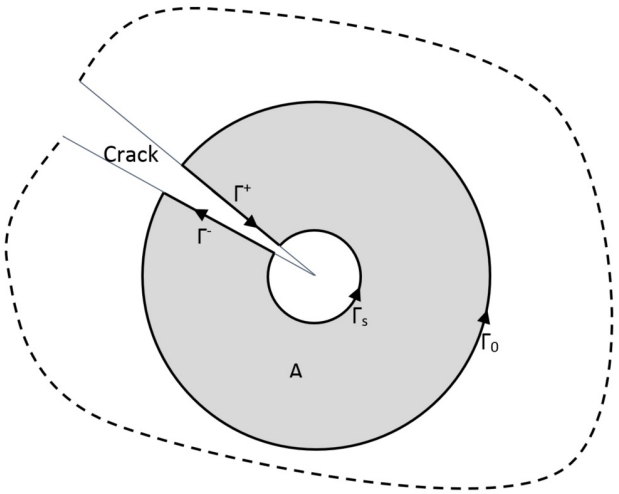

Figure 17: Plot of contours around the crack.

Under pure mode-I conditions, the J-Integral is related to K_I as

$$J = \frac{K_I^2}{E'}, \tag{8}$$

where $E' = E$ for plane stress, $E' = E/(1-\nu^2)$ for plane strain, E is the Young's modulus and ν is the Poisson's ratio. The plane stress condition occurs when a component of the stress tensor that corresponds to any particular surface in a 3D model is zero, whereas the plane strain condition appears when a component of the strain tensor that corresponds to any particular surface in a 3D model is zero.

However, under mixed-mode -I,II loading conditions, i.e. when the mode-I and mode-II loads are simultaneously applied on the structure Fig. 14, the J-integral is related to both SIFs as

$$J = \frac{K_I^2 + K_{II}^2}{E'}. \tag{9}$$

Eq. 9 holds as long as LEFM is applicable. Therefore, further analyses are necessary to individually calculate K_I and K_{II}.

3.1.2 Mixed-mode fracture mechanics: The Interaction Integral.

A 2D structure is under mixed-mode -I,II loading conditions when there are tensional and shear stresses in front of the crack tip. For fatigue purposes, it is inevitable to calculate the SIF of each mode, K_I and K_{II} [22].

Stern et al. [23] and Yau et al. [24] proposed a methodology to calculate each SIF in a mixed-mode situation by applying the interaction integral concept. Assuming that a model with a crack is subject to a mixed-mode loading $S^{(1)}$. The resulting stresses, strains and displacements around the crack are denoted as $\sigma_{ij}^{(1)}$, $\varepsilon_{ij}^{(1)}$ and $u_i^{(1)}$ respectively. In a linear elastic problem, if an auxiliary load randomly selected $S^{(2)}$ is added to the original case Fig. 18, the resulting stresses, strains and displacement are calculated by applying the superposition principle [19]

$$u_i = u_i^{(1)} + u_i^{(2)} \tag{10}$$

$$\sigma_{ij} = \sigma_{ij}^{(1)} + \sigma_{ij}^{(2)} \tag{11}$$

$$\varepsilon_{ij} = \varepsilon_{ij}^{(1)} + \varepsilon_{ij}^{(2)} \tag{12}$$

where $\sigma_{ij}^{(2)}$, $\varepsilon_{ij}^{(2)}$ and $u_i^{(2)}$ are the stresses, strains and displacements associated with $S^{(2)}$.

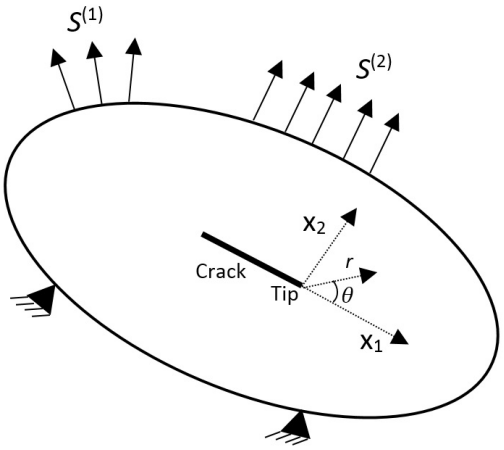

Figure 18: Example of loads $S^{(1)}$ and auxiliary loads $S^{(2)}$ for the interaction integral method.

The substitution of the terms Eq. [10-12] in Eq. 7 results as [19]

$$J^S = \int_A \left\{ \left(\sigma_{ij}^{(1)} + \sigma_{ij}^{(2)}\right) \left(u_{i,1}^{(1)} + u_{i,1}^{(2)}\right) - \frac{1}{2} \left(\sigma_{ik}^{(1)} + \sigma_{ik}^{(2)}\right) \left(\varepsilon_{ik}^{(1)} + \varepsilon_{ik}^{(2)}\right) \delta_{1j} \right\} q_{,j} dA \tag{13}$$

Eq. 13 can be decomposed into three terms

$$J^S = J^{(1)} + J^{(2)} + M^{(12)} \tag{14}$$

where

$$J^{(1)} = \int_A \left\{ \sigma_{ij}^{(1)} u_{i,1}^{(1)} - \frac{1}{2} \sigma_{ik}^{(1)} \varepsilon_{ik}^{(1)} \delta_{1j} \right\} q_{,j} dA \tag{15}$$

$$J^{(2)} = \int_A \left\{ \sigma_{ij}^{(2)} u_{i,1}^{(2)} - \frac{1}{2} \sigma_{ik}^{(2)} \varepsilon_{ik}^{(2)} \delta_{1j} \right\} q_{,j} dA \tag{16}$$

$$M^{(12)} = \int_A \left\{ \sigma_{ij}^{(1)} u_{i,1}^{(2)} + \sigma_{ij}^{(2)} u_{i,1}^{(1)} - \frac{1}{2} \sigma_{ik}^{(1)} \epsilon_{ik}^{(2)} \delta_{1j} - \frac{1}{2} \sigma_{ik}^{(2)} \epsilon_{ik}^{(1)} \delta_{1j} \right\} q_{,j} dA \tag{17}$$

where $M^{(12)}$ is known as the interaction integral.

According to Eq. 9, Eq. (13,15,16) can be expressed as

$$J^{(S)} = \frac{\left(K_I^{(S)}\right)^2 + \left(K_{II}^{(S)}\right)^2}{E'} \tag{18}$$

$$J^{(1)} = \frac{\left(K_I^{(1)}\right)^2 + \left(K_{II}^{(1)}\right)^2}{E'} \tag{19}$$

$$J^{(2)} = \frac{\left(K_I^{(2)}\right)^2 + \left(K_{II}^{(2)}\right)^2}{E'} \tag{20}$$

Considering the superposition principle, for each loading mode the total SIF is the sum of the SIF related to each load [11],

$$K_I^{(S)} = K_I^{(1)} + K_I^{(2)} \tag{21}$$

$$K_{II}^{(S)} = K_{II}^{(1)} + K_{II}^{(2)} \tag{22}$$

Eq. 21 and Eq. 22 can be included in Eq. 18 as

$$J^{(S)} = \frac{\left(K_I^{(1)} + K_I^{(2)}\right)^2 + \left(K_{II}^{(1)} + K_{II}^{(2)}\right)^2}{E'} \tag{23}$$

The substitution of Eq. [19,20,23] in Eq. 14 results as

$$M^{(12)} = \frac{1}{E'}\left(2K_I^{(1)}K_I^{(2)} + 2K_{II}^{(1)}K_{II}^{(2)}\right). \tag{24}$$

The interaction integral in Eq. 14 can be calculated by solving the three load cases, i.e. Eq. 19 when only load $S^{(1)}$ is applied, Eq. 20 when only the load $S^{(2)}$ is applied and Eq. 18 when both loads $S^{(1)} + S^{(2)}$ are applied. The stress, displacement and strain distributions can be retrieved from e.g. the Finite Element Method (FEM). However, Eq. 24 is dependent on the mixed-mode -I,II SIFs. The stress intensity factors can be individually calculated by a proper selection of the auxiliary force $S^{(2)}$ such that results in pure auxiliary modes. For instance, if an auxiliary force results in pure mode-I with a known solution $K_I^{(2)} = 1$ and $K_{II}^{(2)} = 0$, Eq. 24 is reduced to $K_I^{(1)} = \frac{E'}{2}M^{(12)}$. A similar procedure can be done to calculate $K_{II}^{(1)}$. [19]

3.1.3 The Equivalent Stress Intensity Factor and the Crack Growth Direction

Under a mixed-mode crack growth analysis, the crack growth direction is usually set by the direction where the maximum strain energy is released [11]. Assuming that this direction is consistent towards pure mode-I, the Equivalent Stress Intensity Factor K_{Eq} is presented as the SIF corresponding to an infinitely small growth from a mixed-mode to a pure mode-I crack geometrical configuration, Fig. 19. [22]

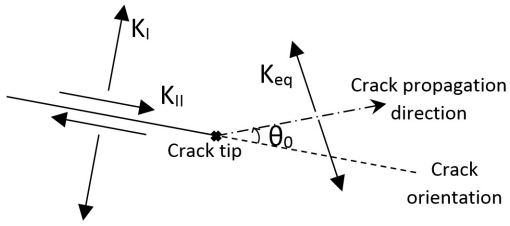

Figure 19: Crack propagation direction following an illustration by Meggiolaro et al. [22]

Under a mixed-mode scenario, the equivalent SIF concept is extremely useful because it opens the possibility to use formulas that were in principle constraint to pure mode-I. The term K_I is directly replaced by K_{eq} in each formula, as Ruiz explains in [25].

There are several criteria to calculate the equivalent SIF. The Irwin or Energy Release criterion [15] shows an approximation, Eq. 25, based on the relations between the energy release rate and the SIFs.

$$K_{Eq,IRWIN} = \left(K_I^2 + K_{II}^2\right)^{1/2} \tag{25}$$

It is also widely used in literature the Tanaka's formulation [26], Eq. 26, which is based on the displacements behind the crack tip that reach a critical value.

$$K_{Eq,TANAKA} = \left(K_I^4 + 8K_{II}^4\right)^{1/4} \tag{26}$$

Another well-known model to calculate the equivalent SIF is the Maximum Circumferential Stress (MCS) criterion, also called the Maximum Tangential Stress (MTS) criterion, proposed by Erdogan and Sih [27]. This criterion considers that the crack growth is oriented in the direction where

the maximum circumferential stress is located. Assuming the MCS this direction is the same as the direction for pure mode-I growth. The Equivalent SIF is formulated as

$$K_{Eq,MCS} = \frac{1}{4}\left(3\cos\frac{\theta_0}{2} + \cos\frac{3\theta_0}{2}\right) K_I - \frac{3}{4}\left(\sin\frac{\theta_0}{2} + \sin\frac{3\theta_0}{2}\right) K_{II} \tag{27}$$

where θ_0 is the pure mode-I crack growth direction Fig. 19 and it is calculated as

$$\theta_0 = 2\tan^{-1}\left(\frac{K_I}{4K_{II}} \pm \frac{1}{4}\sqrt{\left(\frac{K_I}{K_{II}}\right)^2 + 8}\right) \tag{28}$$

Two values can be obtained from Eq. 28. The final selected value is the one that presents the maximum circumferential stress,

$$\sigma_{\theta\theta} = \frac{1}{(2\pi r)^{1/2}} \cos\frac{\theta}{2}\left[K_I \cos^2\left(\frac{\theta}{2}\right) - \frac{3}{2} K_{II} \sin\theta\right] \tag{29}$$

where θ is the polar coordinate around the crack tip, Fig. 20.

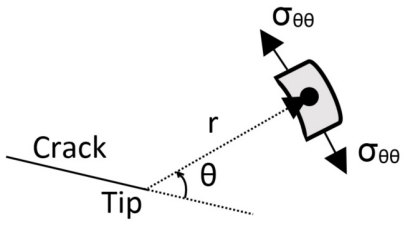

Figure 20: Circumferential direction of the stresses in a polar coordinate system with crack tip as the origin.

Fig. 21 shows the result of different Equivalent SIF formulations. For high values of $|K_{II}/K_I|$, each model behaves differently. Meggiolaro et al. [22] already showed this analysis and they incorporated other criteria such as the strain energy density criterion or the maximum energy release rate criterion. They concluded that at predominant mode I, where $K_I \gg K_{II}$, all these criteria show similar equivalent mixed-mode results. Meggiolaro et al. state that since the presented criteria predicts a path deviation towards a pure mode-I, the model will grow towards a situation where all criteria are essentially the same. Among all equivalent SIF criteria, Meggiolaro et al.

declare that the MCS criterion is a preferred approach due to its simplicity and close form solution.

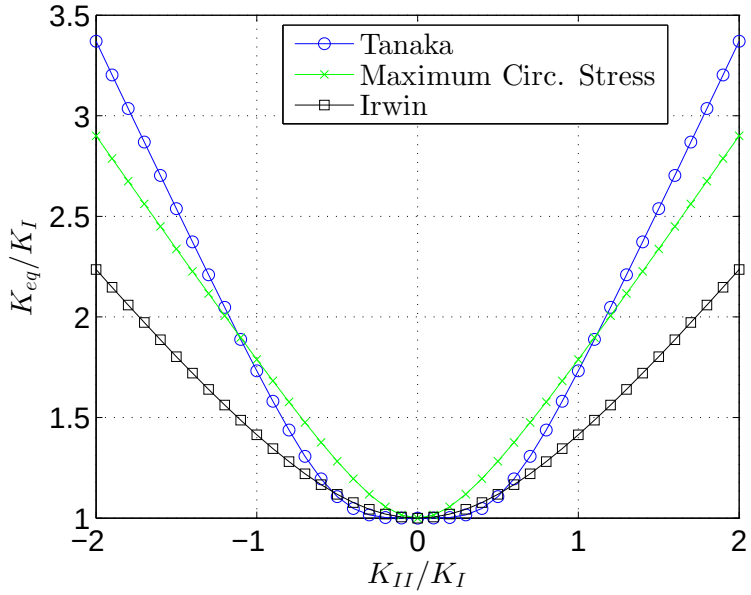

Figure 21: Normalised equivalent SIF for different mix mode SIF and criterion: Tanaka(Eq. 26), Maximum Circ. Stress(Eq. 27) and Irwin(Eq. 25). The graph follows the illustration by Meggiolaro et al. [22].

3.1.4 The plastic zone under plane stress/strain conditions and the application limit for LEFM analysis

The plane stress/strain conditions are widely used in literature as an approach to a 3D problem from a 2D perspective. The shape of the plastic area around the crack tip depends on the condition applied. Irwin defines the most simple approach to this area as a circle in front of the crack tip, with radius

$$2r_{O\varepsilon} = \frac{1}{3\pi}\left(\frac{K_{eq}}{\sigma_{ys}}\right)^2 \tag{30}$$

for plane strain conditions, and

$$2r_{O\sigma} = \frac{1}{\pi}\left(\frac{K_{eq}}{\sigma_{ys}}\right)^2 \tag{31}$$

for plane stress conditions, where $r_{O\epsilon}$ stands for the radius of the plastic zone under plane strain conditions, and $r_{O\sigma}$ denotes the radius of the plastic zone under plane stress conditions.

Another approach to defining the plastic zone is by using the circle of Mohr principles as explained in [11]. The shape of the plastic zone as a function of the angle from the crack tip θ is shown as,

$$r_{O\sigma} = \frac{1}{4\pi}\left(\frac{K_{eq}}{\sigma_{ys}}\right)^2\left[1+\cos\theta+\frac{3}{2}\sin^2\theta\right] \tag{32}$$

for plane stress, and

$$r_{O\varepsilon} = \frac{1}{4\pi}\left(\frac{K_{eq}}{\sigma_{ys}}\right)^2\left[(1-2\nu)^2(1+\cos\theta)+\frac{3}{2}\sin^2\theta\right] \tag{33}$$

for plane strain conditions.

Dowling [16] suggests using the plasticity formulations to elaborate the application limit for LEFM analysis. Among the equations of the plasticity shape presented, Eq. 31 includes the location $(2r_{O\varepsilon}, 0)$ with the highest distance from the crack tip, Fig. 22. Dowling defines the application limit for LEFM analysis as two times that distance,

$$d_{LEFM} \geqslant 4r_{O\varepsilon} = \frac{4}{\pi}\left(\frac{K_{eq}}{\sigma_{ys}}\right)^2, \tag{34}$$

where σ_{ys} is the yielding stress and Dowling [16] defines d_{LEFM} as the distance between the crack tip and a free surface, Fig. 23.

Fig.22a shows the shape of the plastic zone for the two different approaches. In both approaches, the plastic zone related to the plane stress conditions is always larger than the one associated with plane strain conditions. A further analysis, Fig.22b, presents the difference in size between the application limit to LEFM, Eq. 34, and the plastic zones, Eq. [30-33]. [16] [11]

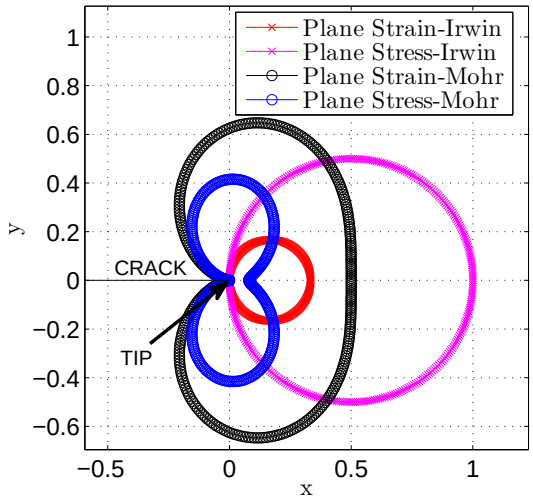

(a)

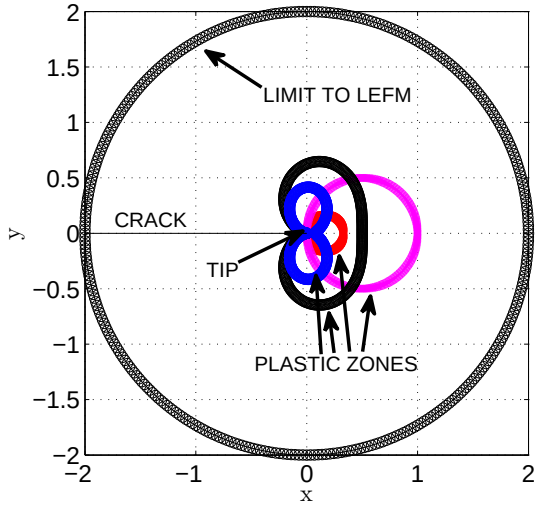

(b)

Figure 22: Shape of the plastic zone in front of the crack tip. Cartesian coordinates x y normalized with respect to $\frac{1}{\pi}\left[\frac{K_{eq}}{\sigma_{ys}}\right]^2$: (a) Plastic Zone delimited by plane stress/strain conditions from two different approaches, the Irwin approach and the Mohr approach Eq. [30-33] [11]; (b) Comparison between the plastic zones and the application limit to LEFM [16].

Fig. 23 illustrates the limit situation where LEFM theory is applicable for three cases.

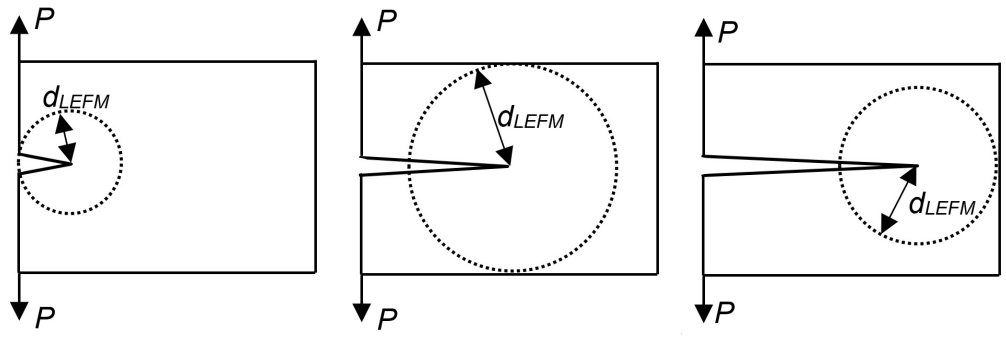

(a) (b) (c)

Figure 23: Three limit situations where the LEFM theory are applicable.

3.1.5 Numerical methods for fracture mechanics

The analysis of the SIF in simple cases can be retrieved through parametric formulation described in e.g. [11]. Closed form solutions only exist for simple problems hardly applicable to the majority of fracture problems posed in real life.

Several numerical methods are normally used to retrieve the SIFs of a crack. Among the possibilities, Anderson [11] suggests the FEM and the Boundary Integral Equation Method (BIE). Anderson states that the BIE is very efficient for calculating unknown tractions and displacements at the surface, but the FEM is more efficient for retrieving internal field quantities, e.g. stresses, strains or displacements.

3.2 Introduction to fatigue analysis from a Linear Elastic Fracture Mechanics perspective

The fatigue crack propagation is commonly defined by two phases, the crack initiation and the crack propagation phase. [12] [28]

3.2.1 Fatigue crack initiation

The fatigue crack initiation is a period in which cracks initiate and start to grow. The crack initiation mechanism is generally governed by slip-band

cracking, inclusions or micro-voids [12] and the crack grows according to the short/small crack growth curves, Fig. 24 [16].

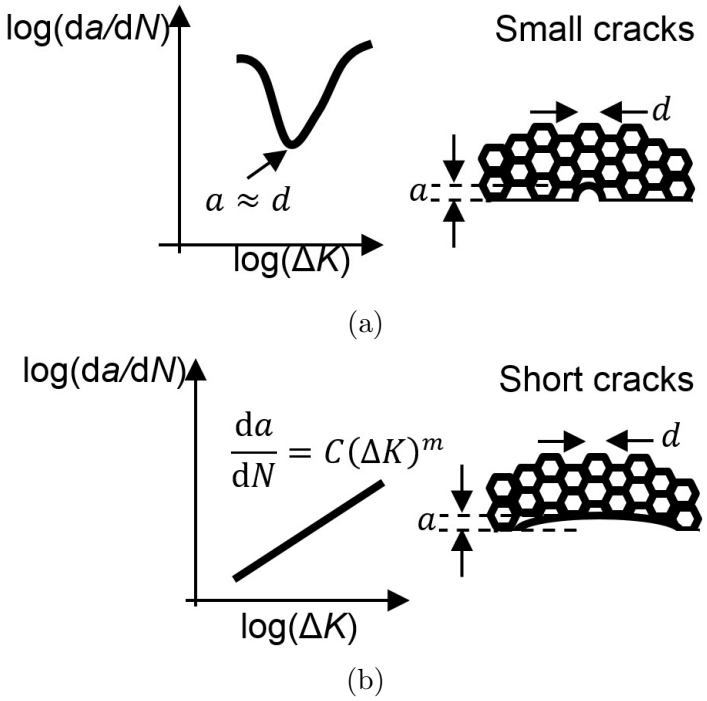

Figure 24: Two types of crack propagation depending on the crack geometry with respect to microstructure: (a) Crack growth rate according to small cracks; (b) Crack growth rate according to short cracks.

The common size of cracks during this phase is usually lower than the limit from which LEFM is applicable, $a < 0.1$ mm ([9],[12]). Lei et al. [28] or Maierhofer et al. [29], among others, conducted several researches about this fatigue period. However, there are no universal formulations that can predict the crack initiation process to date.

3.2.2 Fatigue crack propagation

The fatigue crack propagation is usually divided into three stages, Fig. 25. The Stage I, a non-linear phase where the crack growth rapidly increases, a second stage where the crack growth follows the well-known Paris Law, and a third stage where the crack growth rate approaches the structural collapse.

The Stage II is the most popular, which its expression for mixed-mode fatigue crack propagation is [22]

$$\frac{da}{dN} = C\Delta K_{Eq}^{m} \tag{35}$$

where a is the crack length, N is the number of cycles, and C and m are material parameters.

A discrete form of the Paris Law equation is shown as [16]

$$C\Delta K_{Eq}^{m} = \frac{da}{dN} \approx \frac{\Delta a}{\Delta N} \tag{36}$$

where the crack growth $\Delta a = a_j - a_{j-1}$ is associated with a certain number of load cycles $\Delta N = N_j - N_{j-1}$, and j represents an integer index.

A discrete form of Eq. 35 can be found as [16] 36

$$\Delta a \approx C\Delta K_{Eq}^{m}\Delta N \tag{37}$$

Forman and Mettu [30] proposed including the crack growth rate for the three stages in a single expression

$$\frac{da}{dN} = FC(\Delta K_{Eq})^{m}\frac{\left(1-\frac{\Delta K_{th}}{\Delta K_{Eq}}\right)^{p}}{\left(1-\frac{K_{max}}{K_C}\right)^{q}}, \tag{38}$$

where p and q are material parameters, K_C is the maximum SIF a crack can propagate without immediate failure, F is a crack velocity factor, K_{max} is the maximum SIF a crack propagates according to the Paris Law and ΔK_{th} is the SIF threshold.

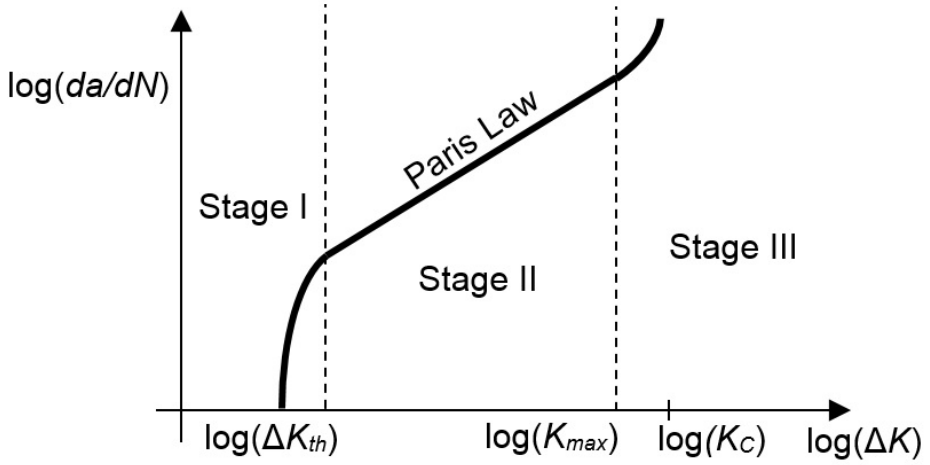

Figure 25: The three crack growth stages of the fatigue crack propagation. The parameter ΔK_{th} is the threshold, K_{max} determines the boundary between the Paris Law regime and the third stage, and K_C is the limit to structural collapse.

In cases of HCF, the most relevant stages to study are I and II. The Stage III is generally neglected [25] since the cycles involved in this stage are very low when compared with the other two.

3.2.3 The overlap between the crack initiation and crack propagation phase

The crack initiation phase and crack propagation phase defined in [12] implies an overlap, Fig. 26 [16]. The first stage of the fatigue crack growth, Fig. 25 is overlapped by the short/small crack growth, Fig. 24. As a consequence, it is not well defined where the crack initiation phase finishes. Maierhofer et al. [29] proposed further formulations to account for this overlap in a modified NASGRO equation. However, it is difficult to present a neat boundary in between the two phases.

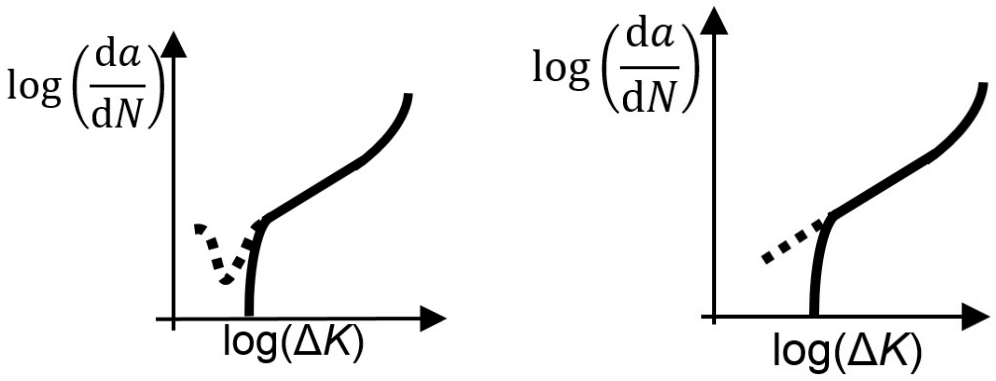

(a) (b)

Figure 26: Overlap in between the crack growth model during the crack initiation phase, denoted in a dash line, and the crack propagation phase, denoted as a continuum line: (a) Initial growth for small cracks; (b) Initial growth for short cracks.

3.2.4 The Crack Closure

Elber [31] was the first to study the effects of crack closure in 1970 when he experimentally noticed that for same stress ranges, decreasing the stress ratio involved lower fatigue crack growth. The crack closure is a mechanical phenomenon that extends the fatigue life of a structure. There are five common types of mechanisms that induce crack closure [11]:

- Corrosion Products: The corrosive waste generated under aggressive environmental conditions can be stacked inside the crack, Fig. 27a.
- Fluid: Cracks of structures immersed in a fluid can include liquids inside, Fig. 27b.
- Roughness: The irregular crack propagation caused by e.g. the T-stresses [32] may result in contact in between the crack faces in some spots, Fig. 27c.
- Plastic induced zone: The high stress values around the crack singularity induce plastic deformations that result into compressive residual stresses, Fig. 27d.

- Transformed Zone: The crack propagation mechanism may induce changes in the metallic composition due to e.g. high temperatures induced by high loading frequency. Metallic changes towards e.g. martensitic induce residual stresses Fig. 27e.

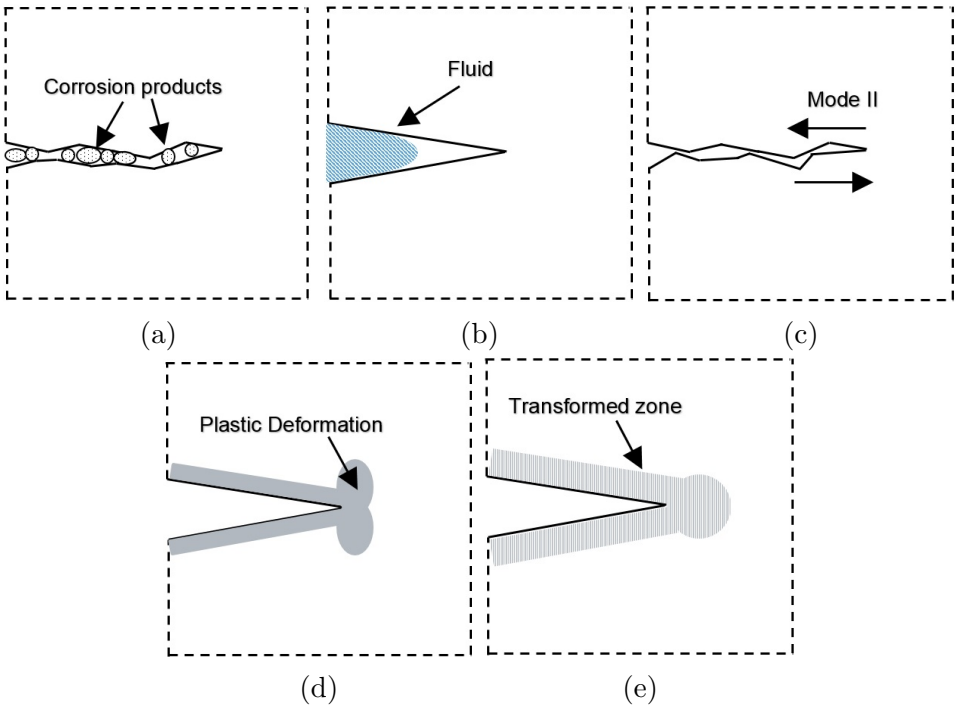

Figure 27: The five typical mechanisms that induce closure effects: (a) The products generated in a corrosive environment; (b) A fluid inside a crack; (c) The roughness of the crack under e.g. mode-II FM analysis; (d) The plasticity induced as crack propagates; (e) The transformed zone, i.e. part of the metal result in a different composition e.g. martensitic.

The corrosion, fluid and roughness closure mechanisms are also known as wedging mechanisms because cracks are prevented from closing completely by different types of obstructions. On the other hand, the plasticity induced situation and transformed zone result in closure effects due to compressive residual stress generation.

Dowling [16] and Anderson [11] show two alternatives to include the crack closure in a fatigue crack propagation model. Dowling shows a relation be-

tween closure effects and Stress Ratio R through the Walker formulation

$$C = \frac{C_0}{(1-R)^{m(1-\gamma)}}, \tag{39}$$

where γ and C_0 are material constants and C and m are the Paris Law parameters from Eq. 35.

Anderson suggests that the crack closure can be included by the term K_{op}, Fig. 28, where adopting the Equivalent SIF concept [25], the effective range is calculated as

$$\Delta K_{eff,eq} = K_{eq}^{max} - K_{op,eq} \tag{40}$$

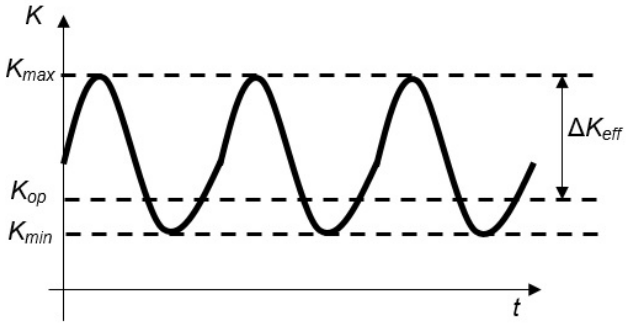

Figure 28: Illustration of the closure SIF K_{op} and the effective SIF range ΔK_{eff}.

Newman [33] proposes a specific formulation for plasticity induced closure problems in metallic structures,

$$f_{eq} = \frac{K_{op,eq}}{K_{eq}^{max}} = \begin{cases} \max(R, A_0 + A_1 R + A_2 R^2 + A_3 R^3) & R \geq 0 \\ A_0 + A_1 R & -1 \leq R < 0 \end{cases} \tag{41}$$

where

$$A_0 = (0.825 - 0.34\alpha + 0.05\alpha^2)[\cos(\pi S^{max}/2\sigma_o)]^{1/\alpha}, \tag{42}$$

$$A_1 = (0.415 - 0.071\alpha)(S^{max}/\sigma_o), \tag{43}$$

$$A_2 = 1 - A_0 - A_1 - A_3, \tag{44}$$

$$A_3 = 2A_0 + A_1 - 1, \tag{45}$$

the parameter S_{max} is the maximum nominal stress, σ_o is the flow stress, i.e. the average between the yield stress σ_{ys} and the ultimate tensile strength σ_u [34], and α is a parameter that varies from $\alpha = 1$ for a plane stress analysis to $\alpha = 3$ for a plane strain analysis. [25]

The analysis of f_{eq} for different parameters in Fig. 29 reveals that the plane stress approach results in the biggest crack closure effects, whereas plane strain conditions present the lowest closure. This result is coherent with the plasticity induced closure theory, since the plane stress condition shows the largest plastic area, Fig. 22 ([11],[16]). Fig. 29 also reveals that, for high Stress Ratios $R > 0.7$, there are no closure effects since $f_{eq} = R$, i.e. $K_{op,eq} = K_{eq}^{min}$.

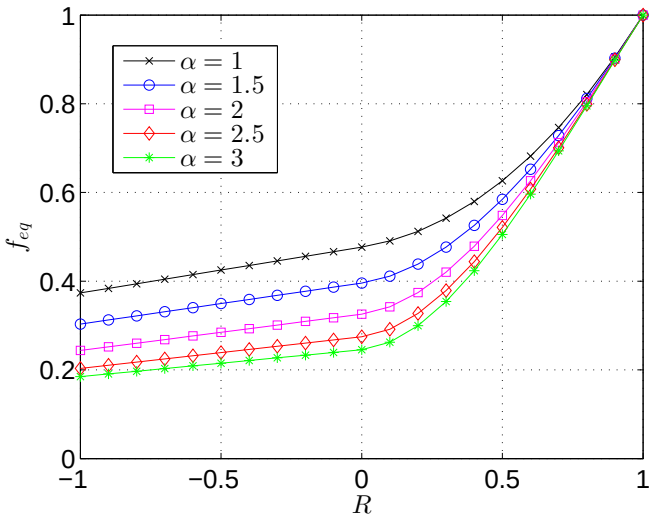

Figure 29: Analysis of the plasticity induced crack closure parameter f_{eq} for different α values [34] and ratio $S_{max}/\sigma_o = 0.3$. The closure effect vanishes as the stress ratio increases.

3.3 Fatigue Formulation for offshore welds under 2D analysis

The fatigue analysis of offshore welds usually includes several characteristics. The initial size of manufacturing defects can lead to a fatigue performance where the crack initiation phase is negligible compared to the crack prop-

agation period [9]. The fracture mechanics approach in literature usually proposes a conservative approach by studying the initial defect in a high stress concentration spot and consider it with a crack shape. However, the manufacturing defects [10] can result in a multiple crack analysis, also known as a Multiple Site Damage (MSD) analysis.

Apart from the MSD analysis, offshore welds include Residual Stresses (RS) and can be subject to environmental aspects that can be detrimental to the structure. The study of these concepts is crucial to understand the fatigue life performance of a weld.

3.3.1 The Multiple Site Damage

Rahman et al. [35], Huang et al. [36], Dundar and Ayhan [37], and Price and Trevelan [38] have performed some of the multiple existing researches about MSD. Seifi et al. studied multiple crack propagation from hollow pre-notched plates whereas Huang et al. studied the MSD in complex welded structures. Dundar et al. and Price et al. developed their own code for MSD fatigue in 2D and 3D analysis.

The MSD fatigue analysis presents several differences with respect to single crack propagation. The author Ruiz [25] shows that the effects of multiple cracks can lead to stress shielding or stress amplification. These effects can be seen by performing Finite Element (FE) studies. However, there are another two MSD peculiarities which require further studies, the closure effects during MSD and the crack coalescence.

The closure effects in Multiple Site Damage

According to the Newman's Eq. 41, the plasticity induced closure effect depends on the 2D conditions imposed, i.e. plane stress, plane strain or mixed conditions. Dowling [16] explains that a 2D model can be considered under plane strain conditions as long as

$$(t_h \cup d) \geq 2.5 \left(\frac{K_{eq}^{max}}{\sigma_{ys}} \right)^2, \tag{46}$$

where t_h is the thickness, d is the distance from the crack to a boundary.

However, as two cracks approach one another, the distance d decreases. Therefore, the plane strain conditions are not satisfied. Dowling [16] suggests that if Eq. 46 is violated, the FM analysis should be performed under plane stress conditions. However, the Dowling's approach dismissed the mixed

conditions, i.e. an interval between plane strain and plain stress conditions where the radios of the plastic zone is

$$\left(2r_{O'} > \frac{1}{3\pi}\left(\frac{K_{eq}^{max}}{\sigma_{ys}}\right)^2\right) \cup \left(2r_{O'} < \frac{1}{\pi}\left(\frac{K_{eq}^{max}}{\sigma_{ys}}\right)^2\right). \tag{47}$$

Rahman et al. [35] already performed an analysis about how the closure effects vary as two cracks approach one another by adjusting the parameter α of Eq. 41 during crack growth. However, their analyses are purely empirical, i.e. the relation between α and cracks proximity is based on a calibration procedure to achieve consistent fatigue results between experiments and crack growth simulations.

Ruiz [25] proposes to address the closure effects in MSD fatigue from a conservative perspective. If the initial conditions are plane strain, this condition is fixed during the entire fatigue analysis. Therefore, the plasticity area is not affected by any change in the 2D conditions as cracks approach one another. As a consequence, cracks grow faster under assuming constant plane strain conditions than varying the conditions during MSD fatigue. On the contrary, if initial plane stress conditions are satisfied, no assumption is needed since this condition will be satisfied during all of the fatigue analysis.

The Crack coalescence

When two cracks approach one another, it is required to evaluate when they will intersect. Skorupa et al. [39] explain the Plastic Zone Link-Up (PZL) criterion, which was initially introduced by Swift [40]. The PZL criterion determines that if the Dugdale's Plastic limits,

$$d_{PZL} = \frac{\pi}{8}\left(\frac{K_{eq}}{\sigma_{ys}}\right)^2, \tag{48}$$

of two cracks are in contact, as shown in Fig. 30, crack coalescence appears.

Skorupa et al. [39] also remark that a more detailed analysis would be the Elasto-Plastic Fracture Mechanics (EPFM) method, which keeps track of the crack tip evolution for large areas plastically deformed. However, PZL is a quicker and simpler solution and is still used for MSD type experiments, even in complex geometry cases [39]. The PZL criterion is in general conservative compared to EPFM, as it skips the plastic behaviour of the structure by directly assuming coalescence.

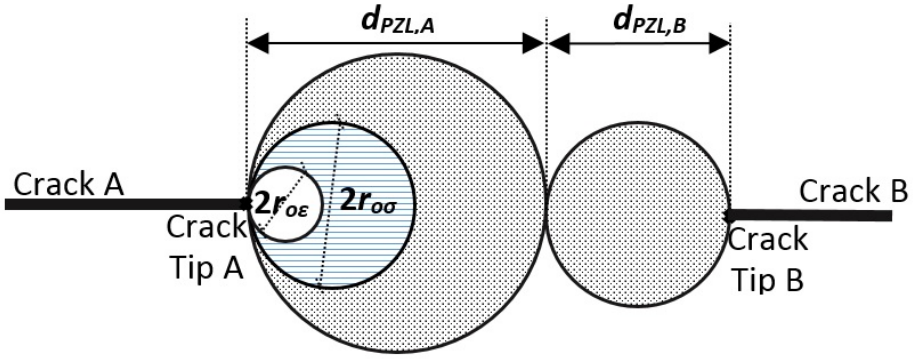

Figure 30: Geometrical position where crack coalescence appears under plane stress/strain conditions. The plastic zone is defined by a radius $2r_{O\epsilon}$ Eq. 30, for strain conditions, and $2r_{O\sigma}$ Eq. 31, for plane stress conditions. The Plastic Zone link-up is delimited by $d_{PZL,A}$ and $d_{PZL,B}$.

Fig. 30 shows the relative size of the plastic zone for plane stress/strain conditions compared to the limits for the PZL

$$d_{PZL,A} = \frac{\pi}{8}\left(\frac{K_A}{\sigma_{ys}}\right)^2, \tag{49}$$

$$d_{PZL,B} = \frac{\pi}{8}\left(\frac{K_B}{\sigma_{ys}}\right)^2, \tag{50}$$

where $d_{PZL,A}$ is the PZL distance for crack tip A, $d_{PZL,B}$ is the PZL distance for crack tip B, K_A is the equivalent SIF associated with tip A and K_B is the equivalent SIF associated with tip B.

The PZL occurs when

$$d_{PZL,AB} \leq d_{PZL,A} + d_{PZL,B} = \frac{\pi}{8}\left(\frac{K_A}{\sigma_{ys}}\right)^2 + \frac{\pi}{8}\left(\frac{K_B}{\sigma_{ys}}\right)^2, \tag{51}$$

Assuming a scenario where $K_A > K_B$, the minimum distance between cracks for a LEFM analysis is

$$d_{LEFM,A} = \frac{4}{\pi}\left(\frac{K_A}{\sigma_{ys}}\right)^2. \tag{52}$$

Fig. 31 shows the comparison between the application limit for LEFM and the limit for PZL. The distance d associated with the application limit of

LEFM is higher for any SIF ratio $\frac{K_A}{K_B}$. Consequently, the LEFM is violated before crack coalescence, Fig. 32.

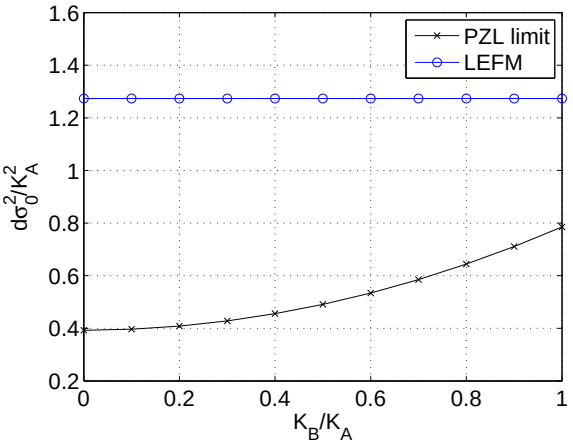

Figure 31: Normalized values between the PZL and LEFM limits between two crack tips: A and B, for different SIF relations K_B/K_A. For the PZL limit study $d = d_{PZL,AB}$ (Eq. 51), whereas for the LEFM limit study $d = d_{LEFM,A}$ (Eq. 52).

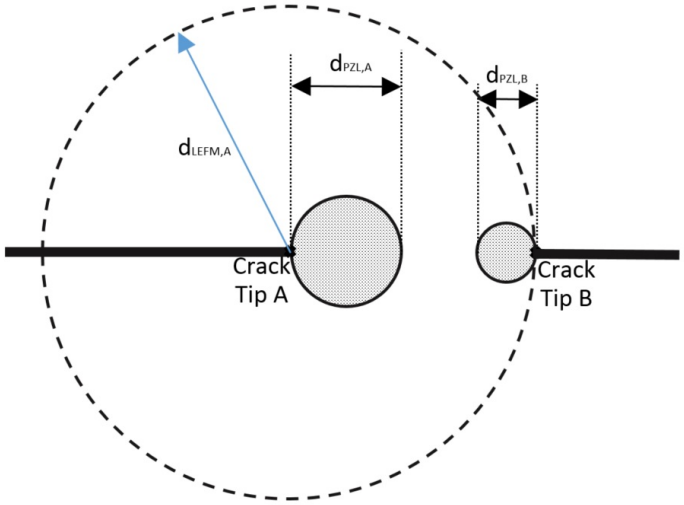

Figure 32: Delimitation of the PZL (Eq. 50) and LEFM (Eq. 52) between two crack tips: A and B.

Ruiz [25] proposes an alternative to PZL criterion by considering crack coalescence once the application limit of LEFM is violated, Eq. 52. This approach is more conservative than PZL criterion since it predicts earlier coalescence, but it respects the LEFM approach.

3.3.2 Residual stress effects in fatigue

Residual stresses result from the manufacturing process of a welded component. During fatigue, tensional residual stresses have a detrimental effect in the life of a structure whereas compressive residual stresses are beneficial.[9]

The Stress-Based methods used to calculate fatigue life of structures relies on S-N curves that implicitly include the residual stress effects. However, the FM approach needs to explicitly include the residual stress as part of the fatigue life calculations.

The residual stresses can be calculated for a limited range of cases through parametric formulation given in standards [5]. For most complex geometries, the Thermo-Mechanical Finite Element Analysis (TMFEA) can be used to estimate the residual stress distribution of a weld. The drawback about TMFEA is the high computational cost when compared with parametric formulation. Finally, the most accurate approach to determine the residual stress values is through experimental methods such as neutron diffraction. The equipment used for these methods is generally costly and time-consuming, usually exceeding the effort for TMFEA.

The residual stress values can subsequently be included in fracture mechanics models through different approaches e.g. weight functions [41] or the modified J-integral [42]. Their results show a remarkable dependency between the residual stress and the crack growth results.

Despite the multiple studies about residual stress in FM models, their applicability in real welded structures face major limitations. Post weld treatments, overloading or creep may develop residual stress relaxation. If compressive residual stress relaxation is not included in fatigue calculations, FM results are conservative. However, if tensional residual stress relaxation is not taken into consideration, calculations can overestimate the fatigue life of the structure.

The high complexity of the residual stress calculations for real and large structures has motivated a need to seek for alternatives. Ruiz and Eder [43] have developed the *Residual Stress Intensity Factors (RSIF) Proportionality Conjecture* as an alternative to implement residual stresses in FM models.

The RSIF addresses the question concerning the maximum growth rate of a crack subject to residual stresses. Assuming a crack under fatigue loading σ_{22} and residual stress σ_R, Fig. 33.

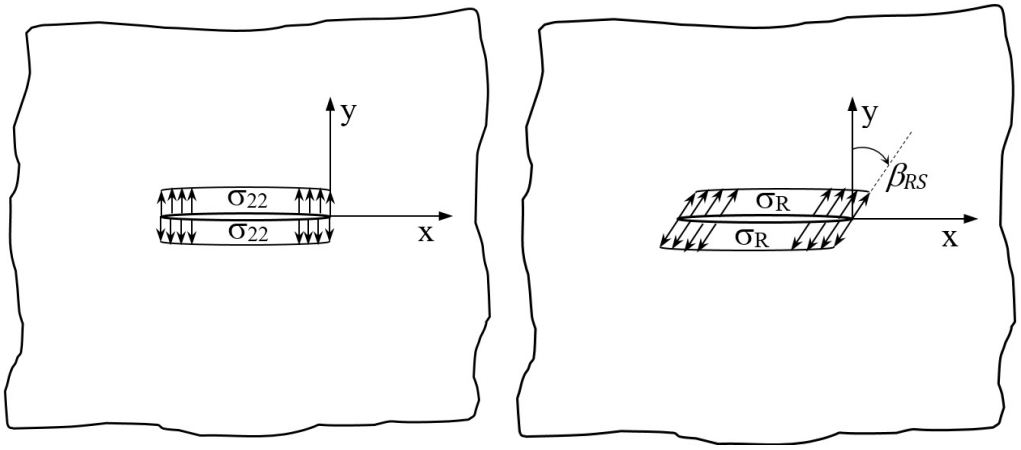

(a) (b)

Figure 33: Infinitely large plane strain/stress domain with horizontal crack of length $2a$ under two simultaneous stresses: a) pure tensional cyclic stress where $\sigma_{22} = \sigma_{22}^{max}$ when maximum stress is applied and $\sigma_{22} = \sigma_{22}^{min}$ when minimum stress is applied. b) RS tilted β_{RS} degrees.

Ruiz and Eder found that the maximum equivalent SIF was found at two conditions: when the RSIF where proportional to the SIF related to the external loading $\beta_{RS} = 0$ degrees, and when residual stress had no effects on SIF calculations $\beta_{RS} = 90$ degrees, Fig. 34.

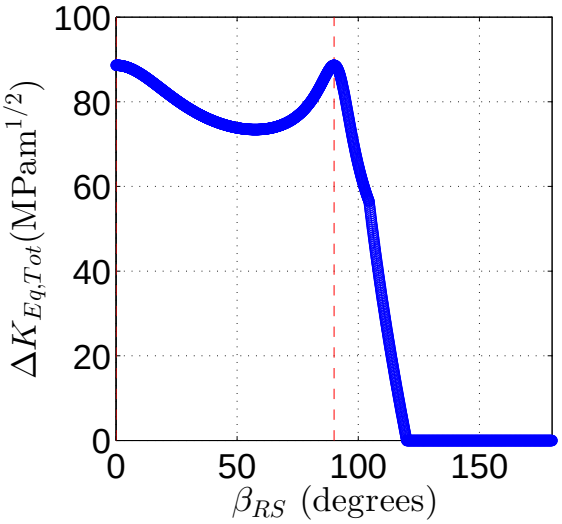

Figure 34: Variation of $\Delta K_{Eq,Tot}$ with respect to the angular orientation β_{RS} of the RS. The illustration shows two peaks which correspond to the same value of $\Delta K_{Eq,Tot}$, at $\beta_{RS} = 0$ degrees, where the RS vector is proportional to the cyclic loading vector σ_{22}, and $\beta_{RS} = 90$ degrees, where the SIF calculations are independent of the RS magnitude.

Ruiz and Eder extended their analysis to a full residual stress domain, where they numerically demonstrated the conjecture:

The residual Stress Intensity Factors (RSIF) Proportionality Conjecture

Assuming any arbitrary crack under cyclic mixed-mode loading conditions, where K_I^{max} and K_{II}^{max} denote the maximum mode-I,-II SIF, and K_I^{min} and K_{II}^{min} denote the minimum mode-I,-II SIF.
Condition: If the external loading is proportional such that the following condition holds:

$$\frac{K_I^{max}}{K_{II}^{max}} = \frac{K_I^{min}}{K_{II}^{min}} \quad \text{where} \quad K_I^{max,min} \geq 0 \text{ and } K_{I,II} \, \epsilon \, \mathbb{R} \tag{53}$$

Conjecture: The RSIF Proportionality conjecture states that the maximum equivalent SIF range $\max(\Delta K_{eq})$ is attained if the RSIF ratio is proportional

to the cyclic loading SIF ratio, according to the following condition:

$$\frac{K_I^{max}}{K_{II}^{max}} = \frac{K_{I,RS}}{K_{II,RS}} \quad \text{where} \quad K_{I,RS} \geq 0 \text{ and } K_{I,II} \in \mathbb{R} \tag{54}$$

where $K_{I,RS}$ and $K_{II,RS}$ are RSIF for mode-I,II.
Corollary: If the RSIF ratio is proportional to the cyclic loading SIF ratio, it follows that the $\max(\Delta K_{eq})$ becomes exclusively a function of the external mode-I,-II SIF.

The *residual Stress Intensity Factors (RSIF) Proportionality Conjecture* is based on the MCS criterion. This conjecture implies that the most conservative crack growth can be achieved by assuming no RS effects and the Paris Law parameters for high stress ratios. As a consequence, no residual stress calculations are needed.

3.3.3 Environmental fatigue

The environment plays a key role in fatigue life performance, especially when the structure is subject to severe corrosion. Xu and Wang [44] presented results about the effects of corrosion pitting on cracks generation in a steel plate. Additionally, Wahab and Sakano [45] studied the corrosion effects in a weld subject to biaxial fatigue loading. The formulation that describe the fatigue crack propagation under a corrosive environment may be different from one study to another. Anderson [11] describes one of the most popular formulations as

$$\frac{da}{dN}_{corrosive} = \Phi \frac{da}{dN}_{Air} + \left(\frac{1}{f}\frac{d\bar{a}}{dt}\right)_{EAC}, \tag{55}$$

where the term $\Phi \frac{da}{dN}_{Air}$ is the cycle-dependent corrosion fatigue and the term $\left(\frac{1}{f}\frac{d\bar{a}}{dt}\right)_{EAC}$ is the time-dependent corrosion fatigue. The parameter Φ is an acceleration factor, $\frac{da}{dN}_{air}$ is given by Eq. 38, f is the loading frequency and $\left(\frac{d\bar{a}}{dt}\right)_{EAC}$ is the average environmental crack growth over a loading cycle.

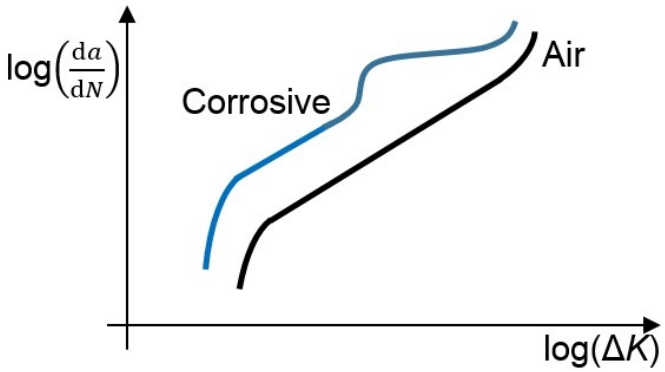

(a)

Figure 35: Crack growth rate as a function of the SIF range for Air or corrosive environment.[11]

In spite of the multiple formulations found in literature, fatigue crack propagation generally involves multiple parameters and complex equations.

3.3.4 The Fracture Mechanics approach to fatigue from the Standards perspective

The standard BS7910 [5] suggests simplifying the FM Eq. 55 by splitting the fatigue crack growth into two linear stages Fig. 36,

$$\frac{da}{dN} = \begin{cases} \Delta C_A(\Delta K_{eq})^{m_A} & \Delta K_{eq} \geq \Delta K_{TP} \\ \Delta C_B(\Delta K_{eq})^{m_B} & \Delta K_{eq} < \Delta K_{TP}, \end{cases} \tag{56}$$

where K_{TP} C_A, m_A, C_B and m_B are material parameters that depend on the environmental conditions and are defined in [5].

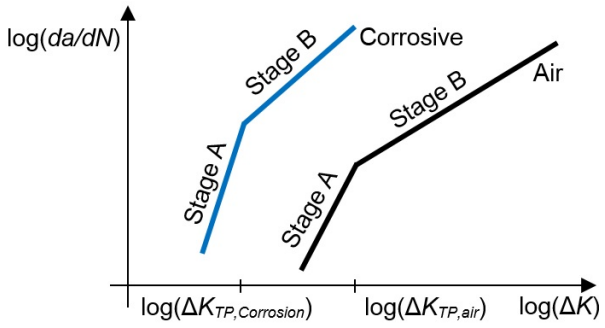

Figure 36: British Standard approach [5]. The FM crack propagation for different environmental conditions is simplified by two linear stages: A and B.

Eq. 56 does not describe the fatigue crack propagation as accurate as Eq. 38 or 35a. However, it is simple, it includes fewer parameters and the material parameters are well documented in standards.

3.3.5 Fatigue crack propagation for variable amplitude loading

During a cycle range ΔN which includes different stress ranges, Anderson [11] suggests calculating the crack growth as the weighted average of the crack growth related to each stress range,

$$\frac{da}{dN} = \frac{\sum_{i=1}^{n} N_i \left(da/dN\right)_i}{\Delta N}, \tag{57}$$

where i is an index that refers to a certain load range, n is the number of different load ranges in a cycle range, and N_i is the number of cycles that correspond to load i and is related to the cycle range as

$$\Delta N = \sum_{i=1}^{n} N_i. \tag{58}$$

Eq. 57 is only applicable when ΔN is small enough so the crack growth associated with the loading signal period $\Delta a = a_j - a_{j-1}$ has a negligible effect on the crack growth rates, i.e. $\left(\left(da/dN\right)_j\right)_i \approx \left(\left(da/dN\right)_{j-1}\right)_i$ for all stress ranges in ΔN.

3.3.6 The Transitional Environmental Protection process for the FM approach

The TEP process under a FM perspective involves the transition between crack generation or growth from environmentally protected conditions to corrosive conditions. Ruiz and Sørensen [1] address this situation by using the crack growth parameters associated with their corresponding environmental condition for each phase during the TEP process, i.e. when the corrosion protection system fails, at $t = t_{TEP}$, the Paris Law parameters change from protected to corrosive conditions. The crack size is adjusted to cope with the crack initiation phase as Ruiz and Sørensen described in [1].

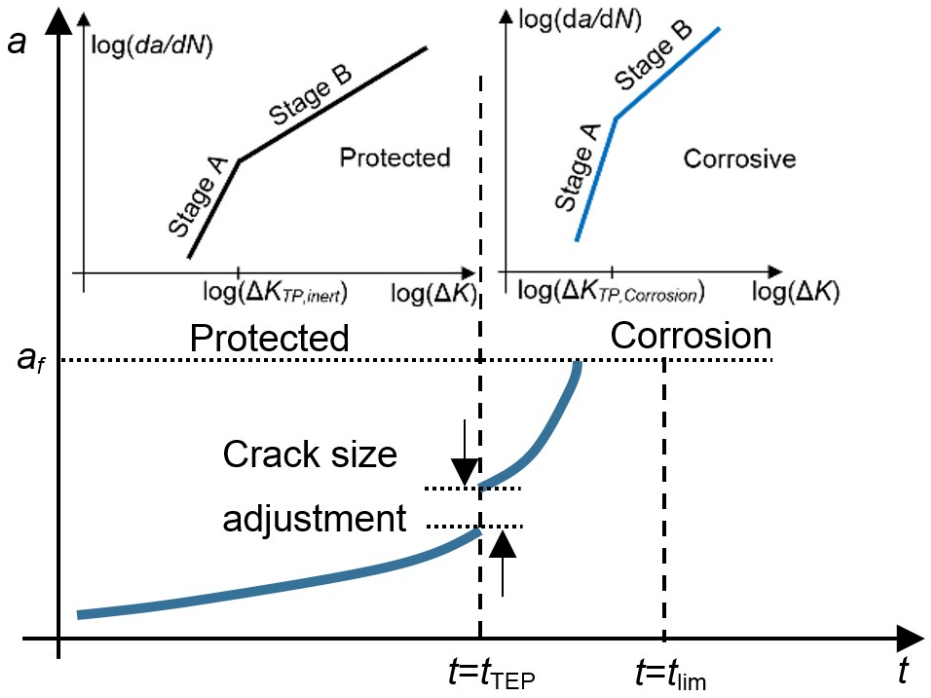

Figure 37: Crack growth analysis for the Transitional Environmental Protection (TEP) process. The crack growth parameters correspond to protected conditions, e.g. air or cathodic protection, until the protection system fails at $t = t_{TEP}$. At that moment, the crack size is adjusted, as described in [1], and the crack growth parameters shift to corrosive conditions.

3.3.7 The fatigue analysis from a Elasto-Plastic Fracture Mechanics approach

In cases where LEFM is not applicable because of high stress values, Elasto-Plastic Fracture Mechanics (EPFM) is suggested [11]. This approach accounts for the non-linear deformation of the structure through different techniques such as e.g. the J-Integral. However, the EPFM calculations usually introduce a higher degree of complexity than the LEFM calculations.

Standards such as [5] and some researchers e.g. ([9],[36],[46]) suggest to use LEFM formulation for fatigue analysis of welds. However, some studies show that stress may be in the order of yield stress and EPFM analysis is necessary [47].

The current research focuses only on LEFM due to its simplicity and efficiency. However, further research is needed to compare LEFM and EPFM fatigue calculations in welds.

4 Probabilistic fatigue analysis

Numerous fatigue life studies use parameters as they were accurately known, following a nomenclature called deterministic. In the analysis of real cases, however, the knowledge about different parameters is limited, and they are normally considered as stochastic. A stochastic variable is a parameter that follows a statistical distribution. Since some variables that affect the fatigue life are stochastic, the concept of a unique value associated with the fatigue life of a real structure vanishes. Instead, probabilistic fatigue deals with the concept probability of failure and reliability.

4.1 Common statistical distributions

The parameters that influence the fatigue life of a structure may follow different statistical distributions. Two of the most common statistical distributions in fatigue analysis are the normal and the log-normal distribution ([48],[49],[50]). The normal distribution function of a stochastic variable Z with mean μ and standard deviation s is calculated as

$$F_Z(Z) = \Phi\left(\frac{Z-\mu}{s}\right) = \int_{-\infty}^{Z} \frac{1}{\sqrt{2\pi}s} e^{-\left(\frac{z-\mu}{\sqrt{2}s}\right)^2} dz \tag{59}$$

where $F_Z(Z)$ denotes the probability of a random value is equal or lower than Z.

The log-normal distribution is defined as

$$F_Z(Z) = \Phi\left(\frac{\ln Z - \mu_Y}{s_Y}\right) = \int_{-\infty}^{Z} \frac{1}{\sqrt{2\pi}s_Y} e^{-\left(\frac{\ln z-\mu_Y}{\sqrt{2}s_Y}\right)^2} dz \tag{60}$$

where $s_Y = \sqrt{\ln\left(\left(\frac{s}{\mu}\right)^2 + 1\right)}$ and $\mu_Y = \ln\mu - \frac{1}{2}s_Y^2$, and μ and s denote the mean and standard deviation related to the parameter Z.

Fig. 38 shows the shape of both statistical distributions. Apart from these two, other probability density functions, e.g. the Weibull distribution, are generally found in the structural fatigue analysis. ([48] [50][12])

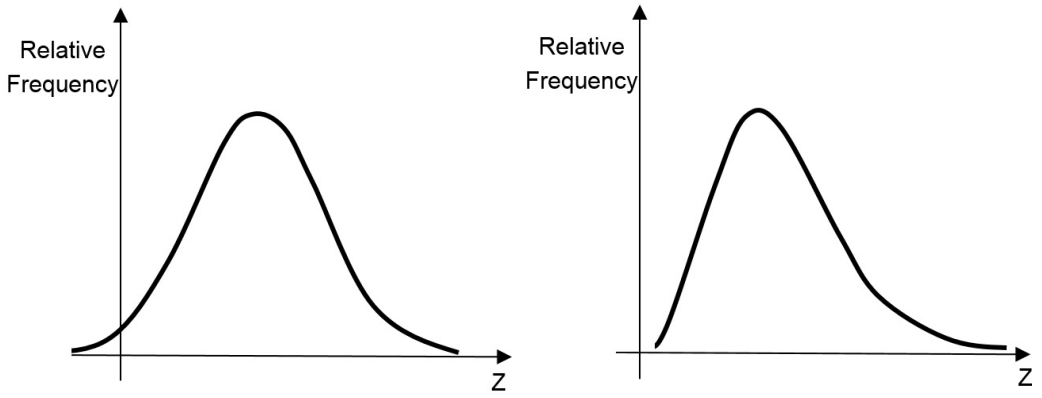

(a) (b)

Figure 38: Shape of a: (a) Normal distribution (b) Log-normal distribution.

4.2 Introduction to reliability

In a probabilistic fatigue analysis, studies evaluate failure in terms of probabilities. The first step is to determine the condition in which failure is assumed. This condition is defined by an equation known as the Limit State equation. There are different formulations of the Limit State equation depending on the method used for fatigue life estimation. SB approach methods are normally defined by a limit state equation according to the damage formulation,

$$g(N, D_f) = D_f - D(N) \tag{61}$$

where $D(N)$ is the damage accumulated after a number of cycles N and D_f is the damage limit for failure.

The limit state equation for the Probabilistic Fracture Mechanics framework can be defined as

$$g(N, a_f) = a_f - a(N) \tag{62}$$

where $a(N)$ is the crack length associated with N cycles and a_f is the crack length before assuming failure of the structure. The parameter a_f is typically half of the width of the cracked specimen [9].

Once the limit state is posed, the failure is considered when $g \leq 0$. For monetary and risk analysis purposes, the general objective is to know what is the probability of the failure of a component for a period of time $P_f(t)$,

i.e. the probability $g \leq 0$ for a time interval t. The concept of probability of failure is directly related to the reliability index as [51]

$$\beta(t) = -\Phi^{-1}[P_f(t)], \tag{63}$$

where β is the reliability index, $P_f(t)$ is the probability a failure event occurs and Φ is the cumulative function of the standard normal distribution,

$$\Phi(Z) = \frac{1}{\sqrt{2\pi}} \int_{-\infty}^{Z} \mathrm{e}^{-z^2/2} \mathrm{dz}. \tag{64}$$

4.2.1 Techniques to calculate the reliability index

There are several techniques to estimate the reliability of a structural case[52]:

- Simulation Techniques: Samples are generated according to the stochastic variables and the probability of failure is estimated by computing the number of samples that fail with respect to the total number of samples generated. The number of samples necessary is found through a convergence analysis.

- First Order Reliability Methods (FORM): The limit state equation is transformed to be a function of normalized, uncorrelated and Normal distributed variables, it is linearised and the reliability index is found through an iteration scheme described in [52].

- Second Order Reliability Methods (SORM): The limit state equation is transformed to be a function of normalized, uncorrelated and Normal distributed variables, it is approximated to a quadratic function and the reliability analysis is found through an iteration scheme described in [52].

Fig. 39 shows an illustration about the first two techniques. The limit state $g(\mathbf{x})$ is defined in coordinates $\mathbf{x} = (x_1, x_2)$, where the values for x_1 and x_2 are stochastic. The region ω_f includes all combination of (x_1, x_2) where failure is assessed. The rest of the space is region ω_s, where no failure is addressed.

A simulation technique is performed and results are shown in Fig. 39b. The samples which result in the failure region ω_f are retrieved, n_{Fail}. The probability of failure is calculated as $P_f = n_{Fail}/n_{Total}$, where n_{Total} is the total number of samples.

Fig. 39a and 39c illustrate how the reliability index is calculated through a FORM technique. The space (x_1, x_2) and function $g(\mathbf{x})$ is transformed into normalized and uncorrelated variables (u_1, u_2) and its corresponding limit state function $g_{\mathbf{u}}(\mathbf{u})$. Through an iterative procedure described, a final straight tangent to the function $g_{\mathbf{u}}(\mathbf{u})$ is achieved, $\beta - \boldsymbol{\alpha}^T \mathbf{u} = 0$, where $\boldsymbol{\alpha}$ is a unitarian vector orthogonal to the tangent and β is the distance of the straight to the origin, which corresponds to the reliability index.

If the limit state equation in the standardized u-space is rather non-linear, the SORM is a good alternative. This quadratic approximation cannot be described in a simple illustration and, therefore, the SORM technique is not included in Fig. 39. Nevertheless, further descriptions can be found in literature [52].

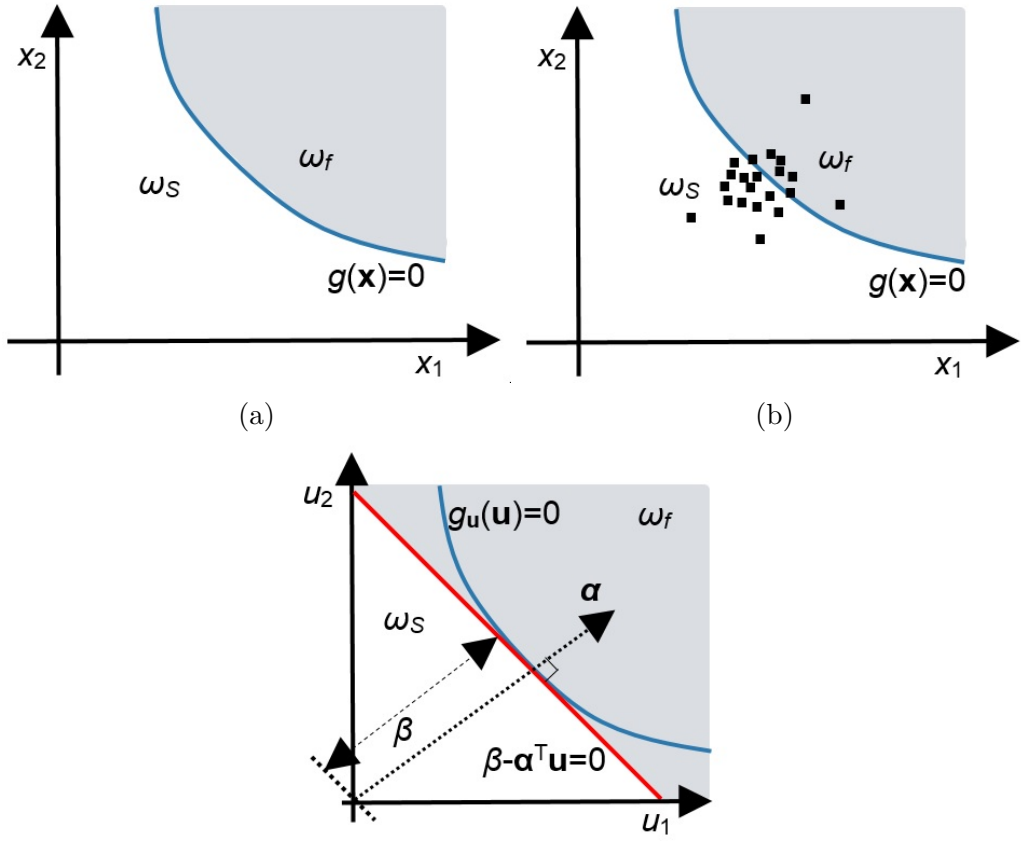

Figure 39: Illustration about different techniques to retrieve the reliability index: (a) Original space (x_1, x_2) and failure function $g(\mathbf{x}) = 0$, ω_s includes the safe region and ω_f includes the failure region; (b) Simulation technique where multiple samples are performed; (c) FORM technique where space and function are transformed according to normalized and uncorrelated variables (u_1, u_2). The function $g_{\mathbf{u}}(\mathbf{u})$ is linearized into a tangent straight denoted in red. The distance from the origin to the straight is the reliability index β.

Among these three techniques, the Simulation Techniques are the most simple and capable to solve non-linear complex problems. A very popular simulation technique is known as the Monte Carlo simulation. This technique is suggested by Straub [12] in order to perform inspection simulations. In a Monte Carlo simulation, a number of samples are generated and the failure

of each sample is evaluated. The main drawback about this method is that the number of samples necessary to reach convergence might be considerably high.

Other simulation techniques may require a lower number of samples than the Monte Carlo simulation. Examples are the Importance Sampling or Monte Carlo sampling excluding the safe area. [52]

4.2.2 Common types of reliability index

The reliability index can be divided into different categories, where the most common ones in the inspection planning framework are the annual reliability index β_t and the accumulated reliability index β_{accum} ([53],[12],[54]). The parameter β_t is related to the probability that the structural failure corresponds to a certain year t, $P(F)_t$. The accumulated reliability index β_{accum} is related to the probability a component will fail before a certain time.

4.3 Influence of MSD and Corrosion in the reliability curves.

The current research has performed a study on how MSD and corrosion affects the accumulated reliability index of a structural case, Fig. 40 [55], where the reliability is measured as a function of the number of loading cycles. The component is subject to a cycling load P and fatigue parameters are taken from the standard BS7910 [5]. Further details of this study are found in [55].

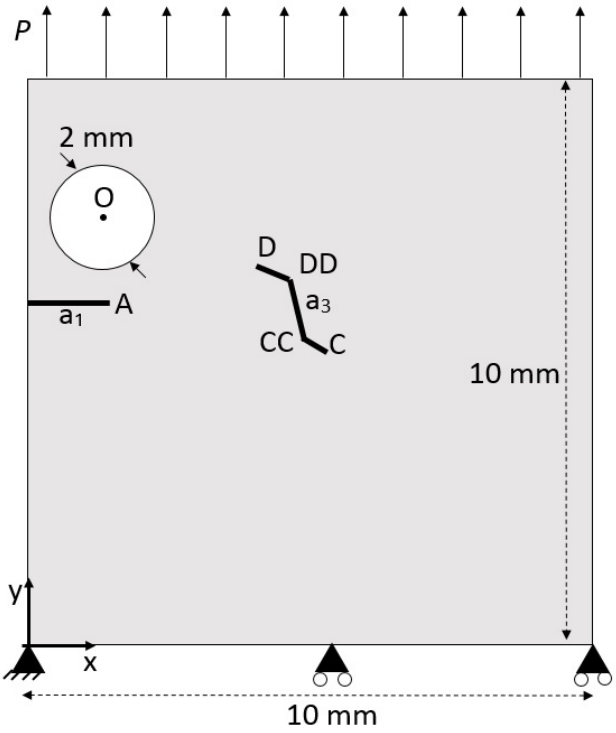

Figure 40: Specimens for fatigue crack propagation under Multiple Site Damage. [55]

The study evaluates two factors affect fatigue life performance. The first factor is the impact of including multiple flaws in the structure. Results showed that there is a noticeable variation of results between single and multiple crack propagation conditions, Fig. 41a. However, this study is performed for a single case and further studies are required to determine what is the minimum number, geometrical size or orientation of cracks that influence the reliability index.

The second factor is the impact of corrosion in the reliability of a structure. Results show that a corrosive environment has a striking effect in reliability results, where same reliability values can be found at cycles of order of magnitude 100 times lower when compared to air conditions, Fig. 41b.

This study concludes that corrosion is an important phenomenon when evaluating the reliability of a structure. However, MSD needs further studies in order to assess its criticality when performing probabilistic fatigue.

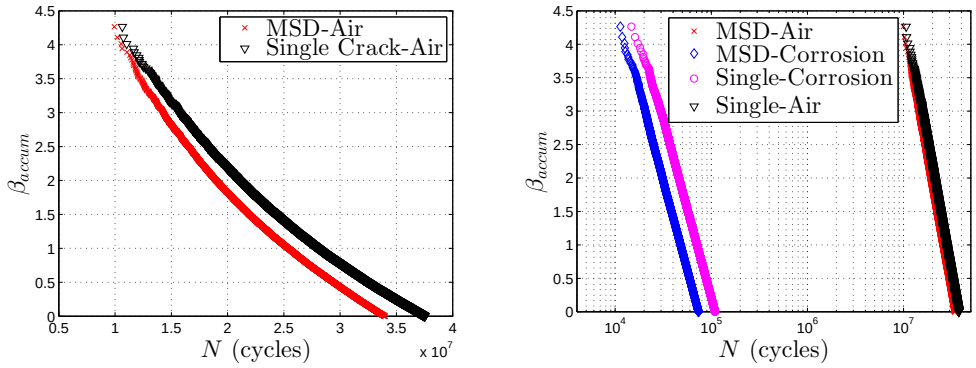

(a) (b)

Figure 41: Reliability analysis of the case Fig. 40 for: (a) Single surface crack growth or MSD fatigue under inert environmental conditions; (b) Comparison with a corrosive environment for single surface crack growth or MSD fatigue.[55]

5 Risk-Based Inspection Planning for Offshore welds from a fracture mechanics perspective

Risk-Based Inspection Planning comprehends all the studies that determine the number and location of inspections through the structural lifetime, as well as the inspection/repair techniques and the repair decisions. It is usually based on two factors:

- The consequences of the failure.
- The likelihood of the failure.

The consequences of failures are determined through different risk assessment procedures, where monetary costs, environmental risks or human losses analyses are involved. This research does not focus on risk assessment, but examples can be found in ([12],[56],[57]).

The likelihood of a structural component failure depends on the inspection plan performed. Each inspection plan may result in different reliability curves, i.e the reliability index results along a period of time. [58]

5.1 Inspection Plan

In the early 1970's, Yang and Trapp ([59],[60]) started to perform deterioration models for inspection planning that updates with time. The optimization of inspection plans for offshore structures was firstly developed by researchers such as Skjong in the 80's [61]. Since then, multiple studies have been performed, e.g. ([62],[63],[64]).

Different inspection procedures are nowadays well spread in the offshore industry. The inspection/repair mechanism is usually divided into three phases:

- A first phase where technicians perform inspections of flaws and report results.
- A second phase where technicians repair the spot where critical cracks are found.
- A third phase where technicians repeat the inspection analysis of the repaired spots.

The inspection plan may have different origins. Some inspection procedures are determined by standards or the authorities of the country where the offshore structure stands. Other inspection plans are developed by technicians from their own experiences. However, these methods can be inefficient and involve high costs.

The fracture mechanics approach to probabilistic inspection planning is becoming popular in the past years. Doshi et al. [58] evaluated the reliability-based inspection planning through fracture mechanics models of ship components. Kim and Frangopol [65] performed simulations for optimum inspection planning of ship hull structures by using FM models and evaluating the impact of the detection delay. These inspection procedures have reached the standards, e.g. DNVGL-RP-0001:2015 [66].

Ruiz and Sørensen [1] evaluates the reliability of offshore welded structures under the TEP process. Their results help to understand the impact of different inspection/repair intervals and environmental conditions in the reliability of a structure. They divided their algorithm into three main steps:

- The structural analysis.
- The reliability calibration.
- The inspection/repair simulation.

5.1.1 Structural analysis.

In the structural analysis step, calculations are executed through e.g. FEM, and the principal stresses and SIF necessary for fatigue analysis are retrieved. Two different structural analysis are performed. The first one is a SB method. The second analysis is a FM calculation of the structure. Lotsberg et al. [53] or Ruiz and Sørensen [1], among others, suggest imposing an initial crack in the FM model. In both cases, a scaled load is submitted and the objective is to retrieve the stresses and SIF that would be later applied in probabilistic fatigue analyses. [1]

5.1.2 Calibration

The DNVGL-RP-0001:2015 [66] suggests to calibrate the FM model against the SB methods as the FM approach generally does not physically describe the crack initiation phase. The calibration is performed by varying different

parameters of the fracture mechanics model, from the initial crack size to the uncertainty of the FM model.

The FM model is calibrated with the SB approach when it presents similar reliability curves. Fig. 42 shows an example of results after calibration for the case described in [1].

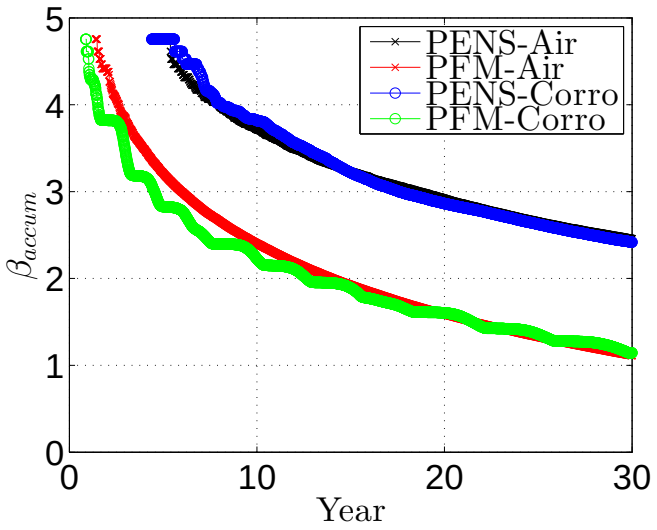

Figure 42: Reliability curves after the calibration for Air and Corrosive conditions. The Probabilistic Fracture Mechanics (PFM) approach is calibrated against the Probabilistic Effective Notch Stress (PENS) approach. The parameters calibrated were the initial crack size and the uncertainty of the FM method.

5.1.3 Inspection/Repair Simulation

Once the FM model is calibrated, multiple Monte Carlo simulations are run for different inspection intervals. Every time a simulation is performed, each of the cracked samples is evaluated through a Probability of Detection (PoD) curve. Fig. 43 shows the example of PoD curve for ultrasonic inspections. Further examples of PoD for different techniques e.g. visual inspection or eddy current can be found in [66].

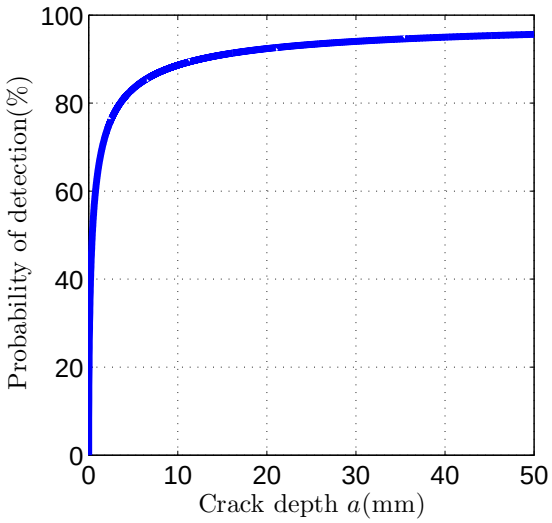

Figure 43: Probability of Detection (PoD) curve for cracks evaluated under Ultrasonic technique. [66]

Every time a crack is detected, a probabilistic inspection plan model deals with two main questions. The first question corresponds to whether the crack size has exceeded the limit a crack can be repaired. The second question is if the crack size is large enough to have a relevant impact on the reliability of the structure for its remaining time in service. Ruiz and Sørensen [1] propose a model where all cracks detected with a size $a < 3$ mm were repaired, where $a = 3$ mm correspond to the limit for repairs through grinding [67]. Other repair strategies could be e.g. TIG dressing or the complete replacement of the welded component.

Literature usually suggests two types of assumptions after a crack is repaired [12]:

- The repaired sample is assumed to not fail for the rest of the operational life.
- The repaired sample behaves as a new sample.

5.2 Case of study: Cost effective inspection plan of the 2D bracket case.

The present research includes a publication [1] where the 2D bracket case was evaluated for an arbitrary and variable amplitude loading condition, Fig. 44.

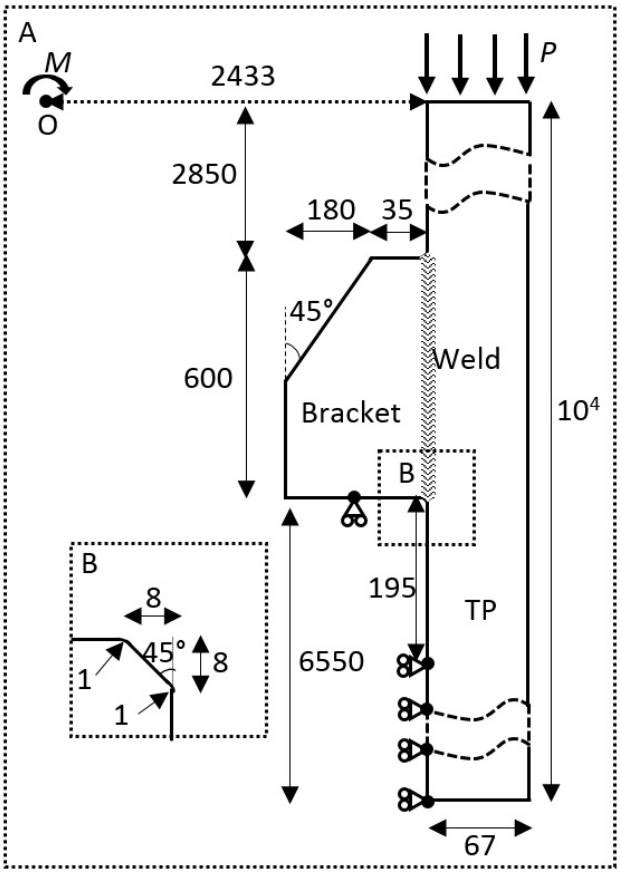

Figure 44: Geometry, constraints and load set-up of the offshore welded component with dimensions in mm.

Fig. 44 is a 2D plane strain simplification of the case Fig. 1b. The case includes a variable distributed load P and moment M located on the upper surface of the model. The reference location of M is O coordinates. A simulation-based probabilistic inspection algorithm [1] is used to calculate the reliability levels for different inspection periods and environmental conditions.

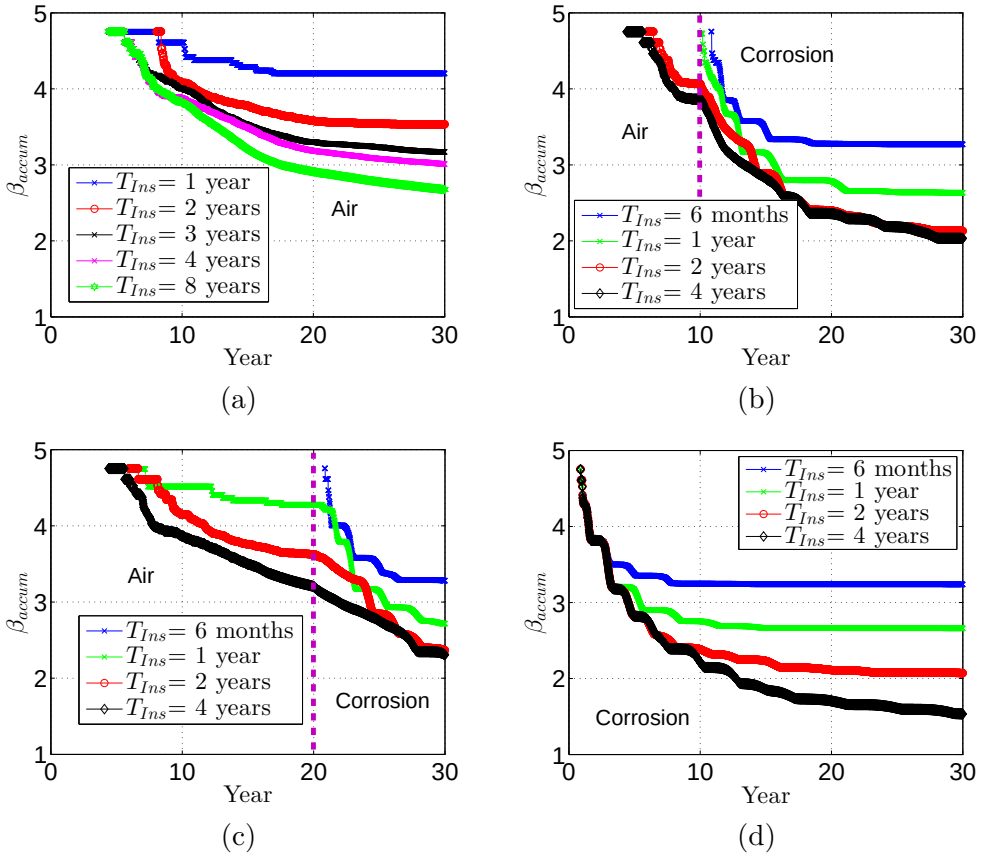

Figure 45: Reliability curves for different inspection interval T_{Ins}: (a) Results for permanent air environmental conditions; (b) Results for TEP process from air to corrosive at $t_{TEP} = 10$ years; (c) Results for TEP process from air to corrosive at $t_{TEP} = 20$ years; (d) Results for permanent corrosive environmental conditions.[1]

This section introduces further calculations of the study in order to show the benefits of applying probabilistic fracture mechanics for inspection plans in the offshore industry. Table 1 presents the different costs involved in maintenance, where C_W is associated to the cost per year of a wind turbine failure, C_P is the average hourly cost of the technicians, C_V is the daily cost of the maintenance vessel, C_U is the daily cost of ultrasonic equipment, C_O are daily costs related to logistic and data analysis of the inspection results and C_{GW} are the daily costs related to the grinding/welding equipment.

The annual interest of the currency is assumed $r = 0.06$ and the costs are dimensionless and based on an arbitrary price index.

Table 1: Cost index of the different factors involved in maintenance. The values are indicative.

C_W	C_P	C_V	C_U	C_O	C_{GW}
15000	1.25	70	3.75	20	1.75

The inspection/repair procedure is performed in 3 days. The first day, six technicians perform an ultrasonic inspection of the bracket. The total amount of hours worked is 14 per day. The cost involved on the first day is

$$C_1 = 1\text{day} \times 14\text{hours}/(\text{people} \times \text{day}) \times 6\text{people} \times C_P + C_V + C_U + C_O. \quad (65)$$

If the crack is detected and its size is $a \leq 3$ mm, technicians grind and weld the detected cracks. The cost involved is

$$C_2 = 1\text{day} \times 14\text{hours}/(\text{people} \times \text{day}) \times 6\text{people} \times C_P + C_V + C_{GW}. \quad (66)$$

Finally, if the crack is repaired, a third day is necessary in order to perform an inspection of the repaired bracket. The cost involved on the third day is the same as the cost related to the first day, $C_3 = C_1$.

The first day corresponds to a cost due to inspection $C_I = C_1$, whereas the second and third day correspond to a cost of repair, $C_R = C_2 + C_3 = C_2 + C_1$. The total expected cost is calculated as [57]

$$E[C_{TOTAL}] = E[C_f] + E[C_I] + E[C_R] \quad (67)$$

where $E[C_f]$ is the expected cost due to structural failure, $E[C_I]$ is the expected cost related to inspections and $E[C_R]$ is the expected cost related to repairs.

Eq. 67 can be formulated in terms of probabilities. The expected cost of failure for 30 years can be expressed as

$$E[C_f] = \sum_{n=1}^{30} P_{t,n}(31 - n)C_W(1 + r)^{-n} \quad (68)$$

where $P_{t,n}$ is the annual probability of failure of the structure, the term $(31 - n)$ is the remaining years in service the wind turbine was designed to

operate and the term $(1+r)^{-n}$ is related to the interest rate.

The expected cost of inspections can be expressed as

$$E[C_I] = \sum_{n=1}^{T_{Total,Ins}} (1 - P_{accum,T_n}) C_I (1+r)^{-T_n} \tag{69}$$

where n is an integer index, $T_n = nT_{Ins}$ is the year when inspection take place, T_{Ins} is the inspection period, $T_{Total,Ins}$ is the total number of inspections planned and the term $(1 - P_{accum,T_n})$ is the survival probability after T_n years. The parameter $T_{Total,Ins}$ is calculated dividing the total number of years by the inspection interval planned.

Finally, the expected cost of repair, including the expected cost of inspections of repaired cracks can be performed as

$$E[C_R] = \sum_{n=1}^{T_{Total,Ins}} (1 - P_{accum,T_n}) P_{d,T_n} (C_R + C_I)(1+r)^{-T_n} \tag{70}$$

where P_{d,I_n} is the probability of repair a crack at year T_n and $(C_R + C_I)$ involves the cost of repair and the cost of inspecting the repaired structure.

The value P_{d,T_n} was calculated in the simulation-based procedure as P_{d,T_n}=$n_{rep,T_n}/n_{tot}$ where n_{rep,T_n} is the number of samples repaired at I year and n_{tot} is the total number of samples, i.e. $n_{tot} = 10^6$ [1].

Note that all the probabilities of failure are dependent of the inspection interval, T_{Ins}. Eq. 68, 69 and 70 are included in Eq. 67, resulting in the expected total cost expression,

$$\begin{aligned} E[C_{TOTAL}] &= \sum_{n=1}^{30} P_{t,n}(31-n) C_W (1+r)^{-n} + \\ &+ \sum_{n=1}^{T_{Total,Ins}} (1 - P_{accum,T_n})(C_I + P_{d,T_n}(C_R + C_I))(1+r)^{-T_n}. \end{aligned} \tag{71}$$

Fig. 46 shows the cost calculated through Eq. 71 for the case in [1]. The result shows different costs for different maintenance intervals and different environmental conditions. Enlarging the isolation of the brackets against corrosion has an enormous reduction in the expected total cost.

The curve for corrosive environment shows another peculiarity, i.e the maximum expected total cost is found at the inspection interval of 8 years.

This result demonstrates that in some cases, it is more effective to avoid any type of maintenance than to perform inefficient inspections.

Fig. 46 also illustrates that the cost curves for different environmental conditions tend to converge as the inspection interval reduces, where the cost associated with the inspection interval of 6 months is essentially the same for all cases. As inspection intervals decrease, the likelihood of failure becomes very small for all cases and most of the costs are driven by inspection/repair procedures.

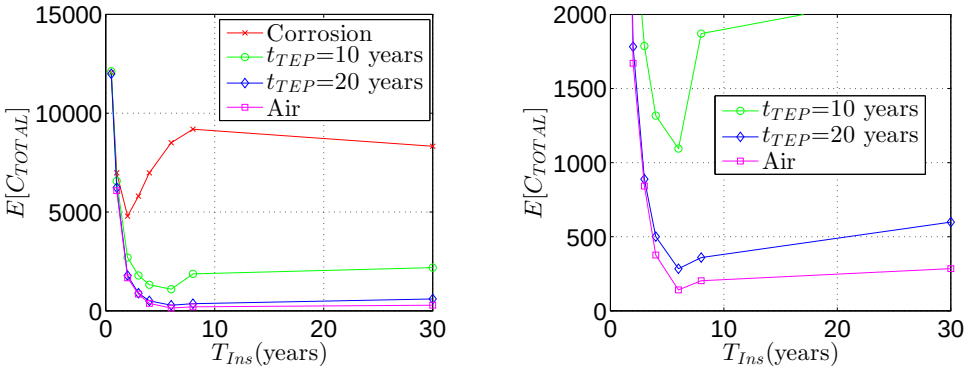

Figure 46: Expected total cost depending on the inspection/repair interval applied to the case [1]. The optimum inspection interval is considered to be at the minimum cost value of each curve. For different environmental conditions, the optimum inspection interval is different as well as the cost: (a) Illustration of the expected total cost curves. (b) Close-up of the cost curves.

Table 2 presents the optimum cost and inspection interval retrieved from Fig. 46. It is worth noticing that depending on the environmental conditions, the optimum inspection interval is different. Furthermore, the environment has a large influence on the inspection costs. A bracket structure subject to air conditions involves a total cost 34 times lower than under corrosive conditions. Enlarging the environmental protection also has a remarkable effect on the total cost.

Table 2: Optimum maintenance interval T_{Ins} the associated cost index for different environmental conditions, from air to corrosive environment. TEP stands for Transitional Environmental Protection from air to corrosion.

Environment	T_{Ins}(years)	$E[C_{TOTAL}]$
Air ($t_{TEP} = 30$ years)	6	141
t_{TEP}=20 years	6	284
t_{TEP}=10 years	6	1095
Corrosive ($t_{TEP} = 0$ years)	2	4792

6 Discussion about the work

The current research describes the theory and numerical results related to the fracture mechanics approach to probabilistic inspection planning of offshore welds for wind turbines. The work focuses on already existing theory and develops new concepts and methods.

The Stress-Based methods explained are assumed to be accurate enough to estimate the life of an offshore weld. However, the present study emphasizes that these methods are not directly applicable for inspection planning and thus, the fracture mechanics approach is introduced. Both, the SB and the FM, include limitations. The SB method cannot describe the crack growth and the FM method cannot describe the crack initiation phase. In order to overcome both limitations, the present work suggests to calibrate FM results with SB results in a similar procedure as the standards and literature suggest.

The calibration between both methods may introduce results oversimplified. Some weld characteristics, such as occlusions or porosity, are not directly described in FM models, but they are assumed to be inside the S-N curves used for the calibration.

Another weld characteristic, the Multiple Site Damage (MSD), is included in an original method developed during this research. The MSD was evaluated for different cases, which confirms the relation between the fatigue life with the number of flaws. However, the Multiple Site Damage in welds requires a deeper analysis in order to evaluate its contribution to the fatigue lifetime and reliability of an offshore weld.

The residual stresses, an inherent characteristic of welds, is considered through the *Residual Stress Intensity Factor (RSIF) Proportionality* conjecture. The RSIF Proportionality Conjecture is an original contribution of this study to the FM analysis of welds. This concept introduces a striking simplification of fatigue calculations of welds by assuming no residual stress and high stress ratios.

The study of offshore welds includes another characteristic, the corrosive environment. The SB methods assume corrosive effects by using S-N curves, which implicitly include those effects. On the other hand, the FM mechanics formulation for corrosive environments is simplified using equations recommended by standards. Corrosion phenomenon, such as pitting or crevice, are assumed to be included inside the S-N curves used for the SB methods. The calibration of the FM model to SB method will implicitly incorporate all the

concepts.

Apart from the simplifications exposed above, the current research focuses on the LEFM analysis of offshore welds. The LEFM approach to weld analysis is common in the scientific community and standards. However, it might not be an accurate approach to the fatigue analysis of welded details. Welds can include high stress locations where a Elasto-Plastic fracture mechanics analysis is more suitable. Further research in this field is necessary in order to compare the deviation between the EPFM and the LEFM.

All the simplifications exposed during this research have served to propose doable FM models that can be applicable for inspection planning in the industry. However, the author wants to emphasize that it is necessary to determine how much these concepts deviate from the real structural behaviour. Therefore, data from experiments can be used to adjust the FM models.

The FM concepts have subsequently been studied from a probabilistic perspective. The probabilistic approach is necessary in order to perform inspection planning simulations of real structures, where the parameters applied in the fatigue analyses are uncertain. This work focuses on how to incorporate the probabilistic analysis in FM models, which is shown Manuscript D.

The probabilistic inspection simulations were performed through the Monte Carlo method. This technique is very common in the inspection planning framework due to its simplicity and accuracy when compared with FORM or SORM simulations. However it might not be the most efficient. As a result, further alternatives to probabilistic simulations should be investigated.

Overall, the concepts described in this work are sufficient enough to elaborate a cost effective model of inspection planning from a fracture mechanics perspective, as shown in Fig. 46. The author believes that the models and methods described are applicable in the offshore industry.

7 Conclusions

This research describes how to reach optimum inspection planning through a fracture mechanics approach. The following conclusions can be drawn:

(i) The present study describes the Stress-Based methods. These methods are commonly used in the offshore industry to estimate the fatigue lifetime. However, the Stress-Based methods do not simulate the crack propagation, an important concept for inspection planning.

(ii) Literature suggests using fracture mechanics methods in order to calculate the crack propagation in welds. Nevertheless, to the best of the author's knowledge, the Fracture Mechanics framework does not present universal formulation for the crack initiation period.

(iii) Fracture mechanics models of welds face the challenge of Multiple Site Damage and residual stresses. The current research has developed an algorithm for fatigue analysis of multiple crack propagation. Additionally, it has demonstrated that under the *RSIF Proportionality Conjecture*, residual stress calculations are not necessary for fatigue calculations from a conservative perspective.

(iv) This work has shown a general description of the corrosive effects on the fatigue analysis of a weld. It includes a novel study about the Transitional Environmental Protection (TEP) process of welded components, i.e. when the corrosion protection system fails after a period of time.

(v) The weld geometrical defects as well as the different corrosion mechanism such as pitting were assumed implicitly in the S-N curves used for the SB approach. The FM models account for these effects as well as the crack initiation period through the calibration against SB methods. The crack growth parameters in FM models depend on environmental conditions.

(vi) A literature review about probabilistic fatigue and inspection planning has been introduced. The current research has developed an algorithm capable of executing inspection/repair simulations through Monte Carlo techniques. The algorithm shows different reliability curves depending on the inspection intervals and environmental conditions.

(vii) The analysis of a 2D bracket weld illustrates the capabilities of the algorithms developed in this research. The method can serve to answer three questions: The most cost-effective inspection interval, the cost involved, and the impact of ageing the corrosion protection system.

(viii) Most of the inspection planning concepts developed in the present work are aligned with the recommendations from the standards, e.g. DNV or BS.

(ix) The FM models exposed in this work are constraint by 2D modelling techniques. A further analysis of 3D modelling techniques is necessary in order to address real fatigue cases.

(x) Further studies are necessary in order to compare the crack growth results from this research with the real structural behaviour of offshore welds for wind turbines. Additionally, cracks may grow from different locations than the root and those situations should be accounted.

8 Impact of the current research and contribution to society

This work introduces a number of novel studies for the sake of reaching feasible solutions for the inspection planning of offshore welds for wind turbines. Firstly, an innovative method for Multiple Site Damage (MSD) is presented in Manuscript A, Appendix A. The publication enhances the knowledge of the scientific community about multiple cracks modelling, and how to evaluate closure effects and coalescence under MSD fatigue.

The research includes another important contribution to the fracture mechanics field: The *Residual Stress Intensity Factor (RSIF) Proportionality Conjecture*. This idea is presented in Manuscript B, Appendix B, and it implies that no residual stress calculations are necessary in order to reach conservative solutions of crack propagation in welds. As a consequence, crack propagation solutions can be reached while avoiding multiple and complex residual stress calculations. The conjecture considerably eases the path towards the fracture mechanics studies of welds. However, further comparisons with experimental data are necessary in order to evaluate this approach.

The author also includes a description of how to address the corrosion topic in the Fracture Mechanics analysis of offshore welds. Manuscript C, Appendix C, exposes the effects of corrosion in a structure with MSD that becomes subject to fatigue loading. Results confirm the importance of environmental conditions for the fatigue analysis.

The research finishes with the inspection planning of welded components under different environmental conditions. Manuscript D, Appendix D, introduces the concept of Transitional Environmental Protection (TEP) process. The TEP process is a common phenomenon in the industry but, to the best of the Author's knowledge, it has not been well described in the academic world. This thesis aims to shed light into this very relevant topic by opening the path to developing new studies about the TEP process. The method proposed in this work can be used to see the impact of corrosion protection systems on optimized inspection planning solutions.

This thesis aims to narrate the most important concepts and methods behind the fracture mechanics approach to optimize inspection planning of offshore welds subject to fatigue loading. The consequence of an optimized inspection plan is a lower maintenance cost in the offshore wind industry. This implies a lower cost of electricity generated from offshore wind turbines.

9 Future Research

The present study serves as a starting point for more advanced future research in the probabilistic inspection planning framework. Some of the improvements and future research proposals are:

(i) Develop crack propagation models and Stress-Based methods in 3D.

(ii) Compare crack propagation simulations with experiments.

(iii) Validate the *RSIF Proportionality Conjecture* with 3D cases and experiments.

(iv) Apply the inspection planning method described in Manuscript D to real offshore structures and compare results.

(v) Include advanced and more precise damage accumulation and fatigue crack propagation formulation in the inspection algorithms developed for Manuscript D.

(vi) Further evaluation of multiple site damage in the reliability of a structure.

(vii) Perform sensitivity analysis of the reliability curve for different types of inspection/repair methods.

(viii) Include the effects of false detection in the inspection plan algorithm.

(ix) Extend the inspection planning of Manuscript D to include variable inspection intervals.

(x) Include Bayesian statistics, i.e. update the probabilistic fracture mechanics model with results from real inspections.

(xi) Include different parameters that influence offshore inspection planning, e.g. the weather forecast or the consequences of failure.

References

[1] Ruiz-Muñoz GA, Sørensen JD. Probabilistic inspection planning of offshore welds subject to the transition from protected to corrosive environment. Submitted.

[2] Guidance notes on risk assessment applications for the marine and offshore oil and gas industry. Houston: American Bureau of Shipping; 2000.

[3] Det Norsk Veritas. Risk-based inspection of offshore topsides static mechanical equipment. DNV-RP-G101. Oslo, Norway: DNV; 201

[4] American Petroleum Institute. Risk-based inspection. API-RP-580. 2nd ed. Washington DC, USA: API; 2009.0.

[5] Committee reference WEE/37. British Standard BS 7910:2013: Guide to methods for assessing the acceptability of flaws in metallic structures. London: BSI; 2013.

[6] DNVGL-RP-C203:2016: Fatigue design of offshore steel structures. 2016.

[7] Jeffus L. Welding: Principles and Applications. 8th ed. Boca Raton: Cengage Learning; 2017.

[8] Haagensen PJ. Notes in Fatigue design of welded structures. Trondheim: NTNU; 2013. PhD course KT8202-Fatigue Analysis, NTNU.

[9] Al-Mukhtar AM. The safety analysis concept of welded components under cyclic loads using fracture mechanics method [dissertation]. Freiberg: Technische Universität Bergakademie Freiberg; 2010.

[10] European committee for standardization. Welding and allied processes-Classification of geometric imperfections in metallic materials- Part 1:Fusion Welding(ISO 6520-1:2007), Trilingual version EN ISO 6520-1:2007. Brussels: CEN; 2007.5

[11] Anderson TL. Fracture Mechanics: Fundamentals and Applications. 3th ed. Boca Raton: CRC Press Taylor & Francis Group; 2005.

[12] Straub D. Generic Approaches to Risk Based Inspection Planning for Steel Structures [dissertation]. Zürich: Swiss Federal Institute Of Technology ETH; 2004.

[13] Chen NZ, Wang G, Soares CG. Palmgren-Miner's rule and fracture mechanics-based inspection planning. Eng Fract Mech 2011; 78: 3166-82.

[14] Westergaard, HM. Bearing Pressures and Cracks. J Appl Mech 1939; 6:49-53.

[15] Irwin GR. Analysis of Stresses and Strains near the end of Crack Traversing a Plate. J Appl Mech 1957; 24:361-4.

[16] Dowling N.E. Mechanical behaviour of materials. 4th ed. London: Springer; 2013.

[17] Ingraffea AR, Grigoriu M. Probabilistic Fracture Mechanics: A Validation of Predictive Capability. Report No. 90-8. Department of structural Engineering, Cornwell University. 1990.

[18] Rice JR. A Path-Independent Integral and the Approximate Analysis of Strain Concentration By Notches and Cracks. J Appl Mech 1968; 35(2):379-386.

[19] Kim J-H, Paulino GH. Consistent Formulation of the Interaction Integral Method for Fracture of Functionally Graded Materials. J Appl Mech 2005; 72:351-364.

[20] Walter MC, Paulino GH, Doodds Jr RH. Interaction integral procedures for 3-D curved cracks including surface tractions. Eng Fract Mech 2005; 72:1635-63.

[21] Kuna M. Solid Mechanics and Its Applications: Finite Elements in Fracture Mechanics. Vol 201. Waterloo: Springer; 2013.

[22] Meggiolaro MA, Miranda ACO, Castro JTP, Martha LF. Stress intensity factor equations for branched crack growth. Eng Fract Mech 2005; 72: 2647-71.

[23] Stern M, Becker EB, Dunham RS. Contour integral computation of mixed-mode stress intensity factors. Int J Fract 1976; 12(3):359-68.

[24] Yau J, Wang S, Corton H. A mixed-mode crack analysis of isotropic solids using conservation laws of elastics. J Appl Mech 1980; 47:335-41.

[25] Ruiz-Muñoz GA. Method to Analyse Multiple Site Damage Fatigue before and after Crack Coalescence. Eng Fract Mech 2017; In press

[26] Tanaka K. Fatigue propagation from a crack inclined to the cyclic tensile axis. Eng Fract Mech 1974; 6: 493-507.

[27] Erdogan F, Sih GC. On the crack extension in plates under plane loading and transverse shear. J Basic Eng 1963; 85: 519-277.

[28] Lei B-M, Tran V-X, Taheri S, le Roux J-C, Curtit F, He M, Wan L, Zhou Y. Toward consistent fatigue crack initiation criteria for 304L austenitic stainless steel under multi-axial loads. Int J Fatigue 2015; 75: 57-68.

[29] Maierhofer J, Pippan R, Gänser H-P. Modified NASGRO equation for physically short cracks. Int J Fatigue 2014; 68: 200-7.

[30] Forman RG, Mettu SR. Behavior of surface and corner cracks subjected to tensile and bending loads in Ti–6Al–4V alloy. In: Fracture Mechanics: 22nd Symposium, Vol. 1 (Eds H.A. Ernst, A. Saxena, D.L. McDowell), ASTM STP 1131, American Society for Testing and Materials, Philadelphia; 1992. p. 519–546.

[31] Elber W. Fatigue Crack Closure under Cyclic Tension. Eng Fract Mech 1970; 2: 37-45.

[32] Walter MC, Paulino GH, Doodds Jr RH. T-stress and its implications for crack growth. Eng Fract Mech 2002; 69:1325-37.

[33] Newman Jr JC. A Crack Opening Stress Equation for Fatigue Crack Growth. Int J Fatigue 1984; 24: 131-5.

[34] Newman Jr JC. A Crack-Closure model for Predicting Fatigue-Crack Growth under Aircraft Spectrum Loading. Hampton: Langley Research Center; 1981 Jan. Report No. NASA-TM-81941.

[35] Rahman S, Ghadimian O, Ranjbaran M. Study on life and path of fatigue cracks in multiple site damage plates. Int J Fatigue 2015; 80: 449-58.

[36] Huang W, Garbatov Y, Soares CG. Fatigue reliability assessment of a complex welded structure subjected to multiple cracks. Eng Struct 2013; 56:868-79.

[37] Dündar H, Ayhan AO. Three-dimensional fracture and fatigue crack propagation analysis in structures with multiple cracks. Comput Struct 2015; 158: 259-73.

[38] Price RJ, Trevelan J. Boundary element simulation of fatigue crack growth in multi-site damage. Eng Anal Bound Elem 2014; 43: 67-75.

[39] Skorupa A, Skorupa M. Riveted Lap Joints in Aircraft Fuselage: Design, Analysis and Properties. 4th ed. Harlow: Pearson; 2012.

[40] Swift T. Widespread fatigue damage monitoring - issues and concerns. In: Proceedings of 5th International Conference on Structural Airworthiness of New and Aging Aircraft: 1993 Jun 16-18; Hamburg, Germany. Bonn: Deutsche Gesellschaft fur Luft- und Raumfahrt; 1993.

[41] Bao R, Zhang X, Yahaya NA. Evaluating Stress Intensity Factors due to Weld Residual Stresses by the Weight Function and Finite Element Methods. Eng Fract Mech 2010; 77: 2550-66.

[42] Seifi R. Effect of Residual Stresses on Fracture Parameters of through Cracks in Welded Plates. Procedia Eng 2011; 10: 1895-900.

[43] Ruiz-Muñoz GA, Eder MA. A conservative approach for Mode I-II fatigue analysis under residual stresses: The RSIF proportionality Conjecture. Submitted.

[44] Xu S-h, Wang Y-d. Estimating the effects of corrosion pits on the fatigue life od steel plate based on the 3D profile. Int J Fatigue 2015; 72: 27-41.

[45] Wahab MA, Sakano M. Corrosion and biaxial fatigue of welded structures. J Mater Process Tech 2003; 143-144: 410-5.

[46] Božić MC. Multiscale fatigue crack growth modelling for welded stiffened panels. Fatigue Fract Engng Mater Struct 2014; 37:1043-54.

[47] Kim JS, Jin TE. Fatigue analysis of nuclear welded structures based on structural stress and elasto-plastic fracture mechanics approach. Key Eng Mat 2005; 297-300: 774-80.

[48] Faber MH, Sørensen JD, Tychsen J, Straub D. Field Implementation of RBI for Jacket Structures. J Offshore Mech Arct Eng 2005; 127(3): 220-6.

[49] Krejsa M, Kala Z, Seitl S. Inspection Based Probabilistic modeling of fatigue crack progression. Procedia Eng 2016; 142: 146-53.

[50] Eltaief M, Chateauneuf A, Bouraoui Ch, Hassine T. Dynamic approach for optimal inspection planning of fatigue cracked components. J Constr Steel Res 2015; 115: 263-75.

[51] Ditlevsen O, Madsen HO. Structural Reliability Methods. Internet ed. 2.2.5. Lyngby: The Technical University of Denmark; 2005.

[52] Sørensen JD. Notes in Structural Reliability Theory and Risk Analysis. Aalborg: AAU; 2011. PhD course Reliability and Risk Analysis of Wind Turbines.

[53] Lotsberg I, Sigurdsson G, Fjeldstad A, Moan T. Probabilistic methods for panning of inspection for fatigue cracks in offshore structures. Mar Struct 2016; 46: 167-92.

[54] Sørensen JD, Ersdal G. Safety and Inspection Planning of Older Installations. J Risk Reliability 2008; 222(3): 403-17.

[55] Ruiz-Muñoz GA. The Effects of Multiple-Site Damage and Corrosion on the Structural Reliability of a Thin Plate with a Hole. In: Željko Božić editor. ICSID 2017. International Conference on Structural Integrity and Durability 2017: Fatigue and Fracture at all Scales (Book of Abstracts); 2017 Aug 15-18; Dubrovnik (Croatia); p. 213-4.

[56] Mohamed K. Optimal Risk-Based Inspection and Maintenance (RBIM) Planning for Process Assets [dissertation]. St John's: Memorial University of Newfoundland; 2012.

[57] Goyet J, Straub D, Michael H. Risk based inspection planning. Revue Française De Génie Civil 2002; 6(3): 448-503.

[58] Doshi K, Roy T, Parihar YS. Reliability based inspection planning using fracture mechanics base fatigue evaluations for ship structural details. Mar Struct 2017; 54: 1-22.

[59] Yang JN, Trapp WJ. Reliability Analysis of Aircraft Structures under Random Loading and Periodic Inspection. AIAA Journal 1974; 12(12): 1623-30.

[60] Yang JN, Trapp WJ. Inspection frequency optimization for aircraft structures based on reliability analysis. Journal of Aircraft 1975; 12(5): 494-6.

[61] Skjong R. Reliability Based Optimization of Inspection Strategies. Proceedings ICOSSAR'85; International Conference on Structural Safety and Reliability; 1985 May 27-29; Kobe (Japan); p. 614-8.

[62] Madsen HO, Sørensen JD, Olesen R. Optimal Inspection Planning for Fatigue Damage of Offshore Structures. Proceedings ICOSSAR'89; International Conference on Structural Safety and Reliability; 1989 Aug 7-11; San Francisco (USA); p. 2099-106.

[63] Zhang C, Gao W, Guo S, Li Y, Yang T. Opportunistic maintenance for wind turbines considering imperfect, reliability-based maintenance. Renew Energy 2017; 103: 606-12.

[64] Pliego-Muragán A, García-Márquez FP, Pinar-Pérez JM. Optimal Maintenance Management of Offshore Wind Farms. Energies 2016; 9(1): 46.

[65] Kim S, Frangopol DM. Optimum inspection planning of minimizing fatigue damage detection delay of ship hull structures. Int J Fatigue 2011; 33: 448-59.

[66] DNVGL-RP-0001:2015: Probabilistic methods for planning inspection for fatigue cracks in offshore structures. 2015

[67] Haagensen PJ, Maddox SJ. IIW Recommendations on Post Weld Improvement of Steel and Aluminium Structures. Cambridge: The International Institute of Welding; 2001 Jul. Report No. XIII-1815-00.

Appendices

Appendix A Method to Analyse Multiple Site Damage Fatigue before and after Crack Coalescence (Manuscript A)

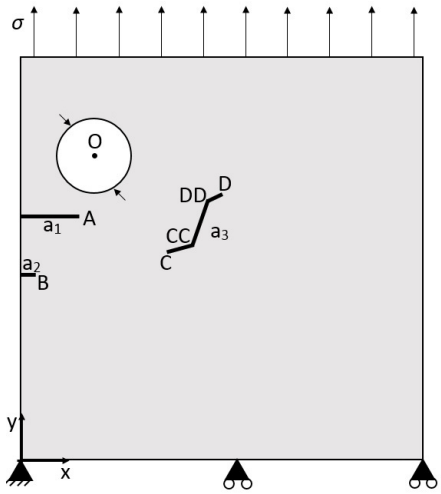

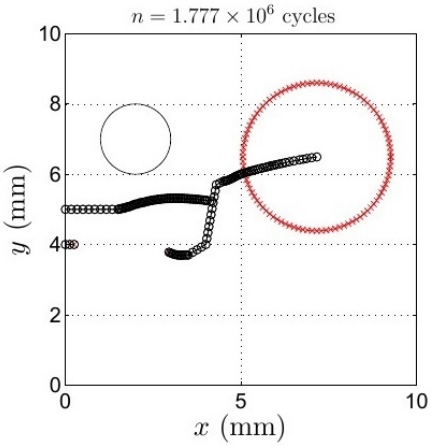

Engineering Fracture Mechanics xxx (2017) xxx–xxx

Contents lists available at ScienceDirect

Engineering Fracture Mechanics

journal homepage: www.elsevier.com/locate/engfracmech

Method to analyse multiple site damage fatigue before and after crack coalescence

G.A. Ruiz-Muñoz *

DONG Energy, Nesa Allé 1, 2820 Gentofte, Denmark
Department of Wind Energy, Technical University of Denmark, 4000 Roskilde, Denmark

ARTICLE INFO

Article history:
Received 10 April 2017
Received in revised form 9 August 2017
Accepted 8 September 2017
Available online xxxx

Keywords:
Multiple site damage
Finite element
Fracture mechanics
Fatigue
Crack closure

ABSTRACT

The Multiple Site Damage is a phenomenon that appears in e.g. aircraft fuselages and weld geometries. This article introduces a method for solving the Multiple Site Damage fatigue in a 2D specimen. The cases studied are for Linear Elastic Fracture Mechanics situations, isotropic materials and crack growth governed by the Paris Law regime. Already known fracture mechanics concepts are merged together in an innovative algorithm that increases computational efficiency by optimizing the number of Finite Element Analyses necessary for fatigue calculations. A new approach to crack coalescence is presented by using the application limit of Linear Elastic Fracture Mechanics. Comparisons with analytical, experimental and other software results have shown the reliability of this method for several cases. A final explanatory example of a plate with multiple cracks and a hole shows the capabilities of the method proposed.

1. Introduction

Multiple Site Damage (MSD) is a phenomenon that occurs when multiple cracks are located in a structure. MSD can appear from multiple stress concentration locations, but also due to e.g. corrosion pitting [1], poor weld manufacturing techniques as explained in ISO 6520-1:2007 [2] or inherent defects in the material. The aircraft fuselage fatigue cases are examples where multiple cracks are analysed in riveted lap joints [3].

A MSD fatigue analysis helps to determine fatigue growth directions, the number of cycles to failure and predominant cracks. These three concepts are coupled and they are relevant to determine e.g. S-N curves or types of failures in a structure. For applications that require high computational resources, e.g. probabilistic fatigue analysis, a method that is able to automatically design MSD Finite Element (FE) models and efficiently simulate fatigue crack growth is preferred.

The MSD has already been studied using FE models by Jiang et al. [4], where the relation between Stress Intensity Factors (SIF) and crack distributions is presented. The fatigue crack propagation of MSD is shown in recent publications by e.g. Dündar et al. [5], Price et al. [6] and Liu et al. [7]. Dündar et al. use enriched finite elements to compute Stress Intensity Factors for different 2D and 3D geometries. On the other hand, Price et al. propose a MSD fatigue analysis applying dual boundary elements. Liu et al. analyse the crack coalescence through the boundary element method for random crack distributions in 2D studies.

* Address: DONG Energy, Nesa Allé 1, 2820 Gentofte, Denmark.
E-mail addresses: g_a.ruiz@hotmail.com, gusru@dongenergy.dk

https://doi.org/10.1016/j.engfracmech.2017.09.011
0013-7944/© 2017 Published by Elsevier Ltd.

Nomenclature

a, a_{lim}	crack length and crack length limit
b	distance between two parallel cracks
b_i	number of divisions for 2D crack modelling
C_0	Paris Law parameter
d	distance between the crack tip and a boundary
d_{LEFM}	distance of the application Limit of LEFM
d_1, d_2	distance between coordinates in 2D crack modelling
d_{lim}	lower limit distance for the 2D crack modelling
E	Young's modulus
f_{eq}	equivalent crack opening factor
F	external loads
h_1, h_2	global mesh size and mesh size around the crack tip
H	height of a specimen
i, j	integer index
K, K_{max}	Stress Intensity Factor (SIF) and maximum SIF
$K_{eq}, K_{eqmax}, K_{eqop}$	equivalent, maximum Equi. and opening Equi. SIF
K_I, K_{II}	SIF for mode I and mode II
m	Paris Law parameter
n, n_{lim}	number of cycles and number of cycles limit
N_1	number of elements around the crack tip
r	radial distance from a crack tip
R	stress ratio
R_1	mesh parameters
t	thickness of the specimen
W	width of a specimen
x, y	Cartesian axis reference
α	crack opening parameter
$\Delta a_{cum}, \Delta a_{Total}$	cumulative and total crack growth
γ	half crack tip angle
θ_0	deviation from the crack tip orientation
ν	Poisson's ratio
σ	external load
$\sigma_{max}, \sigma_{min}$	maximum and minimum nominal stress
σ_o σ_{ys}	flow stress and yield stress
ϕ	crack orientation respect to Cartesian coordinates

The experimental data, however, is scarce. MSD fatigue analysis has already been done by Rahman et al. [8] in the recent years where crack closure was over-imposed to the fatigue numerical model through the Newman's equations.

The coalescence criterion is still a point of discussion. Authors e.g. Rahman et al. [8,3] propose methods such as the Plastic Zone Link-Up (PZL). However, the PZL criterion may reach situations where Linear Elastic Fracture Mechanics (LEFM) is no longer valid and advanced fatigue formulations are required to calculate fatigue life.

The fatigue analysis of multiple cracks requires additional calculations compared to single crack propagation. This publication offers a novel method that optimises the number of Finite Element Analysis (FEA) in a MSD specimen for High Cycle Fatigue (HCF). Cracks are automatically modelled and optimal crack steps are found through the combination of a novel algorithm and convergence analysis.

The study is restricted to 2D specimens, where closure effects are evaluated for MSD mixed mode analysis under plane strain or plane stress conditions. The fatigue analysis only takes into consideration the Linear Elastic Fracture Mechanics (LEFM) approach and assumes that all presented cracks grow according to the Paris Law regime [9]. Crack coalescence is addressed by using the Application Limit of LEFM (ALLEFM). Therefore, the well-known and simple Paris Law formulation is applicable for the entire fatigue analysis. The method presented can operate with complex crack distributions for a large variety of geometries, loads and constraints.

2. Theoretical background

The method explained in this publication combines already known concepts of fatigue, plane strain/stress analysis and boundary analysis. The novelty of this publication is to show how they are merged into a method that is able to perform MSD fatigue analysis before and after crack coalescence, using a low number of FEA for the sake of computational efficiency.

Please cite this article in press as: Ruiz-Muñoz GA. Method to analyse multiple site damage fatigue before and after crack coalescence. Engng Fract Mech (2017), https://doi.org/10.1016/j.engfracmech.2017.09.011

2.1. Fatigue formulation under closure and mixed mode

The Paris Law is a common formulation vastly used in fatigue crack propagation analysis. However, the original equation corresponds to the crack propagation for pure mode-I specimens. Meggiolaro et al. [10] already describes an approach to use the Paris Law for mixed mode conditions by applying the concept of equivalent SIF, K_{eq}. A modification of Meggiolaro's approach, introducing the equivalent opening SIF is shown as

$$\Delta a \approx C_0(K_{eqmax} - K_{eqop})^m \Delta n, \tag{1}$$

where m and C_0 are material parameters, K_{eqmax} is the equivalent maximum SIF, K_{eqop} is the equivalent opening SIF, Δa is the crack growth and Δn is the cycle increment. Assuming that a crack trends to propagate towards pure mode-I [10], K_{eq} is the SIF once a crack propagates an infinitesimally small length from mixed mode towards pure mode-I, Fig. 1. This approach would make valid the use of pure mode-I equations in mixed mode cases. A well-accepted form to calculate the equivalent SIF [11] can be written as

$$\Delta K_{eq} = \frac{\Delta K_I}{2} + \frac{1}{2}\sqrt{\Delta K_I^2 + 4(1.155\Delta K_{II})^2}. \tag{2}$$

There are other alternatives proposed by Meggiolaro et al. [10] to calculate the equivalent SIF, such as the Strain Energy Density criterion or the Maximum Energy Release Rate criterion. All these criteria show similar equivalent mixed mode SIF whenever $K_I \gg K_{II}$, which is a general case in a mixed mode crack propagation under constant loading direction. Meggiolaro et al. [10] already stated that since the presented criteria predicts a path deviation towards a pure mode-I, the cracks will grow towards a situation where all criteria show the same results. The maximum tangential stress (MTS) criterion [12] is preferred because of its simplicity and availability as a closed form solution [10],

$$K_{eqmax} = \frac{1}{4}\left(3\cos\frac{\theta_0}{2} + \cos\frac{3\theta_0}{2}\right)K_{Imax} - \frac{3}{4}\left(\sin\frac{\theta_0}{2} + \sin\frac{3\theta_0}{2}\right)K_{IImax}, \tag{3}$$

where θ_0 is the deviation from the previous crack growth direction,

$$\theta_0 = 2\tan^{-1}\left(\frac{K_{Imax}}{4K_{IImax}} \pm \frac{1}{4}\sqrt{\left(\frac{K_{Imax}}{K_{IImax}}\right)^2 + 8}\right), \tag{4}$$

K_{Imax} is the SIF for mode-I and K_{IImax} is the SIF for mode-II when maximum load is applied. The orientation of the crack propagation angle results in two solutions. The MTS states that the final orientation among both values is the one that results in maximum tangential stress.

Apart from the maximum equivalent SIF calculation, crack closure analysis is necessary as well for Eq. (1). Rahman et al. [8] applies Newman's [13,14] equation for crack propagation under mixed mode conditions to seek a method that could reproduce their experimental results for MSD fatigue. Newman's equation has already been used to validate simulations with experiments in other studies, e.g. [15]. Originally, Newman's equation addresses the closure problems for mode-I SIF in metallic structures. Using the equivalent SIF approach to account mixed mode conditions, Newman's equation is modified to

$$\frac{K_{eqop}}{K_{eqmax}} = f_{eq} \approx \begin{cases} \max(R, A_0 + A_1R + A_2R^2 + A_3R^3) & R \geqslant 0 \\ A_0 + A_1R & -1 \leqslant R < 0 \end{cases} \tag{5}$$

where R is the stress ratio, $A_0 = (0.825 - 0.34\alpha + 0.05\alpha^2)[\cos(\pi\sigma_{max}/2\sigma_o)]^{1/\alpha}$, $A_1 = (0.415 - 0.071\alpha)(\sigma_{max}/\sigma_o)$, $A_2 = 1 - A_0 - A_1 - A_3$ and $A_3 = 2A_0 + A_1 - 1$.

The term f_{eq} is calculated using the right side formulation in Eq. (5). The opening equivalent SIF is the result of $K_{eqop} = f_{eq}K_{eqmax}$.

The term σ_{max}/σ_o is the ratio of the maximum nominal applied stress with respect to the flow stress. The parameter α is 1 for plane stress analysis and 3 for plane strain analysis. The plane stress condition is the condition where the stress vector is

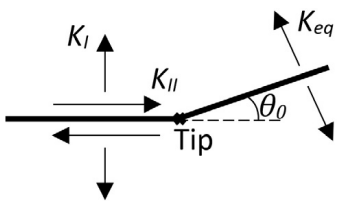

Fig. 1. Illustration of equivalent SIF according to Meggiolaro et al. [10]. Crack propagates from a mixed mode configuration towards pure mode-I.

Please cite this article in press as: Ruiz-Muñoz GA. Method to analyse multiple site damage fatigue before and after crack coalescence. Engng Fract Mech (2017), https://doi.org/10.1016/j.engfracmech.2017.09.011

zero across any particular surface in a 3D model, whereas the plane strain condition occurs when the strain vector is zero across any particular surface in a 3D model.

The crack closure equation proposed by Newman poses an additional challenge for multiple crack propagation. Dowling [16] suggests that plane strain conditions can be addressed as long as $(t \cup d) \geqslant 2.5\left(\frac{K}{\sigma_{ys}}\right)^2$, where t is the thickness, d is the shortest distance from the crack tip to a boundary and σ_{ys} is the yield stress. Following the equivalent stress concept, the plane strain condition for mixed mode is

$$(t \cup d) \geqslant 2.5\left(\frac{K_{eqmax}}{\sigma_{ys}}\right)^2. \tag{6}$$

When a crack grows towards another crack surface, the distance d decreases and plane strain conditions might not be applicable any more. Consequently, the α values in Eq. (5), may decrease from $\alpha = 3$ for plane strain conditions towards $\alpha = 1$ for plane stress conditions. The previous statement means closure effects may increase as a crack approaches another crack surface.

2.2. Crack coalescence: application limit for LEFM analysis

When a crack grows towards another crack surface, a criterion to determine the crack coalescence is required. Skorupa et al. [3] suggest the analysis of Elasto-Plastic Fracture Mechanics Methods (EPFM) to simulate coalescence. However, they recognize the complexity of this approach and recommend simpler methods such as the Plastic Zone Link-Up (PZL) for the sake of computational efficiency.

Another concept appears when a crack approaches a boundary. Dowling [16] explains the overall ALLEFM as $d_{LEFM} \geqslant \frac{4}{\pi}\left(\frac{K}{\sigma_{ys}}\right)^2$, which following the equivalent SIF definition can be approximated to mixed mode conditions as

$$d_{LEFM} \geqslant \frac{4}{\pi}\left(\frac{K_{eqmax}}{\sigma_{ys}}\right)^2. \tag{7}$$

The ALLEFM in Eq. (7) presents a length condition between the crack tip and the closest free surface. As a conservative approach, crack coalescence could be assumed immediately before ALLEFM is violated. The main advantage of using the ALLEFM is that the fatigue analysis always respects the LEFM approach. In addition, the formulation is fairly simple when compared to the EPFM approach.

3. Methodoly to analyze MSD fatigue

The theoretical background explained is evaluated in order to develop a global algorithm that performs the MSD fatigue analysis. The algorithm includes 2D modelling of cracks in a simple and automatic manner, and suitable for efficient execution in the Finite Element Method (FEM) framework.

3.1. 2D crack modelling

The multiple crack propagation analysis requires a flexible system able to evaluate different crack distributions through FEM. The method proposed has the capability to analyse surface and internal cracks. The crack modelling is divided into two stages. The first stage concerns the definition of the crack geometries, see Appendix A. In a second stage, a mesh topology and element type is assigned to the geometry, see Appendix B.

3.2. Description of the algorithm

The algorithm depicted in Fig. 2 performs the multiple crack propagation with the following the steps:

- Initial case: Contains the initial geometry, loads, constraints, mesh parameters and fatigue parameters. An ANSYS script is created.
- Finite Element Analysis: ANSYS calculates the SIFs.
- Fatigue Analysis: The algorithm performs the equivalent SIF calculations following Eq. (3) and, optionally, the equivalent opening SIF calculations given by Eq. (5). The fatigue crack growth is retrieved using the Paris Law formulation Eq. (1) for a certain cycle increment Δn which is pre-set before running the algorithm.
- Application Limit of LEFM (Optional): The user can optionally add the ALLEFM analysis after a certain number of FEA. If visually, the cracks very closely approach the limit Eq. (7), the cracks can be forced to intersect as in Fig. 13 or failure of the structure can be declared. The analysis of an example corresponding to Fig. 8 shows how this option works.
- Crack Growth Update: The cumulative crack growth as well as the mean growth direction are calculated from current and previous fatigue analysis. The number of load cycles is updated for every crack growth update.

Please cite this article in press as: Ruiz-Muñoz GA. Method to analyse multiple site damage fatigue before and after crack coalescence. Engng Fract Mech (2017), https://doi.org/10.1016/j.engfracmech.2017.09.011

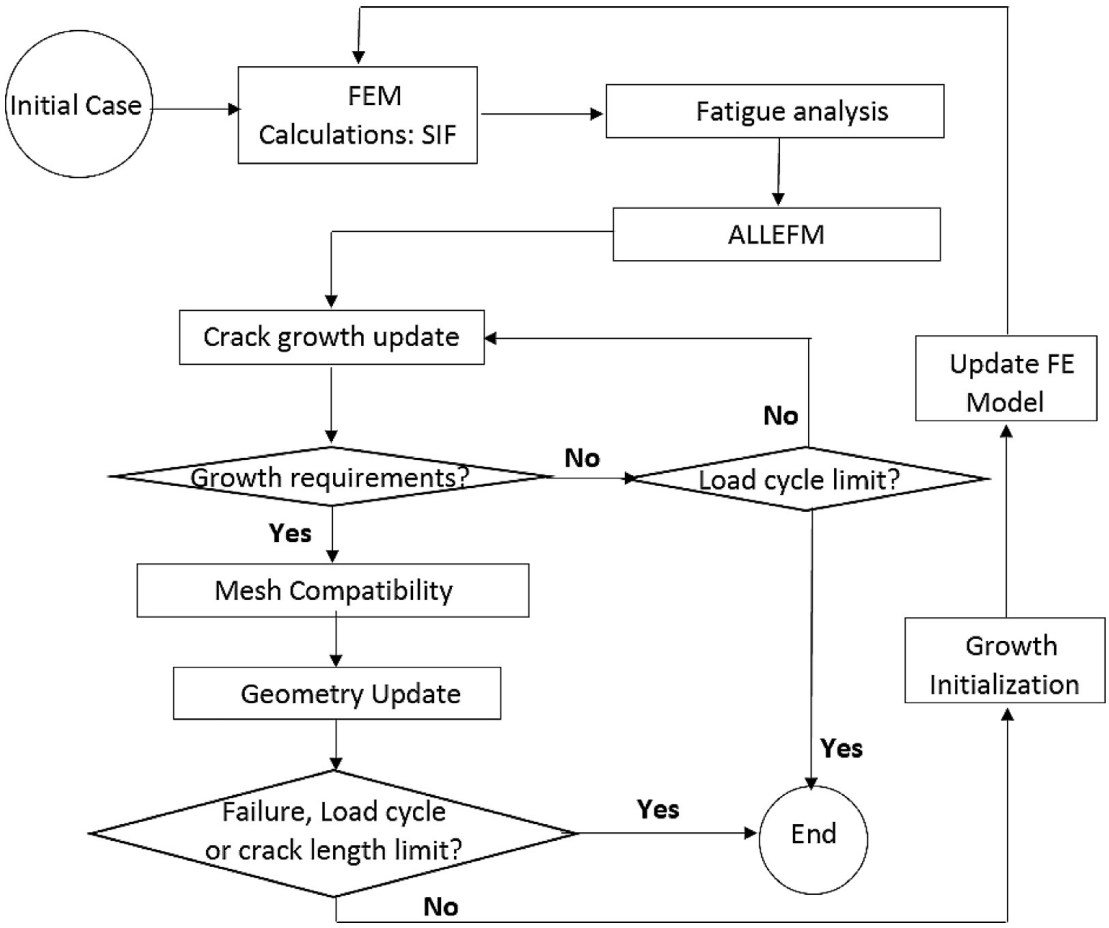

Fig. 2. Algorithm for the multiple crack propagation.

- Mesh Compatibility (Optional): The user can optionally perform a mesh compatibility analysis after a certain number of FEA. If after a visual inspection, the contour around a crack tip is very close to another boundary, the system can be corrected as in the ALLEFM analysis. This option avoids computational failure due to problems with modelling the spider-web mesh.
- Geometry Update: The geometry is updated for crack coalescence or crack tips whose growth increments are higher than a certain limit $\Delta a > \Delta a_{lim}$.
- Growth Initialization: Once a crack tip geometry is updated, its corresponding crack growth parameters are initialized.

The algorithm, shown in Fig. 2, finishes when the number of cycles or any crack length has reached a pre-set limit. Additionally, the user can interrupt the algorithm when failure of the structure is observed in the interface.

The algorithm is executed in a Matlab®-ANSYS® [17,18] system. Matlab performs all calculations except computation of the SIFs, which are calculated by ANSYS.

An explanatory example is plotted in Fig. 3 together with Fig. 4. Fatigue occurs in two crack tips, crack tip 1 and crack tip 2. For each crack tip, a cumulative crack growth variable is initially assigned: $\Delta a_{cum} = 0$. During every cycle increment, the crack growth is added to the cumulative variable as $\Delta a_{cum} = \Delta a_{cum} + \Delta a$. Simultaneously, the crack growth direction is calculated as well. The variable $\overline{\theta_0}$ corresponds to the average of all crack growth directions calculated in the current and previous load cycles.

The multiple crack propagation shown in Figs. 3 and 4 is divided into different stages:

- Initial Stage: The geometry is submitted for FEA. The crack propagation is calculated $\Delta \boldsymbol{a}, \boldsymbol{\theta}_0$. Results are used to calculate Δa_{cum} and $\overline{\theta_0}$ in every cycle increment.
- Stage $\mathcal{A}$: The cumulative crack growth of crack tip 1 has crossed the limit $\Delta a_{cum} > \Delta a_{lim}$. The crack tip 1 location is updated in the geometry through its values Δa_{cum} and $\overline{\theta_0}$. Growth associated with crack tip 1 is initialized. The new geometry is submitted to a FEA. New results for $\Delta \boldsymbol{a}$ and $\boldsymbol{\theta}_0$ are calculated.
- Stage $\mathcal{B}$: Same procedure as Stage $\mathcal{A}$, but applied to crack tip 2.

Please cite this article in press as: Ruiz-Muñoz GA. Method to analyse multiple site damage fatigue before and after crack coalescence. Engng Fract Mech (2017), https://doi.org/10.1016/j.engfracmech.2017.09.011

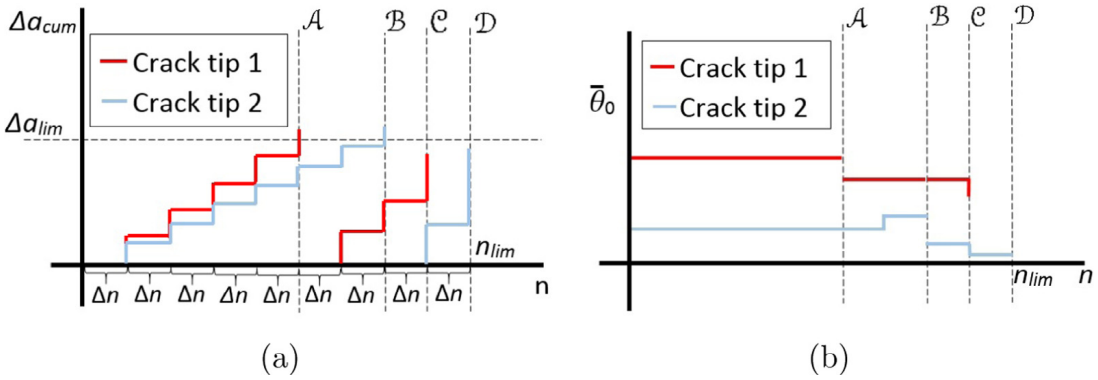

Fig. 3. Illustration of: (a) Cumulative crack growth; (b) Average crack growth.

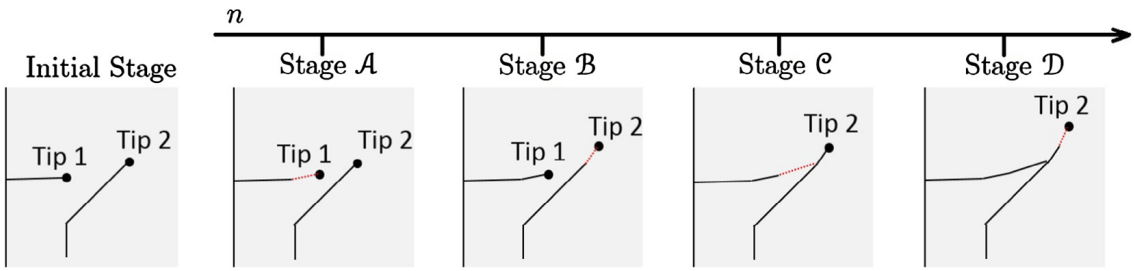

Fig. 4. Crack tip relocation after every stage from Fig. 3.

- Stage $\mathcal{C}$: The geometry is updated and submitted to a new FEA because crack tip 1 has reached the ALLEFM and intersected crack 2. New results for $\Delta \boldsymbol{a}$ and θ_0 are calculated. Crack tip 1 no longer exists for the rest of the analysis.
- Stage $\mathcal{D}$: A limit of cycles is reached and the analysis finishes.

When a crack growth is initialized, its cumulative crack growth is set as $\Delta a_{cum} = 0$. The stage where initialization occurs serves as a starting point for calculating the variables Δa_{cum} and $\overline{\theta_0}$ again. Note that the geometry is submitted to a new FEA only when $\Delta a_{cum} \geqslant \Delta a_{lim}$ or there is crack coalescence. As a consequence, the higher Δa_{lim}, the fewer number of FEA are executed for a given case. The proposed method optimizes the number of FEA executed by doing a convergence analysis reducing Δa_{lim} until results are no longer significantly different.

4. Comparison with analytical results, experiments and other sofware tools

A comparison with other studies can indicate the performance of the proposed method. Firstly, it is necessary to determine adequate values for the mesh parameters. A good parameter set-up can be achieved by benchmarking cases against well-known solutions. Kim et al. [19] evaluated the interaction integral using $h_2/a = 1/32$ and number of contours $N_1 = 8$. The mesh used for all cases in this research is defined by $N_1 = 20$ and $h_2/a \leqslant 1/60$. In this sense, the mesh set-up around the crack tip includes a higher number of elements than in other scientific studies. In addition, the contour radius is generally set to $R/h_2 = 744/100$, which assures several contours around the crack tip, Fig. 14. The spider-web mesh around the crack tip is modelled using the mesh parameters described and the ANSYS command KSCON [18]. The distance limit was considerably low, $d_{lim} = 3R$, to keep sharp shapes of cracks during 2D crack modelling.

The calculations of the SIF are done through the ANSYS command CINT [18], where SIF from the second to the fifth contour is averaged in order to diminish discretisation errors. The first contour is avoided since the mesh set-up does not adjust the first row of nodes to a distance $h_2/4$ from the crack tip [9].

The mesh configuration presents acceptable results, with less than 3% error compared to the analytical solution, in convergence studies for mixed mode and Multiple Site Damage, see Appendices C and D.

4.1. Crack path analysis

The current method is compared with the experiments done by Ingraffea and Grigoriu in [20]. Their results have previously been used for validation of crack growth problems under mixed mode conditions in other publications, e.g. [21]. The material is homogeneous and isotropic, where Young's modulus $E = 380$ MPa. Plane strain conditions are applicable to the geometry [20]. The case approach and the comparison between experiments and the current method are shown in Fig. 5. The

Please cite this article in press as: Ruiz-Muñoz GA. Method to analyse multiple site damage fatigue before and after crack coalescence. Engng Fract Mech (2017), https://doi.org/10.1016/j.engfracmech.2017.09.011

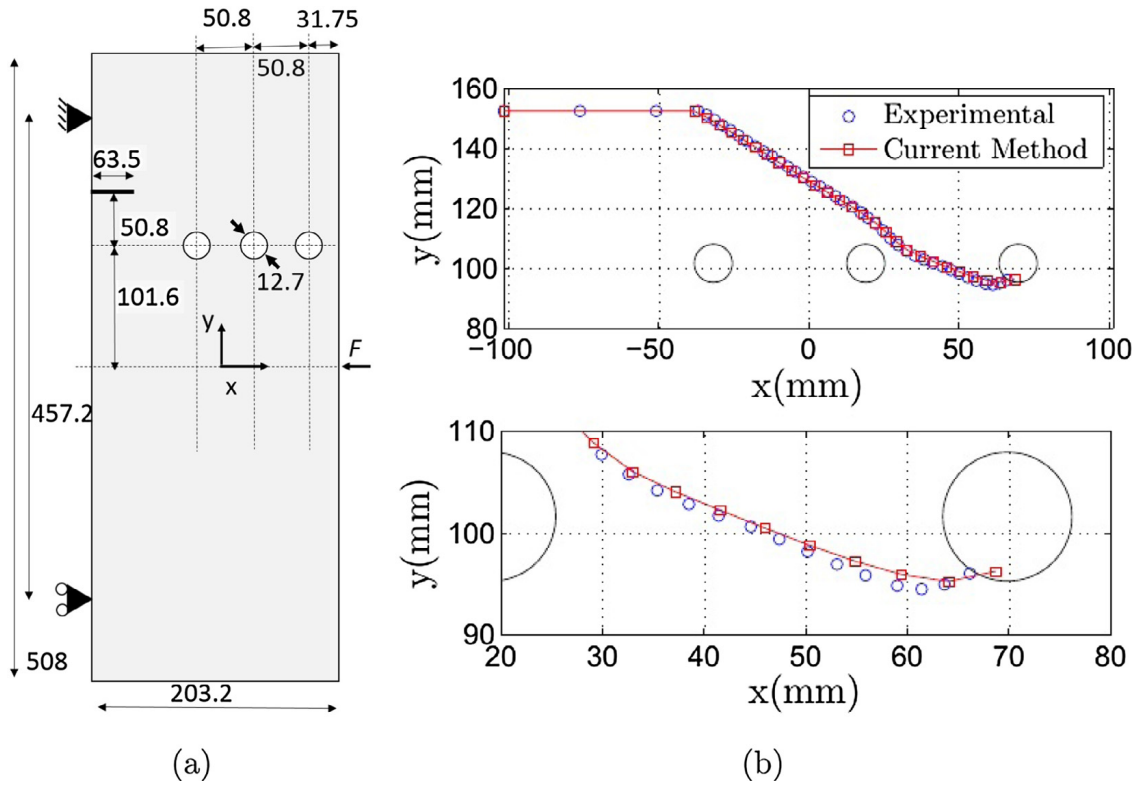

Fig. 5. Crack path analysis: (a) Geometry (mm), load and constraints; (b) Comparison between current method and experimental results from Ingraffea et al. [20]. Dimensions were transformed as 1 in. = 25.4 mm.

crack growth step Δa is set to a fixed value and the crack orientation is calculated by Eq. (4). Note that Eq. (4) does not depend on the absolute value of the force. However, a symbolic force of $F = 5.34$ N was adopted in order to run the FE model. Modifying the value of the load did not have any influence on the crack path.

The contour element size was kept constant during all crack growth $h_2 = D/60 = 12.7/60$ mm in order to keep a small ratio $h_2/a < 1/60$. The radius of the spider-web mesh was $R/h_2 = 744/100$. Convergence analysis for the FE model were performed in two studies: reducing the values of h_1, and reducing the values Δa. In every analysis, one of these two parameters was reduced by half until no significant differences in crack path were observed. The final mesh and crack step configuration were $h_1 = 3.81$ mm and $\Delta a = 4.72$ mm. The resulting mesh includes 7666 elements and 23,436 nodes.

The experimental results from Ingrafea and Grigoriu [20] were only reported as plots. The current study uses WebPlotDigitazer [22], an open source program, to extract data from plots to numerical values. Fig. 5 shows that the method is accurate in predicting crack paths under mixed mode conditions, in particular when the material is isotropic and the crack follows a MTS criterion tendency.

4.2. Two sided crack propagation in a thin plate

The proposed method is compared with the MSD simulations performed by Price et al. [6] and Dündar et al. [5]. Price et al. proposed to analyse the SIFs through a J-integral calculated in a dual boundary element method. One of the analyses concerns the multiple crack propagation of two-sided cracks described in Fig. 6. The same case was later studied by Dündar et al., where they used three dimensional enriched FE to compute stress intensity factors.

The structure is subject to a cycling load with stress ratio $R = 0$ and a stress amplitude of 100 MPa. The Young's modulus of the material is $E = 30$ GPa. The Paris law constants are $C = 10^{-12} \frac{\text{mm/cycle}}{(\text{MPa}\sqrt{\text{mm}})^m}$ and m = 3. The Poisson's ratio is $\upsilon = 0.3$. Since Price et al. and Dündar et Al. do not explicitly mention the closure problem in their publications, the current analysis assumes that closure effects are already included in the Paris Law Parameter C. Thus, Eq. (1) is transformed into

$$\Delta a \approx C(K_{eqmax} - K_{eqmin})^m \Delta n, \tag{8}$$

where K_{eqmin} is calculated in a very similar way as Eq. (3) but applying the minimum load to the structure. The analysis of the case shown in Fig. 6 was evaluated through the present method. The study was approached to plane stress conditions assuming an infinitesimally small thickness compared to the rest of the dimensions. The mesh parameters around the crack tip are $R/h_2 = 750/100$ and $h_2 = 2.5/60$ mm $< a_0/60$, where a_0 is the initial crack length $a_0 = 10$ mm. Three convergence studies

Please cite this article in press as: Ruiz-Muñoz GA. Method to analyse multiple site damage fatigue before and after crack coalescence. Engng Fract Mech (2017), https://doi.org/10.1016/j.engfracmech.2017.09.011

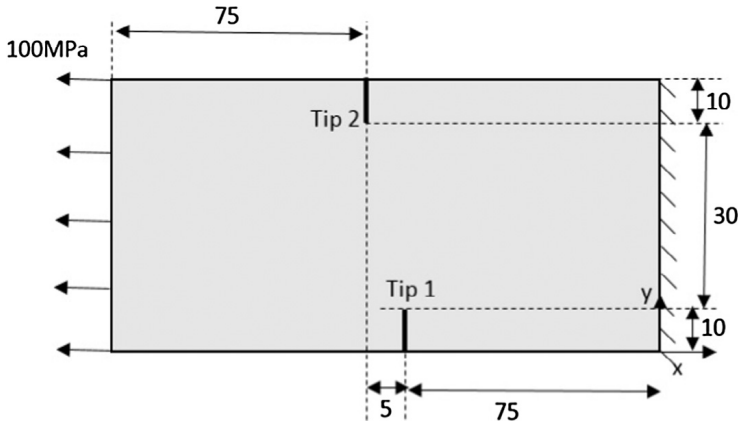

Fig. 6. 2D model shown by Price et al. [6]. Dimensions in mm.

were done reducing $h_1, \Delta a$ and Δn. The crack propagation was studied until structural failure. The values $h_1 = 2.4$ mm, $\Delta a = 0.47$ mm and $\Delta n = 1$ cycle lead to good results in the convergence study. Reducing the parameters to $h_1 = 1.2$ mm or $\Delta a = 0.34$ mm did not make a difference higher than 1.72% in fatigue life. The final mesh includes 7719 elements and 23,522 nodes. The comparison between the three methods is shown in Fig. 7.

The crack growth results predicted by Price seem to be slightly more conservative than those from the current method. However, the method proposed presents a smoother crack path shape when comparing with the other two methods. The tendency of the K_{II} results at crack tip 2 in the current method is similar to the Dündar results, but with lower values. In general, the three methods predict a similar fatigue performance.

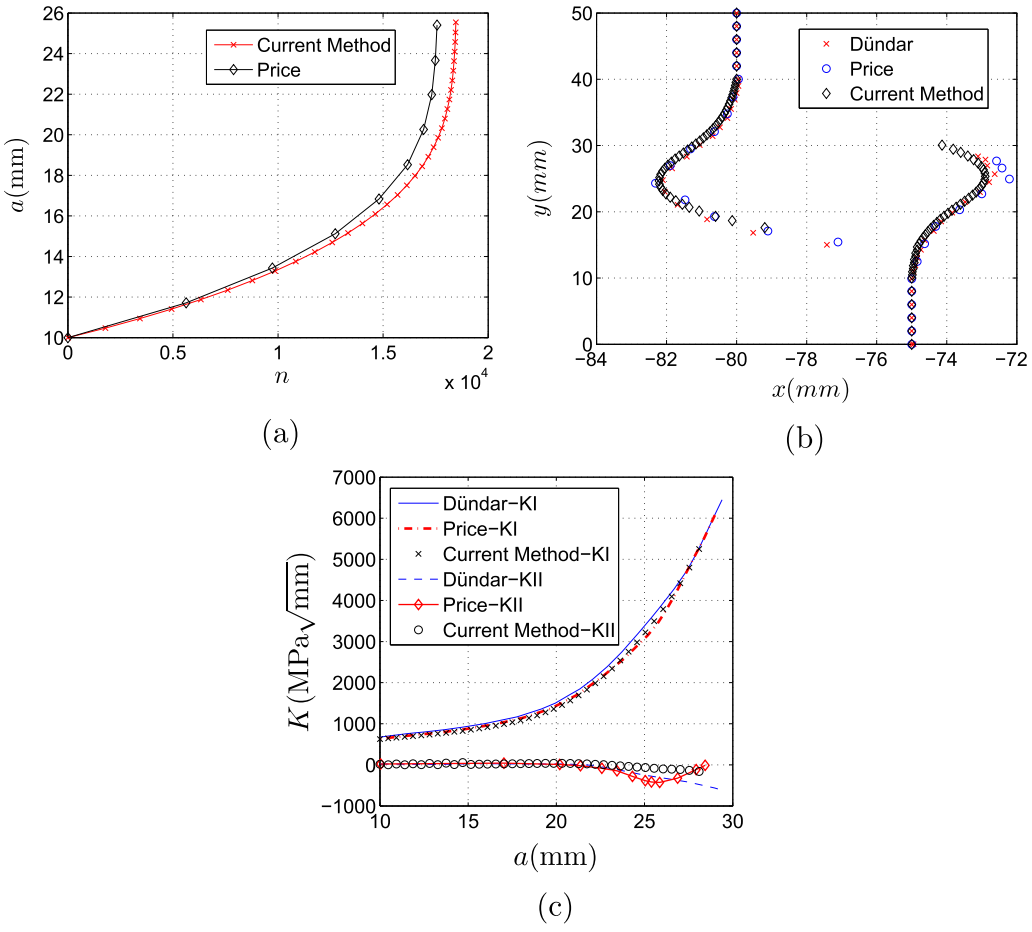

Fig. 7. Comparison between current method versus results from Price et al. [6] and Dündar et al. [5]: (a) Crack growth for crack tip 1; (b) Crack paths; (c) Stress intensity factors of crack tip 2.

Please cite this article in press as: Ruiz-Muñoz GA. Method to analyse multiple site damage fatigue before and after crack coalescence. Engng Fract Mech (2017), https://doi.org/10.1016/j.engfracmech.2017.09.011

An additional analysis of this case is provided in Appendix E, where the crack growths using two different equivalent SIF criteria are compared, Eqs. (2) and (3). The results are essentially the same.

5. Example of study: MSD fatigue analysis of a plate with a hole under a pure tensional cycling load

In this section, the fatigue crack growth in an MSD specimen is solved to show the capabilities of the method. Fig. 8 shows an MSD scenario under mixed mode conditions. A cycling load induces tension into the specimen with a stress ratio $R = 0.1$ and maximum tension σ_{max} = 17.5 MPa. A material with characteristics: Yield Stress σ_{ys} = 458 MPa, $C_0 = 2.5241 \times 10^{-12} \frac{\text{mm/cycle}}{(\text{MPa}\sqrt{\text{mm}})^m}$ and $m = 3.14$ was assumed. The relation between maximum stress and flow stress is assumed $\sigma_{max}/\sigma_o = 0.3$. These values are only representative since the proposed method is valid for the analysis of any metallic structure that can be studied under LEFM and isotropic conditions.

The crack growths are assumed to follow the linear Stage II trend [9]. Two specimens from Fig. 8 are evaluated: One in which the mechanical behaviour follows plane strain conditions and another for plane stress conditions.

The options of ALLEFM analysis and Mesh Compatibility analysis in the algorithm in Fig. 2 are activated for all the fatigue studies. The mesh set-up is the same as in the benchmarked models in Appendices C and D: $N_1 = 20$ and the radius $R/h_2 = 744/100$. The element size around each crack tip is $h_2 = 0.0042$ mm, which leads to a maximum ratio $h_2/a_2 = 0.0168 = 1/60$, where a_2 is the minimum crack length in Fig. 8, $a_2 = 0.25$ mm. As a consequence, the ratio $h_2/a < 1/60$ is kept along all crack growths.

The analysis evaluates all possible crack growths, before and after crack coalescence. In order to find optimal parameters for the fatigue analysis, different convergence studies were done. The procedure followed in each convergence case starts by an initial configuration, Fig. 8. The cracks grow according to the fatigue formulation, Eq. (1), until the fatigue study reaches $n = 1.74 \times 10^6$ cycles, Fig. 9. At this load cycle, the user identifies that the ALLEFM is very close to another surface. The user forces crack coalescence by imposing an artificial crack growth: in this exercise, assigning $\Delta a = 2$ mm to crack tip A ensures that crack coalescence takes place. The algorithm, Fig. 2 corrects the geometry as illustrated in Fig. 13.

Once coalescence is reached, the fatigue analysis continues. The final crack tip configuration immediately before the collapse is shown at $n = 1.777 \times 10^6$ cycles, Fig. 9. The crack distribution in the next cycle increment shows that the ALLEFM has already crossed the surface boundaries of the specimen.

The Mesh Compatibility analysis was also activated for the current analysis. The procedure is the same as when evaluating the ALLEFM. A circular contour as was plotted in Fig. 9 is evaluated but with radius equal to the mesh parameter R in all crack tips. When any of these mesh contours crosses another crack or any other surface, the user has to manually force crack coalescence or failure of the structure. However, in the present study no contour mesh crossed any other crack.

In this example, three convergence analyses were done for plane strain conditions by reducing $h_1, \Delta a_{lim}$ and Δn. The parameters $h_1 = 0.6$ mm, $\Delta a_{lim} = 0.0469$ mm and $\Delta n = 10^3$ cycles are considered adequate enough and they are used for the rest of analysis in this example. Reducing the parameters to $h_1 = 0.3$ mm, $\Delta a_{lim} = 0.0344$ or $\Delta n = 10^2$ cycles did not present any variation in fatigue life higher than 1.24%.

The mesh is based on 1673 elements and 5075 nodes. Fig. 10 shows a comparison between the plane stress and plane strain conditions. Indeed the plane strain analysis leads to a faster fatigue crack growth than in plane stress analysis, as can be deduced from Eq. (5) [13].

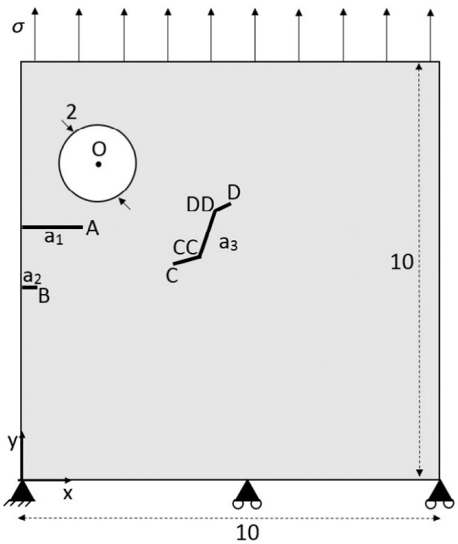

	x	y
A	1.5	5
B	0.25	4
C	3.5	3.7
D	4.5	5.8
CC	4	4
DD	4.3	5.7
O	3	7

Fig. 8. Geometry, loads and constraints for MSD fatigue analysis of a plate with a hole. Dimensions in mm.

Please cite this article in press as: Ruiz-Muñoz GA. Method to analyse multiple site damage fatigue before and after crack coalescence. Engng Fract Mech (2017), https://doi.org/10.1016/j.engfracmech.2017.09.011

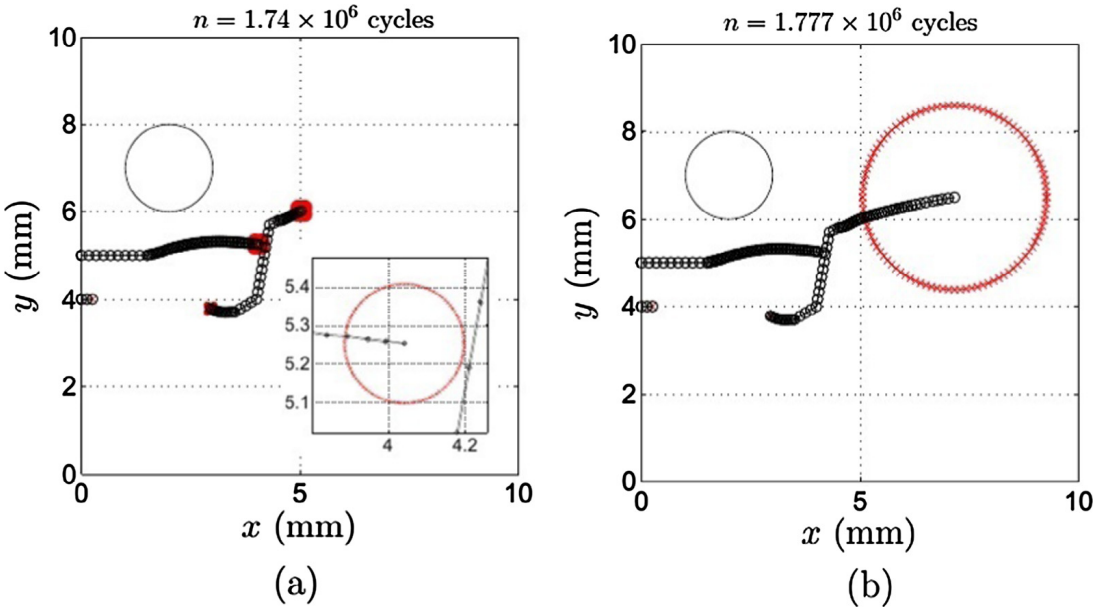

Fig. 9. Analysis of crack propagation under plane strain conditions: (a) First crack coalescence occurs; (b) Last Δn LEFM is applicable.

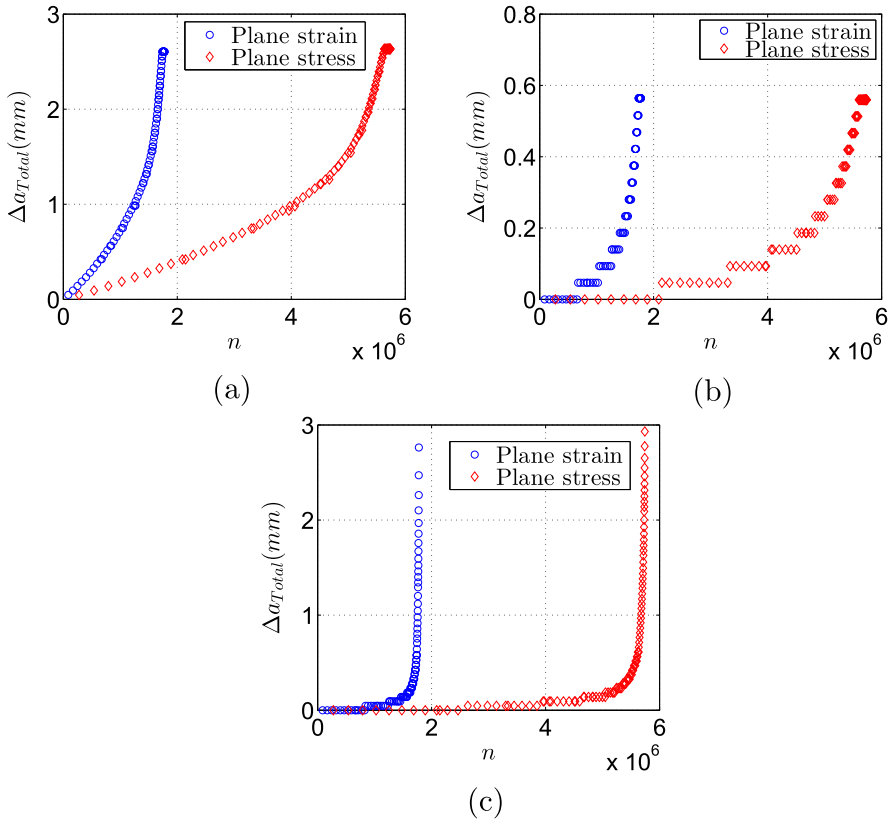

Fig. 10. Comparison of the total crack growth Δa_{Total} between plane stress (Crack closure parameter $\alpha = 1$) and plane strain (Crack closure parameter $\alpha = 3$) analysis: (a) Crack tip A; (b) Crack tip C; (c) Crack tip D.

The Fig. 10 presents a different behaviour of crack growth for every crack tip. The crack growth from crack tip A appears from the beginning of the fatigue study and it accelerates as crack tip A approaches another crack. On the other hand, the crack growth from crack tip D is only significant once crack coalescence appears.

Please cite this article in press as: Ruiz-Muñoz GA. Method to analyse multiple site damage fatigue before and after crack coalescence. Engng Fract Mech (2017), https://doi.org/10.1016/j.engfracmech.2017.09.011

There are some cycles in Fig. 10 where the total crack growth Δa_{TOTAL} is apparently constant. Even though crack growth exists, it is not large enough to present a noticeable modification to the geometry: $\Delta a_{cum} < \Delta a_{lim}$. Fig. 10 only accounts for crack growths once they cross the limit $\Delta a_{cum} \geqslant \Delta a_{lim}$.

A further study is performed to evaluate the computational efficiency of the method. The current results are compared against using a smaller crack growth step, i.e $\Delta a = 0.0252$ mm. Even though the results are very similar, the computational time is increased by 37% when using the smaller crack growth step. This analysis is an example of how computational time is saved by using the value of Δa from the convergence analysis and not smaller values.

6. Discussion of equivalent SIF approach

The concept of equivalent stress approach was introduced in this publication in order to address mixed mode crack propagation problems with equations that were originally formulated for pure mode-I cases. The equivalent SIF concept was described for an infinitesimally small crack growth. The computational analysis approaches that assumption by reducing the crack step Δa until fatigue life results do not significantly vary.

Apart from the scientific background in using equivalent SIF for the Paris Law formulation, e.g. [5,7,10], and the equivalent SIF definition already described, two additional reasons explain the applicability of equivalent SIF. The first reason is the simplicity and closed form solution of all the equations presented in this research. The second refers to an argument in [10]: as cracks propagate towards pure mode-I, the different equivalent stress criterion lead to very similar results. The same concept is used in the present publication: the difference between the equivalent SIF approach and more advance mixed mode formulation decreases with increasing crack growth rate towards pure mode-I.

Consequently, the approach suggested might not be applicable if high mixed mode conditions prevail during crack growth or if the cracks do not grow towards pure mode-I, e.g. some cases of non-proportional loading [23]. Further research is needed to account for these limitations.

7. Further improvements

The system still needs several improvements. The crack coalescence is done manually, which does not lead to a fully automatic process. Moreover, the system cannot do FEA when material is enclosed by two cracks, e.g. when two surface cracks intersect one another. In addition, each FEA requires the ANSYS package to restart, which is computationally time consuming compared to the rest of the operations in the method. Future research needs to reduce the drawbacks mentioned above and benchmark the whole system with a real experimental case of an MSD specimen under fatigue, mixed mode and closure problems. The research could be extended to the analysis of 3D structures, where the complexity of resulting shapes after coalescence would require a more advanced strategy for crack modelling.

8. Conclusions

The current study proposes an innovative method to efficiently design and evaluate MSD fatigue in a 2D structure. Cracks are generated in an FE model by simply assigning coordinates to their vertices. Computational efficiency is reached by a convergence analysis of the crack growth step. The method accounts for closure problems for plane stress and plane strain approaches under mixed mode conditions. The coalescence is addressed using the ALLEFM. Consequently, the simple and well-known Paris Law formulation is applicable for the entire fatigue analysis.

The method has shown good computational time performance by comparison with other crack growth steps. Additionally, the method has proved to give good results for the analysis of SIFs in the tilted crack and the two parallel cracks cases. The system accurately reproduced the results of a crack direction experiment. Finally, a comparison with other existing tools in a multiple crack propagation case has presented good performance.

A multiple crack growth analysis has been studied in a plate with a hole. The method has been able to evaluate crack coalescence by applying ALLEFM. Predominant cracks were easily identified by using the proposed fatigue analysis. The plane strain and plane stress conditions have been compared. Crack growth is faster in plane strain, which is coherent with closure theory.

Several improvements are proposed for future research. Fully automatic crack coalescence or 3D MSD with closure, coalescence and mixed mode conditions are among those improvements.

Funding

This research was supported by the strategic research project Advancing BeYond Shallow waterS (ABYSS), funded by Innovation Fund Denmark, Grant No. 1305-00020B, and in collaboration with DONG Energy. The sponsors have not influenced the outcome of the present publication and the decision to publish was done by the author. The author followed the regulations of his institutions concerning intellectual rights and there are no impediments for publication with respect to intellectual properties.

Please cite this article in press as: Ruiz-Muñoz GA. Method to analyse multiple site damage fatigue before and after crack coalescence. Engng Fract Mech (2017), https://doi.org/10.1016/j.engfracmech.2017.09.011

Acknowledgement

The author thanks all aid from supervisors Christian Niordson, Thomas Østergaard, and especially from Rachel Meyer, Martin Eder and Mathias Stolpe, whose observations gave a great input to this study.

Appendix A. Crack geometry

The theory exposed in the current research is valid as long as crack tip geometries are correctly approximated as infinite sharp edges. Case $\mathcal{A}$ in Fig. 11 shows how surface cracks are modelled. The input coordinates are denoted by O and A_i. First the $\overline{OA}_1$ line is used to reach a model with coordinates $B_1^{(1)},\ldots,B_1^{(6)}$. Then, the internal geometry coordinates A_i are used to generate the geometry of the rest of the 2D crack. The geometry of the cracks follows two characteristics:

- A crack tip angle of 5 degrees is assumed to be small enough to simulate infinite sharp cracks. Therefore $\gamma = 2.5^\circ$ in Fig. 11. The validity of this assumption is checked in Appendix C.
- The method can reproduce finer cracks by modifying the parameter d_{lim}. This parameter establishes a number of divisions b_i in each crack face. For instance, in the Case $\mathcal{A}$, Fig. 11, the segment $\overline{OA_1}$ is divided into three segments $b_1 = 3$ with distance $d_1 = \overline{OA}_1/b_1$. The number of divisions b_1 is found as $|\overline{OA}_1|/b_1 = d_1 \leqslant d_{lim}$ and $|\overline{OA}_1|/(b_1-1) > d_{lim}$. The same procedure is followed to find b_i for the rest of the crack geometry: $\overline{A_iA_j}$.

If d_{lim} is assigned to a large value, the crack representation is coarse, and thus, far away from the infinite crack approach. Fig. 11 shows that in Case $\mathcal{B}$, where $d_{lim} \geqslant \overline{OA}_1$, the crack results in a much coarser shape than in Case $\mathcal{A}$. The use of bisectors to geometrically model cracks ensures that the distance between two parallel crack surfaces is always kept constant. For example, the distance between line $\overline{B_1^{(1)}B_1^{(5)}}$ and line $\overline{B_1^{(2)}B_1^{(6)}}$ is the same as between $\overline{B_1^{(5)}B_2^{(3)}}$ and $\overline{B_1^{(6)}B_2^{(4)}}$.

In the case of internal cracks, Fig. 12, the 2D geometry is built up from one crack tip O_1 all along until the other crack tip O_2. The construction procedure is the same as the surface crack modelling, except that the crack angle $\gamma_1 = 2.5^\circ$ is only assigned to one crack tip. The other angle, γ_2, is a result of the construction.

The present method includes the possibility of coalescence during multiple crack propagation. Fig. 13 shows a typical situation for the coalescence modelling. After a fatigue crack growth calculation, if the new position of the crack tip results at

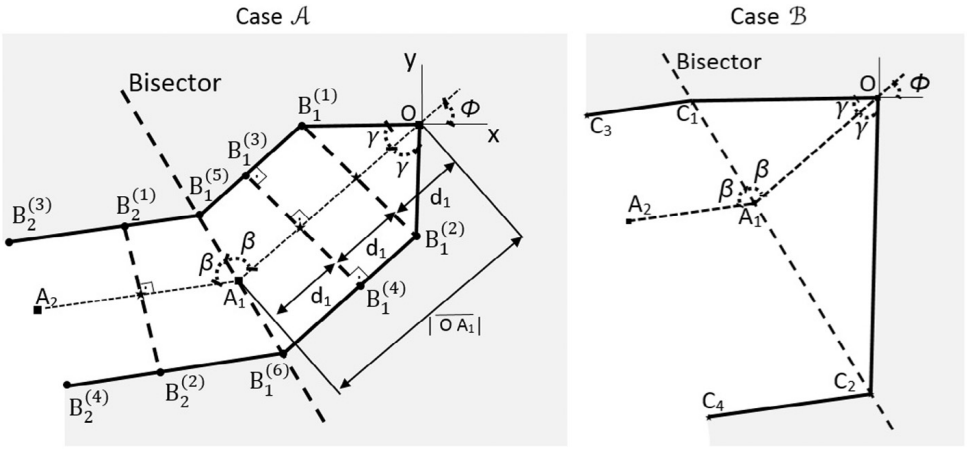

Fig. 11. Two alternatives to model surface cracks. Case $\mathcal{A}$ is used for the method proposed. Case $\mathcal{B}$ results when $d_{lim} \geqslant \overline{OA}_1$ and it is avoided in the current research.

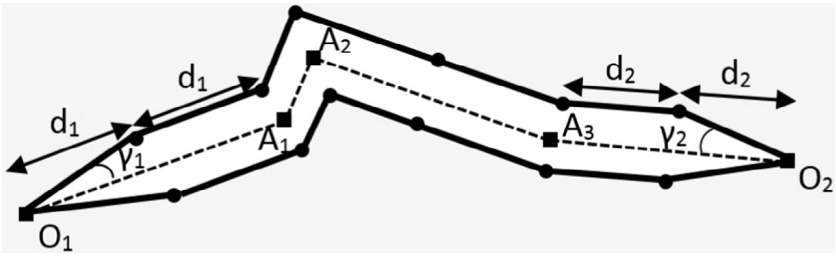

Fig. 12. Modelling of an internal crack. The proposed method is able to model irregular shapes.

Please cite this article in press as: Ruiz-Muñoz GA. Method to analyse multiple site damage fatigue before and after crack coalescence. Engng Fract Mech (2017), https://doi.org/10.1016/j.engfracmech.2017.09.011

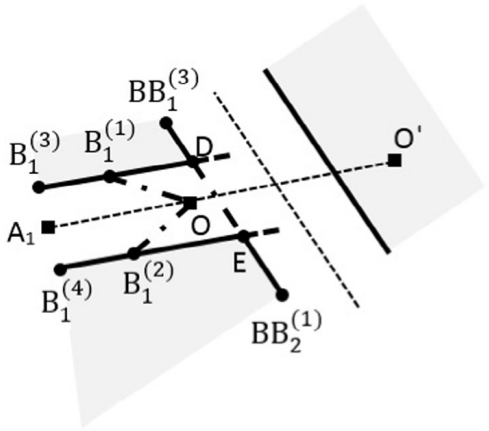

Fig. 13. Modelling crack coalescence. The crack tip is relocated from coordinates O′ to O. The crack tip geometry is then transformed to coalescence geometry.

O′, where one crack crosses another, the crack tip is relocated to a new coordinate at O. Then, the cracks are modelled as shown in Case $\mathcal{A}$, Fig. 11. The D and E coordinates in Fig. 13 are generated, and the lines $\overline{B_1^{(1)}O}$, $\overline{B_1^{(2)}O}$ and $\overline{B_{1'}B_{2'}}$ are deleted. Finally, the D and E coordinates are linked to the rest of the structure.

Appendix B. Element types and mesh topology

Anderson [9] suggests that quadratic elements are normally used for the crack analysis. In the present paper, the 8-node quadratic elements are chosen in order to reduce the level of refinement compared to linear element meshes and the level of complexity of Lagrangian elements. The commercial Finite Element software package ANSYS® Mechanical 16.0 [18] is selected for the fracture mechanics analysis since it includes an element type with the characteristics exposed, PLANE 183. In addition, ANSYS is able to calculate the mixed mode SIFs by applying the principles of the Interaction Integral [24].

The required parameters for the mesh modelling in ANSYS are shown in Fig. 14. The element size at the boundaries and distant from the crack tip is h_1, whereas the element size around the crack tip is h_2. The radius of the spider-web mesh is R. In addition, the mesh set up needs to include the number of elements around the crack tip, N_1.

Appendix C. Mixed mode SIF of tilted crack in plate under pure tension

Fig. 15 shows the analysis of a tilted crack with geometries $H/a = 40$, $W/a = 20$ and $\phi = 30^\circ$. The analytical expression can be found in [9] as $K_I = K_{I(0)} \cos^2 \phi$ and $K_{II} = K_{I(0)} \cos \phi \sin \phi$, where $K_{I(0)} = \sigma\sqrt{\pi a}$ follows a case of infinite width and height, and σ is a tensional load. Convergence is found at 1673 elements and 5075 nodes. Doubling the width and height of the geometry did not present any significant variation. As a consequence, the infinite width and height approach is considered a valid assumption. In addition, results obtained by reducing the crack angle γ to half are not significantly different. Thus, the assumption $\gamma = 2.5^\circ$ to represent an infinite sharp crack is considered adequate for the method. Finally, varying the angle to $\phi = 0^\circ, \phi = 10^\circ$ and $\phi = 20^\circ$ shows errors below 3% between numerical and analytical results.

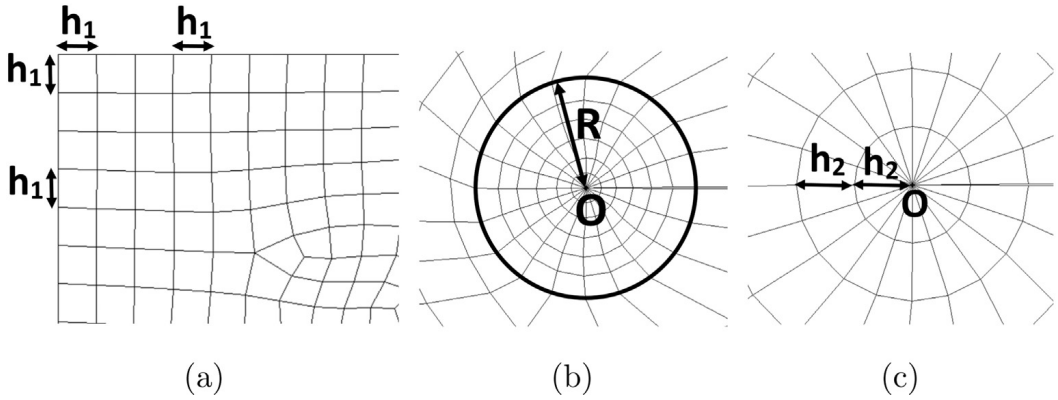

Fig. 14. Different mesh parameters for the FE model: (a) Global mesh; (b) Spider-web mesh; (c) Element size around the crack tip.

Please cite this article in press as: Ruiz-Muñoz GA. Method to analyse multiple site damage fatigue before and after crack coalescence. Engng Fract Mech (2017), https://doi.org/10.1016/j.engfracmech.2017.09.011

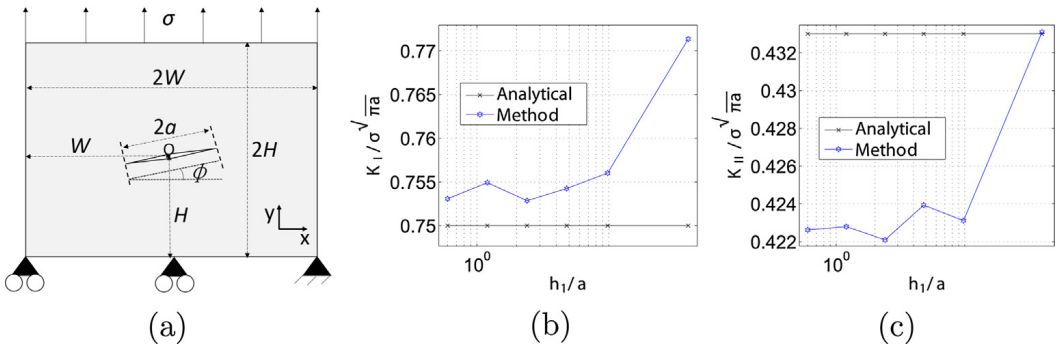

Fig. 15. Analysis of a tilted crack under pure tension: (a) Geometry, loads and constraints; (b) Mode-I SIF comparison; (c) Mode-II SIF comparison.

Appendix D. SIF of two paralel cracks in a plate under pure tension

Fig. 16 shows the analysis of SIFs of two parallel cracks under pure tension. The results are compared with the computational results from Jiang [4], where $W/a = 4$ and $b/a = 1$. A ratio of $H/a = 20$ was assumed to be large enough for infinite height analysis. The SIF are compared with the analytical solution of a central crack $K_0 = \sigma\sqrt{\pi a}$. Convergence is reached at 1010 elements and 3053 nodes. Calculations doubling the height do not result in any change of SIF at the scale of results shown in this exercise. Consequently, the present example agrees well with infinite height assumptions. In addition, results from other crack tips are not significantly different.

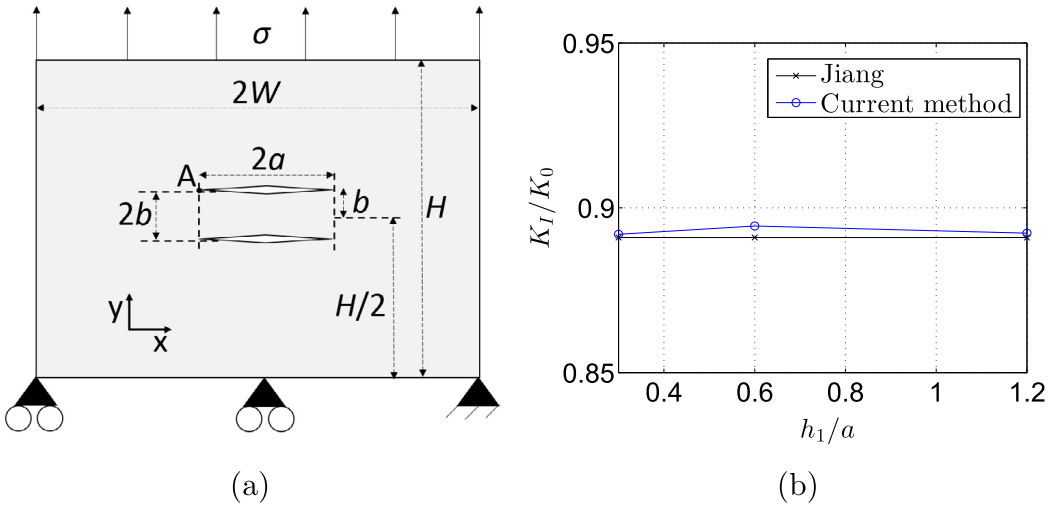

Fig. 16. Analysis of 2 parallel cracks under pure tension: (a) Geometry, loads and constraints; (b) SIF comparison for crack tip A.

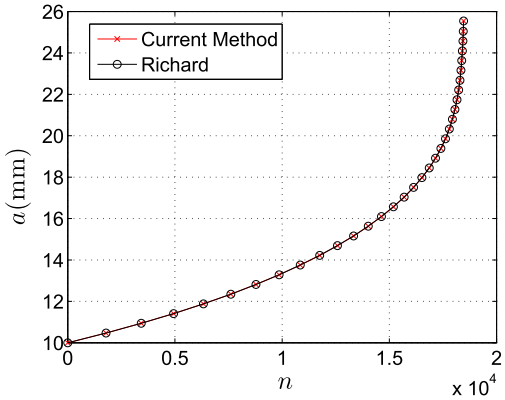

Fig. 17. Case of study from Section 4.2 about fatigue analysis of crack tip 1. Comparison between using current method Eq. (3) and the equation proposed by Richard et al. [11], Eq. (2). Results are essentially the same since smooth crack propagation under mixed mode presents $K_I \gg K_{II}$.

Please cite this article in press as: Ruiz-Muñoz GA. Method to analyse multiple site damage fatigue before and after crack coalescence. Engng Fract Mech (2017), https://doi.org/10.1016/j.engfracmech.2017.09.011

Appendix E. Comparison between different Equivalen SIF formulations

The case in Fig. 6 is evaluated using the equivalent SIF range proposed in Eq. (2). A comparison between the proposed method using Eq. (3) and using Eq. (2) is shown in Fig. 17. The results are essentially the same, as the relation $K_I \gg K_{II}$ is kept during crack propagation. This finding is coherent with that stated from Meggiolaro et al. [10], where all crack path are toward pure mode-I in every single crack growth, and therefore different equivalent SIF criteria are linked to very similar results.

References

[1] Xu S, Wang Y. Estimating the effects of corrosion pits on the fatigue life of steel plate based on the 3D profile. Int J Fatigue 2015;72:27–41.
[2] European committee for standardization. Welding and allied processes-Classification of geometric imperfections in metallic materials-Part 1: fusion welding (ISO 6520-1:2007), Trilingual version EN ISO 6520-1:2007. Brussels: CEN; 2007.
[3] Skorupa A, Skotupa M. Riveted lap joints in aircraft fuselage: design, analysis and properties. 4th ed. Harlow: Pearson; 2012.
[4] Jiang ZD, Zeghloul A, Bezine G, Petit J. Stress intensity factors of parallel cracks in a finite width sheet. Eng Fract Mech 1990;35:1073–9.
[5] Dündar H, Ayhan AO. Three-dimensional fracture and fatigue crack propagation analysis in structures with multiple cracks. Comput Struct 2015;158:259–73.
[6] Price RJ, Trevelan J. Boundary element simulation of fatigue crack growth in multi-site damage. Eng Anal Bound Elem 2014;43:67–75.
[7] Liu YJ, Li YX, Xie W. Modeling of multiple crack propagation in 2-D solids by the fast multipole boundary element method. Eng Fract Mech 2017;172:1–16.
[8] Rahman S, Ghadimian O, Ranjbaran M. Study on life and path of fatigue cracks in multiple site damage plates. Int J Fatigue 2015;80:449–58.
[9] Anderson TL. Fracture mechanics: fundamentals and applications. 3rd ed. Boca Raton: CRC Press Taylor & Francis Group; 2005.
[10] Meggiolaro MA, Miranda ACO, Castro JTP, Martha LF. Stress intensity factor equations for branched crack growth. Eng Fract Mech 2005;72:2647–71.
[11] Richard HA, Sander M, Fulland M, Kullmer G. Development of fatigue crack growth in real structures. Eng Fract Mech 2008;75:331–40.
[12] Erdogan F, Sih GC. On the crack extension in plates under plane loading and transverse shear. J Basic Eng 1963;85:277–519.
[13] Newman Jr JC. A crack opening stress equation for fatigue crack growth. Int J Fracture 1984;24:131–5.
[14] Newman Jr JC. A Crack-Closure model for Predicting Fatigue-Crack Growth under Aircraft Spectrum Loading. Hampton: Langley Research Center; 1981 Jan. Report No. NASA-TM-81941.
[15] Maierhofer J, Pippan R, Gänser HP. Modified NASGRO equation for physically short cracks. Int J Fatigue 2014;59:200–7.
[16] Dowling NE. Mechanical behavior of materials. 4th ed. London: Springer; 2013.
[17] Matlab Documentation. Version R2013b; 2013.
[18] ANSYS Documentation. Version 16.0.0; 2014.
[19] Kim J-H, Paulino GH. Finite element evaluation of mixed mode stress intensity factors in functionally graded materials. Int J Numer Meth Eng 2002;53:1903–35.
[20] Ingraffea AR, Grigoriu M. Probabilistic Fracture Mechanics: A Validation of Predictive Capability. Report No. 90-8. Department of structural Engineering, Cornwell University; 1990.
[21] Bittencourt TN, Wawrzynek PA, Ingraffea AR, Sousa JLA. Quasi-automatic simulation of crack propagation for 2D LEFM problems. Eng Fract Mech 1996;55:321–34.
[22] Rohatgi, A. WebPlotDigitalizer Version 3.10. [Accessed 2016 Aug] Available from: URL: <http://arohatgi.info/WebPlotDigitizer/>.
[23] Zerres P, Vormwald M. Review of fatigue crack growth under non-proportional mixed-mode loading. Int J Fract 2014;58:75–83.
[24] Kuna M. Solid mechanics and its applications: finite elements in fracture mechanics, vol. 201. Waterloo: Springer; 2013.

Please cite this article in press as: Ruiz-Muñoz GA. Method to analyse multiple site damage fatigue before and after crack coalescence. Engng Fract Mech (2017), https://doi.org/10.1016/j.engfracmech.2017.09.011

Appendix B A conservative approach for Mode I-II fatigue analysis under residual stresses: The RSIF Proportionality Conjecture (Manuscript B)

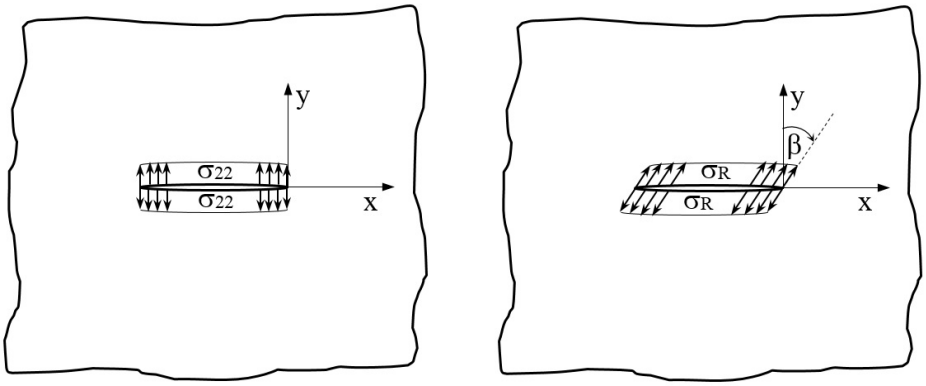

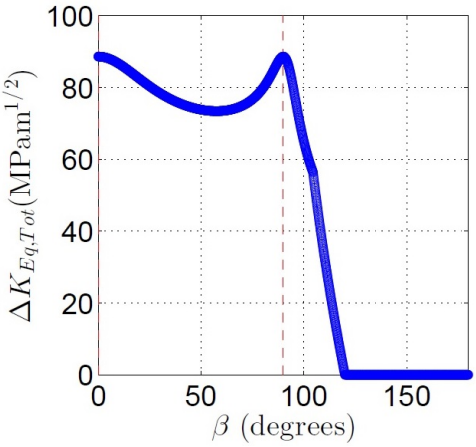

$$\frac{K_I^{max}}{K_{II}^{max}} = \frac{K_{I,RS}}{K_{II,RS}}$$

A conservative approach for Mode I-II fatigue analysis under residual stresses: The RSIF Proportionality Conjecture.

G.A. Ruiz Muñoz[a,b,*], M.A. Eder[b]

[a] *Ørsted, Nesa Allé 1, 2820 Gentofte, Denmark*
[b] *Department of Wind Energy, The Technical University of Denmark (DTU), 4000 Roskilde, Denmark*

Abstract

Residual stresses are a crucial aspect of fatigue life predictions of welded structures. However, their implementation in fatigue crack growth simulations can be tedious. In this paper, a novel approach is proposed which considers the effects of residual stresses in a worst-case scenario by applying the *Maximum Tangential Stress Criterion* and maximising the crack growth rate. Results demonstrate that computationally demanding analysis of residual stresses can be avoided by assuming the residual stress intensity factors are proportional to the stress intensity factors induced by the externally applied cyclic load. This approach is referred to as the *Residual Stress Intensity Factors (RSIF) Proportionality Conjecture*, which is particularly useful for inspection planning of complex structures subject to mixed-mode crack propagation situations, where the computational recovery of current residual stress states by consideration of their temporal evolvement is cumbersome.

*Mobile Phone:0045-99557811
Email address: g_a.ruiz@hotmail.com & gusru@orsted.dk (G.A. Ruiz Muñoz)

Keywords: Residual stresses, Mixed mode, Fatigue, Crack, Weld

Nomenclature

a	Crack length.
Δa	Crack growth.
Δa_f	Final crack growth.
Δa_{lim}	Crack growth limit.
a	Crack length.
C	Paris Law parameter.
F	External load.
K_{Eq}	Equivalent Stress Intensity Factor(SIF).
K_{Eq}^{max}, K_{Eq}^{min}	Maximum and minimum equivalent SIF.
$K_{Eq,Tot}^{max}$, $K_{Eq,Tot}^{min}$	Maximum and minimum equivalent total SIF.
K_I, K_{II}	SIF for mode-I and mode-II.
$K_{I,RS}$, $K_{II,RS}$	Residual stress SIF(RSFI) for mode-I and mode-II.
$K_{I,App}^{max}$, $K_{II,App}^{max}$	Maximum SIF of the periodic load for mode-I and -II.
$K_{I,App}^{min}$, $K_{II,App}^{min}$	Minimum SIF of the periodic load for mode-I and -II.
$K_{I,Tot}^{max}$, $K_{II,Tot}^{max}$	Maximum total SIF for mode-I and mode-II.
$K_{I,Tot}^{min}$, $K_{II,Tot}^{min}$	Minimum total SIF for mode-I and mode-II.
K_{IC}	Fracture toughness.
m	Paris Law parameter.
n	Number of nodes.
N	Number of cycles.
p	Domain parameter.

Nomenclature

r	Distance from the crack tip.
R	Stress ratio.
R_{Appl}	Stress ratio corresponding to the cyclic load.
x, y	Cartesian axis reference.
Δa_{Total}	Total crack growth.
ΔK_{Eq}	Equivalent SIF range.
$\Delta K_{Eq,Tot}$	Equivalent SIF range including cyclic loads and RS.
β	RS orientation.
ε_1	Relative error.
λ	Load ratio.
θ	Crack propagation direction.
θ^{max},θ^{min}	Crack propagation direction for maximum and minimum load.
$\sigma_{\theta\theta}$	Tangential stress around the crack tip.
σ_R	Residual Stress(RS).
σ^{max}, σ^{min}	Maximum and minimum nominal stress.

1. Introduction

New fatigue life predictive methods for welded connections (e.g. in offshore structures) become increasingly important for industry in order to improve reliability in the design of new large-scale structures and for inspection planning of existing structures. Accurate numerical fatigue life prediction of welded connections faces three major challenges: the first concerns computational efficiency required for time history analysis of complex and extensive

multi-axial stress histories; the second is posed by complex part and weld geometries; the third concerns knowledge about the present conditions of the welded zone such as flaw sizes, flaw distribution and Residual Stresses (RS) fields, to name a few.

Any welding seam has been subject to thermal processes and inherently incorporates geometrical imperfections as e.g. stated in [1]. The welding process induces RS in the weld seam itself, as well as in the parental material in close vicinity of the weld, typically referred to as the Heat Affected Zone (HAZ). According to Al-Mukhtar [2], the RS can either be tensional or compressive, where the first is detrimental and the latter beneficial for the fatigue life of a component.

Two major techniques used to estimate the fatigue life of a weld exist to date: the Stress Based (SB) approach and the Fracture Mechanics (FM) approach. The stress based methods, e.g hot spot stress approach, predict failure through stress extrapolation techniques together with experimental S-N curves stipulated in standards such as DNVGL-RP-C203 [3]. The experimental S-N curves correspond to welds which inherently incorporate RS effects. The benefits of the SB methods are mainly versatility and computational efficiency. However, SB methods do not track crack propagation over time, which is an important feature for inspection planning [4].

On the other hand, the FM models allow for crack propagation analysis where the RS distributions are required for an accurate fatigue life prediction. The three major methods to obtain RS distributions are the parametric formulation, Thermo-Mechanical Finite Element Analysis (TMFEA) and the experimental methods. The parametric formulations of RS are found in stan-

dards, e.g. BS7910 [5], where closed-form solutions for RS fields are provided. However, the number of parametric formulations is limited to a small range of rather simplistic geometries.

The TMFEA calculates the RS field by simulating the welding procedure [6]. This method can be applied to any arbitrary geometry. Nevertheless, TMFEA is computationally demanding in comparison to parametric formulation techniques.

Finally, the RS field can be measured through experimental characterisation methods such as e.g. neutron diffraction [7]. Such characterisation techniques result in realistic RS distributions. However, these experiments are costly and time-consuming, usually exceeding the effort necessary for TMFEA.

The effects of such obtained RS distributions can subsequently be considered in fracture mechanics-based models through different approaches. Bao et al. [8] proposed a method to impose RS using weight functions. Alternatively, Seifi [9] suggests to impose the RS as an initial state and calculate the Stress Intensity Factors (SIFs) through a modified J-Integral equation. Sumi et al. [10] investigated the effect of biaxial RS on the fatigue life. Their results show a considerable dependency of both crack path and crack propagation rate on RS - emphasising the importance of their consideration.

It is noteworthy to mention that post-weld treatments, e.g. post-weld heat treatment, can change the initial RS distribution as pointed out by Pingsha [11]. Moreover, the RS may relax and be altered over time due to creep [12] or external loading processes [13].

Two main RS relaxation mechanisms can be observed: tensional RS relax-

ation and compressive RS relaxation. Since the tensional RS is detrimental to the life of a structure [2], if tensional RS relaxation is not accounted for in the FM model, the fatigue life prediction is considered conservative. Conversely, if compressional RS relaxation is disregarded, the predicted fatigue life can be overestimated.

Despite the availability of sophisticated RS analysis techniques, their application to existing structures faces practical limitations. The prediction of RS distributions and their relaxation over time in a multitude of different welded connections of large scale structures, e.g. wind farms, bear high levels of uncertainty and require a high computation effort all of which renders the RS distributions highly impractical.

This paper proposes a novel, conservative and computationally efficient approach to evaluate the effect of RS distributions on numerical fatigue life prediction, primarily intended for inspection planning of large scale structures. In the aforementioned context, conservative refers to an overestimation of the predicted propagation rate in comparison to the expected rate occurring in reality. That is to say, the real crack propagation rate is conservatively approximated from the lower bound. This stipulation ensures conservative inspection intervals which are based on the estimation of the crack depth over time, as e.g. Sørensen shows in [14]. The analyses presented are restricted to cases of positive external loading ratios and crack propagation is assumed to belong to the Paris Law regime, as described in [15].

The main implication of the proposed method is the possibility of avoiding RS analysis in the framework which significantly decreases computation

time. The effects of RS are considered in an analytically derived - worst-case scenario - numerically evaluated at every crack propagation step. Additionally, the formulation and findings presented can be directly extrapolated to other combinations of static or quasi-static loading with a cyclic load.

2. Fracture mechanics approach to fatigue analysis under RS.

Inspection plans demand mechanisms to predict and track crack propagation over time [4]. Since large scale structures typically involve multi-directional stress states, a mixed-mode crack propagation method is usually required. A FM approach can predict crack propagation under mixed-mode conditions [15]. The FM analysis of welds is commonly done within the realm of Linear Elastic Fracture Mechanics (LEFM), as discussed by e.g. Ahmed [2] and Barosoum [16]. The striking advantage of LEFM is its simplicity, allowing for superposition in addition to computational efficiency, compared to advanced models such as e.g. Elasto-Plastic Fracture Mechanics (EPFM) [15]. Assuming LEFM and mixed-mode I-II, the crack propagation can be described through the modified Paris Law formulation [17, 18, 19]

$$da/dN = C(\Delta K_{Eq})^m, \tag{1}$$

where m and C are material parameters, a is the crack length, N is the number of cycles and ΔK_{Eq} is the equivalent Stress Intensity Factor(SIF) range. The parameter C increases by increasing the stress ratio.[20]

The equivalent SIF range can be written as

$$\Delta K_{Eq} = K_{Eq}^{max} - K_{Eq}^{min}. \tag{2}$$

where K_{Eq}^{max} is the maximum equivalent SIF and K_{Eq}^{min} is the minimum equivalent SIF in a load cycle. Among the different equivalent SIF formulations literature provides, the K_{Eq} corresponding to the Maximum Tangential Criterion (MTC) [21] is preferred because of its availability of a closed form solution [17], which can be written as

$$K_{Eq} = K_I f(\theta) + K_{II} g(\theta), \tag{3}$$

where

$$f(\theta) = \frac{1}{4}\left(3\cos\frac{\theta}{2} + \cos\frac{3\theta}{2}\right), \tag{4}$$

$$g(\theta) = -\frac{3}{4}\left(\sin\frac{\theta}{2} + \sin\frac{3\theta}{2}\right) \tag{5}$$

and θ is the crack propagation direction.

According to the MTC, the crack propagation can be calculated as

$$\theta = 2\tan^{-1}\left(\frac{K_I}{4K_{II}} \pm \frac{1}{4}\sqrt{\left(\frac{K_I}{K_{II}}\right)^2 + 8}\right) \tag{6}$$

Eq. 6 results in two angles. The one that corresponds to the maximum tangential stress, is the crack propagation direction,

$$\sigma_{\theta\theta} = \frac{1}{(2\pi r)^{1/2}}\cos\frac{\theta}{2}\left[K_I\cos^2\left(\frac{\theta}{2}\right) - \frac{3}{2}K_{II}\sin\theta\right], \tag{7}$$

where $\sigma_{\theta\theta}$ is the tangential stress and r is the distance from the crack tip.

The mixed-mode crack propagation formulation seems fairly straight forward. However, the complexity increases when including the RS. The RS can be considered by applying superposition principles [16],

$$K_{I,Tot}^{max} = K_{I,Appl}^{max} + K_{I,RS}, \tag{8}$$

$$K_{I,Tot}^{min} = K_{I,Appl}^{min} + K_{I,RS}, \tag{9}$$

where $K_{I,Appl}$ is the mode I SIF corresponding to the external loading and $K_{I,RS}$ is the mode I SIF corresponding to RS. A similar procedure can be applied to mode II crack propagation, where

$$K_{II,Tot}^{max} = K_{II,Appl}^{max} + K_{II,RS}, \tag{10}$$

$$K_{II,Tot}^{min} = K_{II,Appl}^{min} + K_{II,RS}. \tag{11}$$

The application of superposition principles can be extended to calculate the equivalent SIF range necessary for the mixed-mode Paris law,

$$\Delta K_{Eq,Tot} = K_{Eq,Tot}^{max} - K_{Eq,Tot}^{min}. \tag{12}$$

Using the MTC given by Eq. 3 and the superposition equations described in Eqs.(8-11), the terms from Eq. 12 are calculated as

$$\begin{aligned} K_{Eq,Tot}^{max} &= K_{I,Tot}^{max} f(\theta^{max}) + K_{II,Tot}^{max} g(\theta^{max}) = \\ &= (K_{I,Appl}^{max} + K_{I,RS}) f(\theta^{max}) + (K_{II,Appl}^{max} + K_{II,RS}) g(\theta^{max}), \end{aligned} \tag{13}$$

$$\begin{aligned} K_{Eq,Tot}^{min} &= K_{I,Tot}^{min} f(\theta^{min}) + K_{II,Tot}^{min} g(\theta^{min}) = \\ &= (K_{I,Appl}^{min} + K_{I,RS}) f(\theta^{min}) + (K_{II,Appl}^{min} + K_{II,RS}) g(\theta^{min}). \end{aligned} \tag{14}$$

Substitution of Eq. 8 and Eq. 10 into Eq. 6 gives the corresponding angular crack propagation

$$\theta^{max} = 2\tan^{-1}\left(\frac{K_{I,Appl}^{max} + K_{I,RS}}{4(K_{II,Appl}^{max} + K_{II,RS})} \pm \frac{1}{4}\sqrt{\left(\frac{K_{I,Appl}^{max} + K_{I,RS}}{K_{II,Appl}^{max} + K_{II,RS}} \right)^2 + 8} \right) \tag{15}$$

whereas substitution of Eq. 9 and Eq. 11 into Eq. 6 gives

$$\theta^{min} = 2\tan^{-1}\left(\frac{K_{I,Appl}^{min} + K_{I,RS}}{4(K_{II,Appl}^{min} + K_{II,RS})} \pm \frac{1}{4}\sqrt{\left(\frac{K_{I,Appl}^{min} + K_{I,RS}}{K_{II,Appl}^{min} + K_{II,RS}} \right)^2 + 8} \right)$$

(16)

The introduction of $K^{max}_{Eq,Tot}$ and $K^{min}_{Eq,Tot}$ with a different associated crack propagation direction, i.e. $\theta^{max} \neq \theta^{min}$, leads to variations in the crack propagation direction during a single load cycle, Fig. 1. Lucht [22] proposed to update the geometry of the crack in every load cycle using the direction

$$\theta = \frac{\theta^{min} K^{min}_{Eq,Tot} + \theta^{max} K^{max}_{Eq,Tot}}{K^{min}_{Eq,Tot} + K^{max}_{Eq,Tot}}. \tag{17}$$

Lucht's equation is a simplification of the Spievak et al. proposal [23].

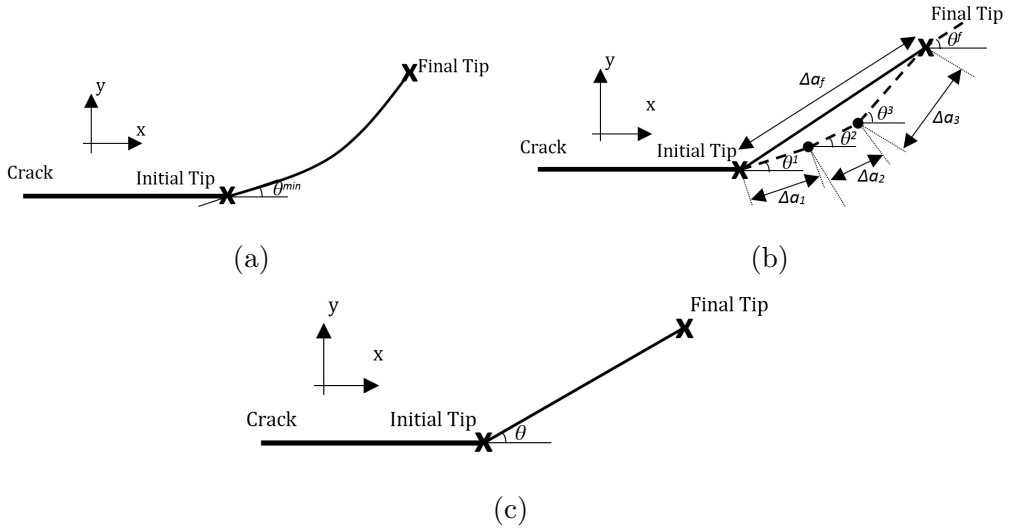

Figure 1: Three schemes for crack growth under one non-proportional loading cycle: (a) Realistic crack growth where direction continuously varies during the load cycle. (b) The crack propagation is discretized into crack growth steps with growth Δa_i and orientation θ^i. The resulting growth corresponds to Δa_f and θ^f [23]. (c) Crack growth calculated by the weighted average [22], Eq. 17.

The total equivalent SIF range from Eq. 12 can subsequently be included in the Paris Law formulation Eq. 1. The relocation of the crack tip depends

on the crack growth speed and the crack growth direction, Eq. 17.

Inspection of Eqs. (1,8-12) shows that fatigue growth depends on RS. A way to circumvent the necessity of determining the RS field would be to prove that a RS distribution exists in which Eq. 1 results in the highest crack growth rate and simultaneously ceases to be a function of $K_{I,RS}$ and $K_{II,RS}$. The solution to this problem is not straightforward since the crack relocates during cyclic loading. That is, any RS distribution which maximises $\Delta K_{Eq,Tot}$ does not necessarily lead to the most conservative growth situation, owing to crack tip roaming which might eventually decrease $\Delta K_{Eq,Tot}$ in subsequent load steps. The next two sections aim to shed some light on this circumstance.

3. A conservative RS field: The RSIF Proportionality Conjecture

In the quest for the most conservative RS distribution which maximises the fatigue growth rate, the following issues need to be addressed:

- The effect of the RS on the crack growth rate da/dn at every crack tip relocation.
- The effect of crack tip relocation on da/dn in a mixed-mode load step for a given RS configuration.

3.1. Illustrative case

An illustrative example is presented to investigate the most conservative RS field. A crack with length $2a$=2 mm is located in an infinitely large plate under plain stress/strain conditions. The material is considered isotropic and linearly elastic. Fig. 2a shows the traction stress distribution along

the crack induced by an uniaxial cyclic tensile load with maximum value $\sigma_{22}^{max} = 100\,\mathrm{MPa}\sqrt{\mathrm{m}}$ and a cyclic stress ratio $R_{Appl} = 0.5$. Fig. 2b shows a uniformly distributed residual stress traction $\sigma_R = 200\,\mathrm{MPa}\sqrt{\mathrm{m}}$, inclined with respect to the crack an angle β. The question posed is: which is the orientation β that results in the fastest crack growth propagation?

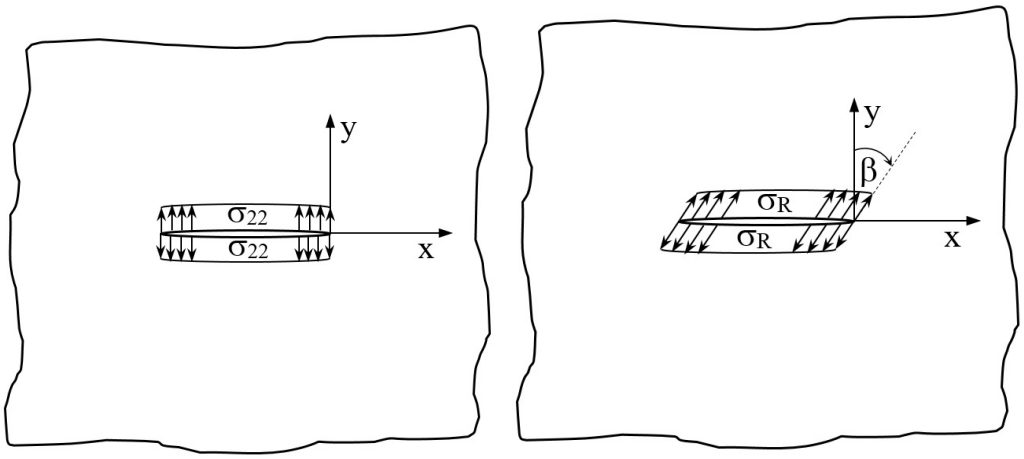

(a) (b)

Figure 2: Infinitely large plane strain/stress domain with horizontal crack of length $2a$ under two simultaneous stresses: a) pure tensional cyclic stress where $\sigma_{22} = \sigma_{22}^{max}$ when maximum stress is applied and $\sigma_{22} = \sigma_{22}^{min}$ when minimum stress is applied. b) RS tilted β degrees.

The crack growth rate in Fig. 2 is determined by Eq. 1. The parameter m and C depend on the stress ratio [20] [5] where a conservative approach is obtained by the adoption of C and m values for high stress ratios. Finally, for maximum growth rate, $\Delta K_{Eq,Tot}$ needs to be maximised, where this parameter generally is a function of the RS field.

Applying the superposition principle and formulation for mixed-mode SIF

[15], the mixed-mode SIF for example Fig. 2 are calculated as

$$K_{I,Tot}^{max} = \left(\sigma_{22}^{max} + \sigma_R \cos^2\beta\right)\sqrt{\pi a}, \tag{18}$$

$$K_{II,Tot}^{max} = \sigma_R \sin\beta\cos\beta\sqrt{\pi a}, \tag{19}$$

$$K_{I,Tot}^{min} = \left(R_{Appl}\sigma_{22}^{max} + \sigma_R \cos^2\beta\right)\sqrt{\pi a}, \tag{20}$$

where $R_{Appl} = \sigma_{22}^{min}/\sigma_{22}^{max}$, and $K_{II,Tot}^{min} = K_{II,Tot}^{max}$.

The corresponding equivalent SIF are

$$K_{Eq,Tot}^{max} = \sqrt{\pi a}\left[\left(\sigma_{22}^{max} + \sigma_R \cos^2\beta\right) f(\theta^{max}) + \sigma_R \sin\beta\cos\beta\, g(\theta^{max})\right], \tag{21}$$

$$K_{Eq,Tot}^{min} = \sqrt{\pi a}\left[\left(R_{Appl}\sigma_{22}^{max} + \sigma_R \cos^2\beta\right) f(\theta^{min}) + \sigma_R \sin\beta\cos\beta\, g(\theta^{min})\right], \tag{22}$$

where θ^{max} and θ^{min} are the crack growth directions calculated using Eq. 6, and $f(\theta^{min})$ and $g(\theta^{min})$ are calculated through Eq. 4 and Eq. 5.

The value of $\Delta K_{Eq,Tot}$ is calculated as $\Delta K_{Eq,Tot} = K_{Eq,Tot}^{max} - K_{Eq,Tot}^{min}$.The orientation β that results in the maximum $\Delta K_{Eq,Tot}$ is calculated as

$$\frac{d(\Delta K_{Eq,Tot})}{d\beta} = 0. \tag{23}$$

The analytical approach for solving Eq. 23 presents difficulties since Eq. 23 includes a boolean function when solving θ^{max} and θ^{min} using Eq. 6. Instead, Eq. 21 and Eq. 22 are solved numerically. Fig. 3 shows the $\Delta K_{Eq,Tot}$ as a function of the RS orientation angle β. Two peaks with the same value of $\Delta K_{Eq,Tot}$ are shown. The first peak occurs at β=0, where the vector σ_R is proportional to the cyclic loading. A second peak appears where σ_R is parallel to the crack, i.e. the RS have no effect on SIF calculations.

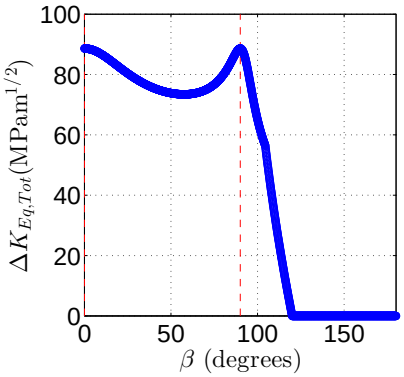

Figure 3: Variation of $\Delta K_{Eq,Tot}$ with respect to the angular orientation β of the RS. The illustration shows two peaks which correspond to the same value of $\Delta K_{Eq,Tot}$, at $\beta = 0$ degrees, where the RS vector is proportional to the cyclic loading vector σ_{22}, and $\beta = 90$ degrees, where the SIF calculations are independent of the RS magnitude.

From Fig. 3, it can be deduced that the maximum $\Delta K_{Eq,Tot}$ is found when either the RS tensor components are proportional to the cyclic stress components or when the RS have no effect on the SIF. In both cases, $\Delta K_{Eq,Tot}$ is the same as not including RS in the SIF calculations.

3.2. Numerical Crack Growth analysis for the different RS distributions

The case from Fig. 2 includes the analysis of the stresses σ_{22} and σ_R. However, in a generic case it might not be possible to analytically find the relation between stresses and SIF, i.e. $\Delta K_{Eq,Tot}(\sigma_{22}^{max}, \sigma_{RS}, ...)$. As a consequence, the next analyses are performed in terms of SIF. From Eq. 12, and using Eq. 13 and Eq. 14, the RS that present the highest $\Delta K_{Eq,Tot}$ fulfil

$$\partial(\Delta K_{Eq,Tot})/\partial K_{I,RS} = 0 \quad \text{and} \quad \partial(\Delta K_{Eq,Tot})/\partial K_{II,RS} = 0. \tag{24}$$

The Eq. 24 includes the same boolean expression as in Eq. 23. As a result, a numerical approach is suggested in order to find the RSIFs that lead to

the highest crack growth. The following studies are based on dimensionally-normalised parameters.

3.2.1. Numerical analysis of a single case

In the following case, Eq. (13-16) are normalized with $K^{max}_{I,Appl}$ and included in Eq. 12. A ratio $K^{min}_{I,Appl}/K^{max}_{I,Appl} = 0.2$ and mixed-mode conditions $K^{max}_{I,Appl}/K^{max}_{II,Appl} = 5$ are adopted. The numerical domain is included in a matrix with 100x100 nodes. Fig. 4a shows that the 3D surface has a distinct maximum in the form of a linear ridge in the domain. Fig. 4b shows a vertical section through the surface from which it can easily be seen that the peak indeed occurs at the closest position to $K_{I,RS}/K_{II,RS} = K^{max}_{I,Appl}/K^{max}_{II,Appl} = 5$. Consequently, it can be inferred that the maximum $\Delta K_{Eq,Tot}/K^{max}_{I,Appl}$ is found when the RS are proportional to the externally applied stresses $K_{I,RS}/K_{II,RS} = K^{max}_{I,Appl}/K^{max}_{II,Appl}$. Henceforth, this situation will be referred to as the *The RSIF Proportionality Conjecture*.

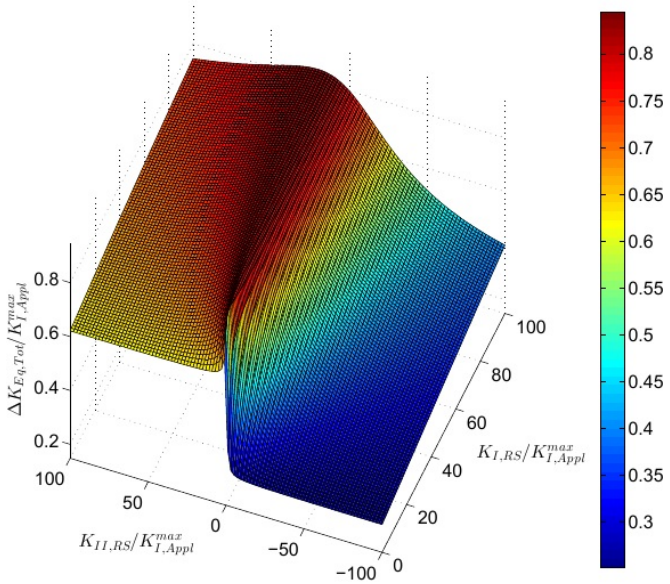

(a)

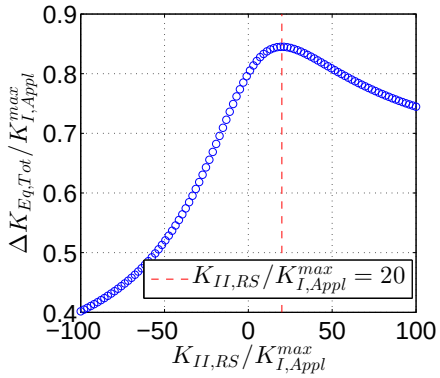

(b)

Figure 4: Normalized values of $\Delta K_{Eq,Tot}$: (a) 3D surface for different $K_{I,RS}/K^{max}_{I,Appl}$ and $K_{II,RS}/K^{max}_{I,Appl}$. As $K_{I,RS}/K^{max}_{I,Appl}$ decreases, the peak width also decreases. However, no singularities are reached; (b) Vertical section of the 3D surface taken at position $K_{I,RS}/K^{max}_{I,Appl} = 100$. The maximum peak is close to $K_{I,RS}/K_{II,RS} = 100/20 = 5 = K_{I,Appl}/K_{II,Appl}$.

3.3. The RSIF Proportionality Conjecture

Assuming any arbitrary crack under cyclic mixed-mode loading conditions, where K_I^{max} and K_{II}^{max} denote the maximum mode-I,-II SIF, and K_I^{min} and K_{II}^{min} denote the minimum mode-I,-II SIF.

Condition: If the external loading is proportional such that the following condition holds:

$$\frac{K_I^{max}}{K_{II}^{max}} = \frac{K_I^{min}}{K_{II}^{min}} \quad \text{where} \quad K_I^{max,min} \geq 0 \text{ and } K_{I,II} \, \epsilon \, \mathbb{R} \tag{25}$$

Conjecture: The RSIF proportionality conjecture states that the maximum equivalent SIF range $\max(\Delta K_{eq})$ is attained if the RSIF ratio is proportional to the cyclic loading SIF ratio, according to the following condition:

$$\frac{K_I^{max}}{K_{II}^{max}} = \frac{K_{I,RS}}{K_{II,RS}} \quad \text{where} \quad K_{I,RS} \geq 0 \text{ and } K_{I,II} \, \epsilon \, \mathbb{R} \tag{26}$$

where $K_{I,RS}$ and $K_{II,RS}$ are RSIF for mode-I,II.

Corollary: If the RSIF ratio is proportional to the cyclic loading SIF ratio, it follows that the $\max(\Delta K_{eq})$ becomes exclusively a function of the external mode-I,-II SIF.

3.3.1. Demonstration of the RSIF Proportionality Conjecture on the entire RS field

In an attempt to make a general investigation, the RS domain is extended in order to investigate if the *RSIF Proportionality Conjecture* leads to the highest $\Delta K_{Eq,Tot}/K_{I,Appl}^{max}$ for any RS configuration. The RS domain is defined in a 200x200 matrix with $K_{II,RS}/K_{I,Appl}^{max}$ ranging from $-100p$ to $100p$ and $K_{I,RS}/K_{I,Appl}^{max}$ ranging from 0 to $100p$. The parameter, p given by Eq. 27,

is used to establish a RS SIF domain whose magnitude is up to 100 times larger than that induced by external loading.

$$p = \max(1, |K^{max}_{II,Appl}/K^{max}_{I,Appl}|) \tag{27}$$

Subsequently, the $\Delta K_{Eq,Tot}/K^{max}_{I,Appl}$ maxima are retrieved for every $K^{max}_{II,Appl}/K^{max}_{I,Appl}$ together with their location in terms of $K_{II,RS}/K_{I,RS}$. Fig. 5 compares the $\Delta K_{Eq,Tot}/K^{max}_{I,Appl}$ maxima along the ordinate with those at $K_{II,RS}/K_{I,RS}$ along the abscissa. It shows that the maxima are all located along the first median at $K_{II,RS}/K_{I,RS} \approx K^{max}_{II,Appl}/K^{max}_{I,Appl}$, confirming the validity of the *RSIF Proportionality Conjecture*.

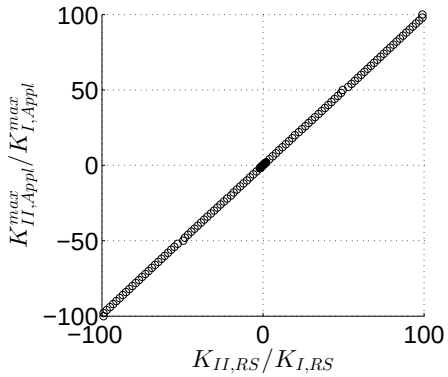

Figure 5: Locations where the maximum $\Delta K_{Eq,Tot}/K^{max}_{I,Appl}$ appears for different RS combinations. Results follow a nearly straight line with $K_{II,RS}/K_{I,RS} = K^{max}_{II,Appl}/K^{max}_{I,Appl}$.

Fig. 6 depicts the relative error distribution ε_1 defined as the maximum deviation between the predicted $K_{I,RS}/K_{II,RS} = K^{max}_{I,Appl}/K^{max}_{II,Appl}$ and the actual value of $K_{I,RS}/K_{II,RS}$ that satisfies the $\max(|\Delta K_{Eq,Tot}|)$. Fig. 6 shows that the error decreases with increasing grid node density, which implies that

$$\lim_{n \longrightarrow \infty} \max(\Delta K_{Eq,Tot}) = \Delta K_{Eq,Tot}(K_{I,RS}/K_{II,RS} = K^{max}_{I,Appl}/K^{max}_{II,Appl}) \quad (28)$$

for $n > 0$, $n \epsilon \mathbb{N}$.

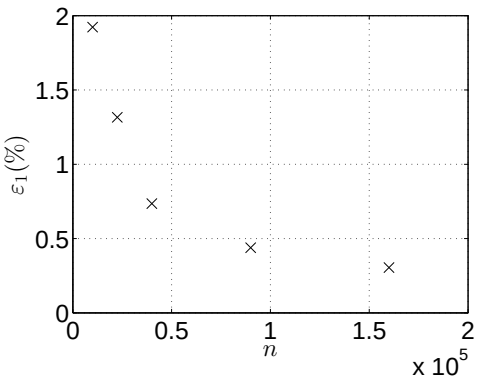

Figure 6: Deviation between $\max(\Delta K_{eq})$ with respect to the condition $K_{eq}(K_{I,RS}/K_{II,RS} = K^{max}_{I,Appl}/K^{max}_{II,Appl})$ for mesh grids from n =100x100 to 400x400.

The results presented in Fig. 5 and Fig. 6 show the highest $\Delta K_{Eq,Tot}/K^{max}_{I,Appl}$ is found when the *RSIF Proportionality Conjecture* is satisfied.

Further studies show that the *RSIF Proportionality Conjecture* holds for different RS magnitudes, e.g. 1000 times smaller or 2 times larger compared to stresses induced by external loading. Furthermore, the results appear to be insensitive to the load ratio, validated for $R = 0$, 0.2, 0.5 and 0.9.

3.3.2. The RSIF Proportionality Conjecture: Implications

The *RSIF Proportionality Conjecture* implies the following simplification

$$\frac{K_{I,RS}}{K_{II,RS}} = \frac{K^{max}_{I,Appl}}{K^{max}_{II,Appl}} \longrightarrow \frac{K^{max}_{I,Appl} + K_{I,RS}}{K^{max}_{II,Appl} + K_{II,RS}} = \frac{K^{max}_{I,Appl}}{K^{max}_{II,Appl}}. \quad (29)$$

Applying Eq. 29 to Eq. 15, the crack propagation angle is

$$\theta^{max} = 2\tan^{-1}\left(\frac{K^{max}_{I,Appl}}{4(K^{max}_{II,Appl})} \pm \frac{1}{4}\sqrt{\left(\frac{K^{max}_{I,Appl}}{K^{max}_{II,Appl}}\right)^2 + 8}\right). \tag{30}$$

Since the external minimum loading is assumed to be proportional to the external maximum loading, i.e. $K^{min}_{I,Appl}/K^{min}_{II,Appl} = K^{max}_{I,Appl}/K^{max}_{II,Appl}$, the crack propagation is $\theta^{min} = \theta^{max} = \theta$. Therefore, Eq. 13 and Eq. 14 are simplified, and Eq. 12 can be expressed as follows

$$\Delta K_{Eq,Tot} = f(\theta)(K^{max}_{I,Appl} - K^{min}_{I,Appl}) + g(\theta)(K^{max}_{II,Appl} - K^{min}_{II,Appl}) \tag{31}$$

Consequently, the *RSIF Proportionality Conjecture* leads to a formulation, Eq. 30 and Eq. 31, where no RS values are necessary. Thus, assuming the *RSIF Proportionality Conjecture*, conservative values of $\Delta K_{Eq,Tot}$ are calculated and no RS field is needed for the FM calculations.

Further numerical analysis shows the same $\Delta K_{Eq,Tot}$ under the *RSIF Proportionality Conjecture* and under no RS field.

4. Crack tip relocation

The *RSIF Proportionality Conjecture* addresses the highest da/dn. However, the crack growth rate varies with crack tip relocation. A crack growth considered to be conservative needs to follow a path which consistently exhibits the highest $\Delta K_{Eq,Tot}$ of all possible crack relocation directions. Anderson [15] showed that the maximum energy release rate of a crack with an infinitesimally small kink under mixed-mode conditions occurs in a pure mode-I kink orientation. From that it can be deduced that the highest fatigue crack growth speed occurs in a pure mode-I direction which can be

predicted by the MTS criterion. Since the maximum $\Delta K_{Eq,Tot}$ occurs when RSIF are proportional to SIF associated to the cyclic loads, the resulting crack growth occurs in a direction $\theta^{max} = \theta^{min}$ always towards pure mode-I, and thus, in the direction of the maximum crack propagation rate.

5. Application of the RSIF Proportionality Conjecture to a plate with three holes and a punctual cyclic load.

In this section, a representative numerical example is used to investigate the fatigue crack propagation for five different cases shown in Tab. 1. Each case is associated with a different RSIF configuration.

Table 1: SIF values for different RS conditions. The cases $\mathcal{A}$ and $\mathcal{B}$ represent RS configurations which are not propotional to the stresses induced by external loading. Case $\mathcal{C}$ represents a fatigue growth situation under the absence of RS. Case $\mathcal{D}$ and $\mathcal{E}$ represent situations in which the *RSIF Proportionality Conjecture* is satisfied.

Case	$K_{I,RS}$(mm)	$K_{II,RS}$(mm)
$\mathcal{A}$	$2K^{max}_{I,Appl}$	0
$\mathcal{B}$	$K^{max}_{I,Appl}$	0
$\mathcal{C}$	0	0
$\mathcal{D}$	$2K^{max}_{I,Appl}$	$2K^{max}_{II,Appl}$
$\mathcal{E}$	$K^{max}_{I,Appl}$	$K^{max}_{II,Appl}$

Fig. 7 shows the geometry, boundary conditions and load set-up of the numerical example. The decision to use this geometry and load set-up was inspired by the research from Ingraffea et al. [24]. The peak load of $F = 3$ kN with a load ratio of $R_{Appl} = 0.57$ was chosen.

The Paris Law parameters are listed in Table 2. The fracture toughness is chosen as $K_{IC} = 3345 \frac{\mathrm{N}}{\mathrm{mm}^{3/2}}$(Corresponding to 105.79 MPa$\sqrt{\mathrm{m}}$), a typical value for structural carbon steel [25].

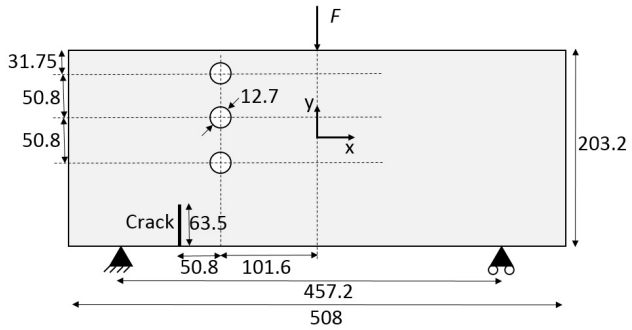

Figure 7: A simply-supported plate with three holes subject to a concentrated load. All dimensions in mm. Plane strain conditions are chosen for the fatigue analysis.

Table 2: Paris Law Parameters following the BS 7910 [5] for $R > 0.5$.

ΔKeq(N/mm)	$C \frac{\mathrm{mm/cycle}}{(\mathrm{MPa}\sqrt{\mathrm{mm}})^m}$	m
≤ 144	$2.1 \cdot 10^{-17}$	5.1
> 144	$1.29 \cdot 10^{-12}$	2.88

The crack propagation method, the mesh characteristics as well as mesh convergence studies used for this analysis can be found in [18], where mesh convergence analyses were performed. The method proposed in [18] was chosen due to its reliability when comparing against experiments, analytical results and other software tools. The algorithm was executed within a Matlab®-ANSYS®[26] [27] set-up, where the crack tip SIFs were obtained by Finite Element Analysis (FEA). The crack growth is calculated through the Paris Law, using the equivalent SIF formulation given in Eq. 1, where

the Equivalent SIF range is computed according to Eq. 12. The geometry is updated and a new FE model is created after every crack propagation stage Δa_{lim}, where Δa_{lim} is found through a convergence analysis.

In this example, the method was restricted to single-crack growth. The crack growth orientations are updated for every crack stage using Eq. 17.

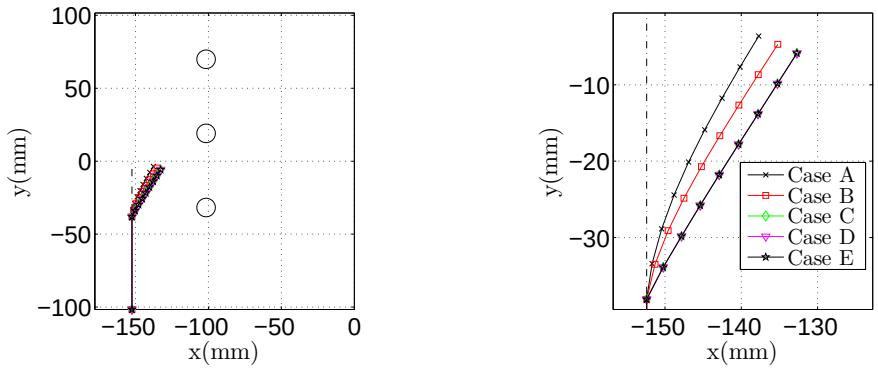

(a) (b)

Figure 8: Crack paths for the five different cases: (a) Crack paths shown in true relative scale to the beam structure. All crack paths are kinking to the right towards the holes; (b) Close-up of the hatched area indicated in (a). Crack paths of cases $\mathcal{C}$ $\mathcal{D}$ and $\mathcal{E}$ coincide. Crack paths $\mathcal{A}$ and $\mathcal{B}$ exhibit increased curvature with a smaller initial kinking slope with a preferential direction towards pure mode-I.

Fig. 8 shows the predicted fatigue crack paths for the five cases given, where the dashed line represents the path evaluated when only pure mode-I K_I is used for fatigue crack growth formulations. The crack path predicted for case $\mathcal{C}$ coincides with those predicted for cases $\mathcal{D}$ and $\mathcal{E}$. However, the crack paths follow a trend towards the pure mode-I path in cases $\mathcal{A}$ and $\mathcal{B}$ as $K_{I,RS}$ is increased (see Fig. 8 and Table 2). All crack growth analyses finished at the

same crack growth distance, which was selected arbitrarily. The maximum SIF magnitude in these analyses was $1774.7\frac{\mathrm{N}}{\mathrm{mm}^{3/2}}$, still considerably lower than the fracture toughness.

Fig. 9 shows the crack path lengths versus the number of cycles. It is worth noticing a strong dependency of the crack propagation rate on the RS distribution where cases $\mathcal{A}$ and $\mathcal{B}$ clearly present the lowest rates compared to the remaining cases.

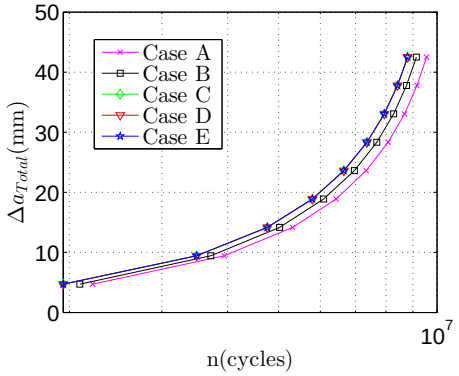

Figure 9: Curves n vs Δa_{Total}, where Δa_{Total} is the total crack growth. The cases where RS are proportional to the externally induced stresses show the same fatigue performance as without RS: cases $\mathcal{C}$, $\mathcal{D}$ and $\mathcal{E}$. Misaligment leads to a lower fatigue rate: cases $\mathcal{A}$ and $\mathcal{B}$

6. Discussion

The results presented in Fig. 9 show that in situations where the RS field is not proportional to the externally-induced stress field, $\Delta K_{Eq,Tot}$ strongly depends on the RS magnitude. In those cases, an increase of the RS magnitude decreased $\Delta K_{Eq,Tot}$, which consequently led to a lower fatigue crack propagation rate.

A numerical proof of principle demonstrates that the application of the MTS criterion through Eq. 12 leads to a maximum $\Delta K_{Eq,Tot}$ if the *RSIF Proportionality Conjecture* is met. Non-proportional stress fields lead to a lower crack propagation rate. The striking advantage of the *RSIF Proportionality Conjecture* is that $\Delta K_{Eq,Tot}$ is no longer a function of the RS magnitude and distribution. Consequently, the calculation of RS fields in the domain can be avoided for the sake of computational efficiency.

It needs to be stressed that the *RSIF Proportionality Conjecture* follows a non-physical albeit conservative assumption in which the RS field is proportional to the externally-induced stress field after every cycle. It is important to mention that although $\Delta K_{Eq,Tot}$ is independent of the RS magnitude, the latter clearly has an influence on the Paris law parameters - with a distinct dependency on low stress ratios.

In the numerical examples presented, the analysis was restricted to positive and high stress ratios, where there are no closure effects [28]. Mixed-mode situations under negative stress ratios pose a different configuration since $K^{min}_{I,Appl} = 0$ and $K^{max}_{I,Appl}/K^{max}_{II,Appl} \neq 0$, thus $K^{min}_{I,Appl}/K^{min}_{II,Appl} \neq K^{max}_{I,Appl}/K^{max}_{II,Appl}$. In those cases the *RSIF Proportionality Conjecture* no longer holds. Moreover, the current approach might disregard cases at which crack paths with lower propagation rates reach a free surface earlier than those with the highest propagation rate, as the current definition of conservatism is only related to crack propagation rate.

The findings in this publication raise the intriguing question as to whether high tensional RS must always be considered detrimental to the fatigue life of a structure. In cases of high load ratios where tensional RS are not sig-

nificantly affecting the Paris Law Parameters, the effect of non-proportional RSIF could even prolong the fatigue life of structures.

Another issue concerns that cyclic loads in conjunction with residual stresses, which may induce non-proportional loading, i.e. $K_{I,Tot}^{max}/K_{II,Tot}^{max} \neq K_{I,Tot}^{min}/K_{II,Tot}^{min}$, where in some cases [29] [30] the validity conditions for the MTS criterion might not be fulfilled. Further research is required to clarify these matters.

According to the theory applied, in cases with multiple pure mode-I configurations, e.g. biaxial loading [15], further analysis is required to ensure that the pure mode-I relocation is indeed leading to the fastest growth.

7. Conclusions

The following conclusions can be drawn:

(i) The RSIF Proportionality Conjecture states that the maximum equivalent SIF range $\Delta K_{Eq,Tot}$ is attained if the RSIF ratio is proportional to the external cyclic load induced SIF. If the RSIF proportionality condition is fulfilled, $\Delta K_{Eq,Tot}$ becomes independent of the RSIF magnitudes.

(ii) Under fulfilment of the RSIF proportionality condition, the highest fatigue crack propagation speed - and therefore the most conservative situation - is attained when Paris law parameters for high stress ratios are adopted, where no closure effects appear. This conservative approach does not require RS calculations.

(iii) The proposed conservative approach is especially suitable for inspections of welded large scale multi-component structures where the anal-

ysis of multiple current RS states based on their temporal evolution is associated with high uncertainty levels - which is generally the case in the construction industry.

Acknowledgement

The authors are grateful for the support and scientific advice of Christian Frithiof Niordson, Thomas Østergaard and Mathias Stolpe.

Funding

The research is supported by the research project Advancing BeYond Shallow waterS (ABYSS), funded by Innovation Fund Denmark, Grant no. 1305-00020B, and in collaboration with Ørsted. The funding source had no influence in the outcome or in the decision to publish the manuscript.

References

[1] European committee for standardization. Welding and allied processes-Classification of geometric imperfections in metallic materials- Part 1:Fusion Welding(ISO 6520-1:2007), Trilingual version EN ISO 6520-1:2007. Brussels: CEN; 2007.5

[2] Al-Mukhtar AM. The safety analysis concept of welded components under cyclic loads using fracture mechanics method [PhD dissertation]. Freiberg: Technische Universität Bergakademie Freiberg; 2010.

[3] DNVGL-RP-C203:2016: Fatigue design of offshore steel structures. 2016.

[4] Straub D. Generic approaches to risk based inspection planning for steel structures [PhD dissertation]. Zürich: Swiss Federal Institute of Technology Zürich; 2004.

[5] Committee reference WEE/37. British Standard BS 7910:2013: Guide to methods for assessing the acceptability of flaws in metallic structures. London: BSI; 2013.

[6] Mullins J, Gunnars J. Guide to methods for assessing the acceptability of flaws in metallic structures. Stockholm: Swedish Radiation Safety Authority; 2013 Jan. Report No. 2013:01.

[7] International Atomic Energy Agency. Measurement of residual stress in materials using neutrons. Vienna: IAEA; 2005 Jun. Report No. IAEA-TECDOC-1457.

[8] Bao R, Zhang X, Yahaya NA. Evaluating Stress Intensity Factors due to Weld Residual Stresses by the Weight Function and Finite Element Methods. Eng Fract Mech 2010; 77: 2550-66.

[9] Seifi R. Effect of Residual Stresses on Fracture Parameters of through Cracks in Welded Plates. Procedia Eng 2011; 10: 1895-900.

[10] Sumi Y, Yang C, Wang ZN. Morphological aspects of fatigue crack growth Part II-Effects of stress biaxiality and welding residual stress. Int J Fract 1996; 82: 221-35.

[11] Pingsha D, Shaopin S, Jinmiao Z. Analysis of residual stress relief in post-weld heat treatment. Int J Pres Ves Pip 2014; 122: 6-14.

[12] Hossain S, Truman CE, Smith DJ, Peng RL, Stuhr U. A study of the generation and creep relaxation of triaxial residual stresses in stainlees steel. Int J Solids Struct 2007; 44: 3004-20.

[13] Farajian M, Nitschke-Pagel T, Dilger K. Mechanisms of Residual Stress Relaxation and Redistribution in Welded High-Strength Steel Specimens under Mechanical Loading. Welding in the World 2010; 54: 366-74.

[14] Sørensen JD. Framework for Risk-based Planning of Operation and Maintenance for Offshore Wind Turbines. Wind Energy 2009; 12: 493-506.

[15] Anderson TL. Fracture Mechanics: Fundamentals and Applications. 3th ed. Boca Raton: CRC Press Taylor & Francis Group; 2005.

[16] Barsoum Z, Barsoum I. Residual stress effects on fatigue life of welded structures using LEFM. Eng Fail Anal 2009; 16(1): 449-67.

[17] Meggiolaro MA, Miranda ACO, Castro JTP, Martha LF. Stress intensity factor equations for branched crack growth. Eng Fract Mech 2005; 72: 2647-71.

[18] Ruiz-Muñoz GA. Method to Analyse Multiple Site Damage Fatigue before and after Crack Coalescence. Eng Fract Mech 2017;(In press)

[19] Price RJ, Trevelan J. Boundary element simulation of fatigue crack growth in multi-site damage. Eng Anal Bound Elem 2014; 43: 67-75.

[20] Dowling NE. Mechanical behavior of materials. 4th ed. London: Springer; 2013.

[21] Erdogan F, Sih GC. On the crack extension in plates under plane loading and transverse shear. J Basic Eng 1963; 85: 519-25.

[22] Lucht T. Analysis of Cracks in Large Diesel Engines. PhD thesis. DCAMM Special Report No. S103. Technical University of Denmark. Lyngby; 2007.

[23] Spievak LE, Wawrzynek PA, Ingraffea Ar, Lewicki DG. Simulating fatigue crack growth in spiral bevel gears. Eng Fract Mech 2001; 68: 53-76.

[24] Ingraffea AR, Grigoriu M. Probabilistic Fracture Mechanics: A Validation of Predictive Capability. Final report. Ithaca: Dept of Civil and Environmental Eng, Cornell University; 1990 Aug. Report No. 90-8.

[25] Bouchard R, Shen G, Tyson WR. Fracture toughness variability of structural steel. Eng Fract Mech 2008; 75: 3735-42.

[26] The MathWorks, Inc. Matlab Documentation. Version R2013b; 2013.

[27] ANSYS, Inc. ANSYS Documentation. Version 18.0.0; 2018.

[28] Newman Jr JC. A Crack-Closure model for Predicting Fatigue-Crack Growth under Aircraft Spectrum Loading. Hampton: Langley Research Center; 1981 Jan. Report No. NASA-TM-81941.

[29] Zerres P, Vormwald M. Review of fatigue crack growth under non-proportional mixed-mode loading. Int J Fatigue 2014; 58: 75-83.

[30] Plank R, Kuhn G. Fatigue crack propagation under non-proportional mixed mode loading. Eng Fract Mech 1999; 62: 203-29

Appendix C The effects of multiple-site damage and corrosion on the structural reliability of a thin plate with a hole (Manuscript C)

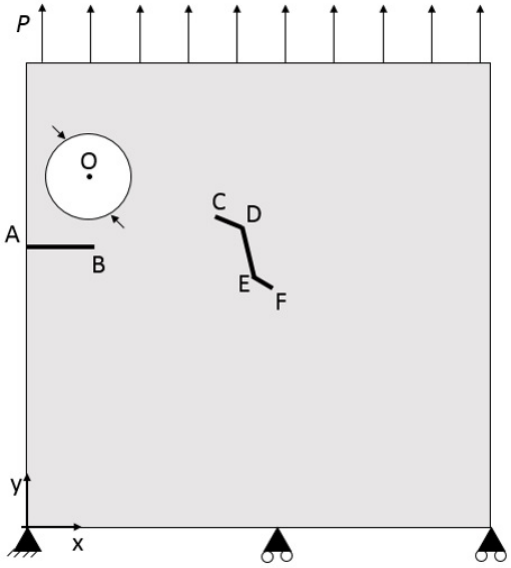

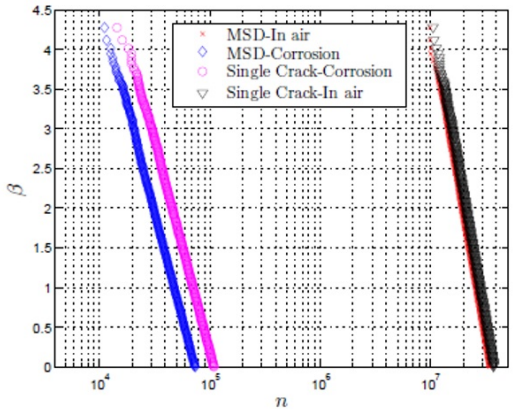

THE EFFECTS OF MULTIPLE-SITE DAMAGE AND CORROSION ON THE STRUCTURAL RELIABILITY OF A THIN PLATE WITH A HOLE.

G.A. Ruiz-Muñoz[1,2,]

[1]*Technical University of Denmark, Department of Wind Energy, Frederiksborgvej 399, 4000 Roskilde, Denmark*
[2]*DONG Energy, Nesa Allé 1, 2820 Gentofte, Denmark*

Abstract: The present research shows the influence of multiple cracks and corrosion on the reliability of a given structural case. The fatigue analysis is performed using a fracture mechanics approach and assuming Linear Elastic Fracture Mechanics conditions. The Paris Law parameter *C* is considered as a stochastic parameter and Monte Carlo simulations are performed for one million samples. The results show that corrosion has a very high impact on reliability curves, when compared to in air studies. Including an inner crack in the model slightly reduces the reliability of the structure. This study serves to shed some light on the structural reliability topic, which is an important concept for inspection planning.

Keywords: Reliability, Multiple Cracks, Fatigue, Corrosion

1. Introduction

The offshore wind turbine industry is facing challenges regarding efficient inspection planning of their structures. The combination of fatigue and corrosion lead to reduced life of wind turbines. In addition, corrosion can lead to multiple cracks, also known as Multiple Site Damage (MSD). Offshore components such as welds can also include different MSD distributions. The analysis of MSD has already been included in several studies e.g. [1] and [2].

Once the wind turbine operates, one possibility to extend its lifetime is through maintenance. Maintenance usually follows conservative guidelines that may result in inefficient and costly inspection planning. The inspection planning is linked to reliability curves [3]. Accurate reliability curves are therefore necessary for cost efficient probabilistic inspection planning [4].

A fracture mechanics model can be used to simulate the crack propagation and reliability in a model. Fracture mechanics approaches based on Finite Element Methods (FEM) are generally more accurate than those base on parametric formulation. In addition, parametric formulations are limited to a range of geometries or flaw configurations [5]. The drawback of using FEM is the high computational demand, where millions of different simulations required in a probabilistic set-up can be impractical.

The inspection planning in offshore wind turbines has served as an inspiration to the develop a research in calculating reliability curves from a fracture mechanics perspective. A simple structure is studied to evaluate the effects of free corrosion and MSD. The crack propagation is simulated once for every environmental and crack distribution condition. Results can give a perspective of how corrosion and MSD influence the reliability curves. The consequence of this study can later be extrapolated to study the influence of these two phenomena in inspection planning.

The reliability curves are determined by assuming only one parameter as stochastic: a crack growth parameter from the Paris Law equation [5]. Further investigations can improve the modelling and results by assuming more variables as stochastic, e.g. initial crack length.

2. Theoretical background.

The Paris Law is a well-accepted formulation to describe fatigue in the second crack growth region. In a mixed mode crack growth environment, the Paris Law formulation can be written [6] as

$$\frac{\mathrm{d}a}{\mathrm{d}n} = C\left(\Delta K_{eq}(a)\right)^{m}, \tag{1}$$

where a is the crack length, n is the load cycle and ΔK_{eq} is the equivalent Stress Intensity Factor. The values C and m are material parameters.

There are different approaches to calculate ΔK_{eq}. Meggiolaro et al. [6] consider the Maximum Tangential Stress Criterion (MTS) because of its simplicity and closed-form solution.

Assuming already existing cracks which growths correspond to the second crack growth region, and a very small fatigue life associated to the third crack growth region [5], the total fatigue life can be calculated from a mathematical transformation of Eq. 1 [5] to

$$\int_0^{n_f} \mathrm{d}n = n_f = \int_{a_{initial}}^{a_f} \frac{\mathrm{d}a}{C\left(\Delta K_{eq}(a)\right)^m} = \frac{1}{C}\int_{a_{initial}}^{a_f} \frac{\mathrm{d}a}{\left(\Delta K_{eq}(a)\right)^m} = \frac{1}{C}B, \qquad (2)$$

where B is a parameter that depends on the geometry, loads, constraints and m. Loads and geometries are usually evaluated as stochastic parameters in probabilistic fatigue, e.g. [4] and [7]. However, in this research those parameters are assumed as deterministic for the sake of simplicity. Consequently, B is also considered as a deterministic parameter. The index f is associated with failure. A characteristic from Eq. 2 is the relation

$$B = C_j n_{fj} = C_i n_{fi}. \qquad (3)$$

where i and j is the index for different values of C. For a given B, the Eq. 3 can be used to efficiently calculate the life of a structure for different values of C. Considering C as a stochastic parameter, the analysis of fatigue would be done from a probabilistic perspective. Therefore, multiple fatigue lives are calculated for different values of C. The calculations of multiple lives can be performed through a Monte Carlo simulation, as explained in [6]. Different fatigue lives will serve to calculate accumulated probability of failure and, therefore, reliability curves a structure.

3. Reliability analysis of a thin plate with a single crack, multiple cracks and corrosion.

The fatigue analysis of a thin steel plate is done through a fracture mechanics approach and assuming Linear Elastic Fracture Mechanics (LEFM). The geometry in Fig. 1 is considered suitable for plane stress modelling. The analysis of mixed mode crack propagation conditions by Ingraffea et al. [8] has inspired the location of a hole on the current structure. The actual location of cracks allows to investigate the effects of surface and inner cracks in fatigue. The material characteristics are assumed as E=210 GPa and ν=0.3. The crack propagation is assumed to belong to the Paris Law regime, where parameters are obtained from the standard BS7910 [9]. The corrosion effects are accounted for by assigning a different Paris Law parameter distribution.

Table 1. Paris Law Parameters for steel, R<0.5 and single slope approach. The symbol μ is the mean and σ is the standard deviation. [9]

Specimen	C (μ, lognormal)	C (μ +2σ)	m(deterministic)
In air	$3.98\text{x}10^{-13}$	$6.77\text{x}10^{-13}$	2.88
Freely corroding in marine environment	$1.27\text{x}10^{-7}$	$1.93\ \text{x}10^{-7}$	1.3

The model shown in Fig. 1 is loaded under uniform cycling pressure with maximum value P=17.5 MPa and stress ratio R=0.1. The coordinates of the crack vertices are given in Table 2.

The crack propagation system and the criterion to assume failure is based on the method from [10], where the equivalent SIF are calculated through the MTS criterion and the fatigue analysis is calculated using Eq. 4. Single crack propagation and MSD fatigue is evaluated in the present research.

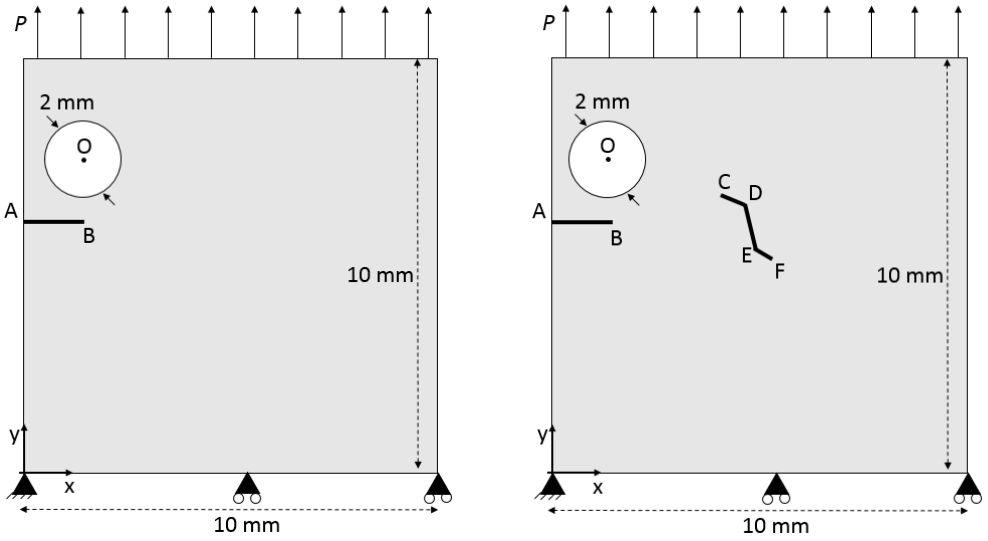

Fig. 1. Specimens for fatigue crack propagation: a) Single crack; b) MSD.

Table 2. Geometrical location of crack vertices.

Coordinate	x(mm)	y(mm)
A	0	5.2
B	1.5	5.2
C	3.5	5.8
D	4	5.7
E	4.3	4
F	4.5	3.7
O	3	7

For every environmental condition and crack disposition, a method explained in [10] is performed once. Fatigue life results are included in Eq. 3 to calculate *B*. The results of the *B* parameter for the four different cases is presented in Table 2.

Table 2. Different values of *B* for the four cases. *B* in $\left(\frac{\text{mm}}{(\text{MPa}\sqrt{\text{mm}})^m}\right)$.

Environment	Flaw distribution	*m* (deterministic)	*B*
In air	Single	2.88	1.43×10^{8}
In air	MSD	2.88	1.29×10^{8}
Freely corroding in marine environment	Single	1.3	1.26×10^{5}
Freely corroding in marine environment	MSD	1.3	8.53×10^{4}

The Fig 2. shows the crack shape of the MSD case immediately before the collapse of the structure. The circle around the crack tip represents the application limit for LEFM. Once the boundary is in contact with the edges of the specimen, the structure is assumed to collapse. Further details about this mechanism can be found in [10]. The same procedure is followed for single crack propagation.

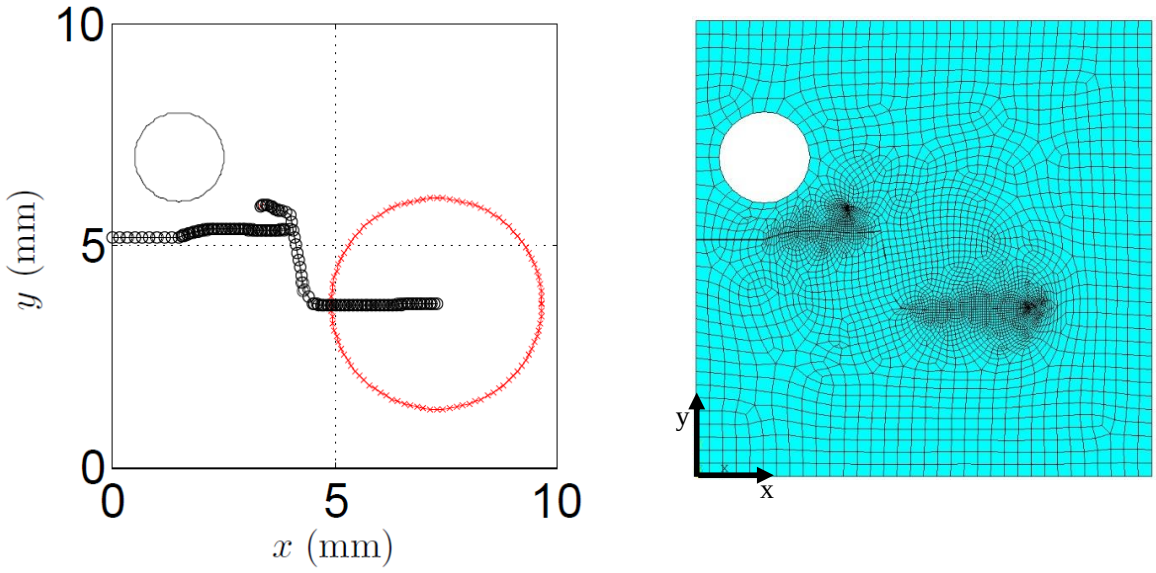

a) b)

Fig. 2. Crack disposition immediately before failure: a) Geometry of cracks. When the red circle is in contact with an external boundary, LEFM is no longer valid and failure is assumed [10]; b) Finite Element mesh of the structure with 12999 nodes and 4191 elements.

For each case in Table 2, one million samples are computed through a Monte Carlo [11] analysis of Eq. 3. Each sample corresponds to a realization of the *C* distribution. The results of different fatigue lives are transformed to accumulated probabilities of failure as

$$P_f(n) = \frac{N_f(n)}{N}, \quad (4)$$

where $P_f(n)$ is the accumulated probability of failure for a cycle n, $N_f(n)$ is the total number of failures and N is the total number of samples, $N = 10^6$. The accumulated reliability index is calculated as

$$\beta(n) = -\Phi^{-1}(P_f(n)), \quad (4)$$

where Φ^{-1} is the inverse function of the standardized normal function [11].

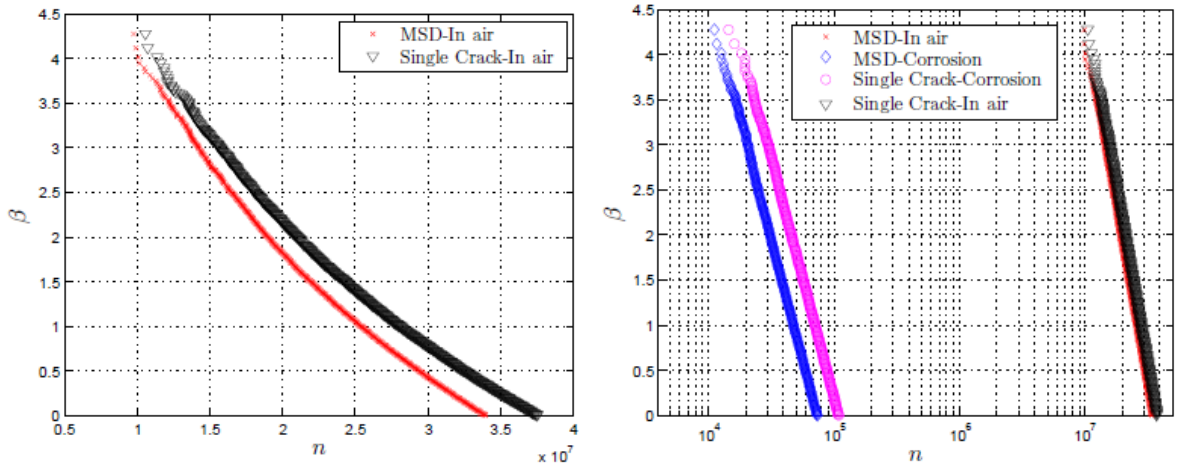

a) b)

Fig. 3. Reliability analysis for single and multiple cracks: a) In air; b) In air and corrosion.

Fig. 3 shows that imposing an inner crack to the model decreases the reliability of a structure. However, its impact is not as striking as the environmental conditions. Future studies of different crack dispositions may help to analyse the influence of MSD in reliability curves. The reliability analyses can be extended to include the results of inspections allowing the reliability curves to be updated given the inspection results; which can serve as the basis for planning of inspections.

4. Conclusions

The reliability curves of a thin plate under fatigue where calculated by a combination of a fracture mechanics approach and Monte Carlo simulations. Four different cases were studied to evaluate the effects of corrosion and MSD on reliability. Corrosion reduces reliability by three orders of magnitude when compared to results from an in-air environment. On the other hand, imposing an internal crack only slightly changes reliability results. The same analysis can be used to evaluate the influence of different crack set-up on the reliability of a structure. Since the inspection planning is related to reliability curves, corrosive conditions may have a significant impact in periodicity of inspections, whereas imposing multiple flaws may not have such large influence.

Acknowledgements and funding

The author thanks all aid from supervisors Mathias Stolpe and John Dalsgaard Sørensen, whose observations gave a great input to this study. This research was supported by the strategic research project Advancing BeYond Shallow waterS (ABYSS), funded by Innovation Fund Denmark, Grant no. 1305-00020B, and in collaboration with DONG Energy. The sponsors have not influenced the outcome of the present publication and the decision to publish was done by the author. The author followed the regulations of his institutions concerning intellectual rights and there are no impediments for publication with respect to intellectual properties.

References

[1] Price RJ, Trevelan J. Boundary element simulation of fatigue crack growth in multi-site damage. Eng Anal Bound Elem 2014; 43: 67-75.

[2] Liu YJ, Li YX, Xie W. Modeling of multiple crack propagation in 2-D solids by the fast multipole boundary element method. Eng Fract Mech 2017; 172: 1-16.

[3] DNV GL AS. Probabilistic methods for planning of inspection for fatigue cracks in offshore cracks in offshore structures. Recommended practise DNVGL-RP-0001; 2015.

[4] Sørensen JD. Framework for Risk-based Planning of Operation and Maintenance for Offshore Wind Turbines. Wind Ener 2009; 12: 493-506.

[5] Anderson TL. Fracture Mechanics: Fundamentals and Applications. 3th ed. Boca Raton: CRC Press Taylor & Francis Group; 2005.

[6] Meggiolaro MA, Miranda ACO, Castro JTP, Martha LF. Stress intensity factor equations for branched crack growth. Eng Fract Mech 2005; 72: 2647-71.

[7] Sørensen JD, Toft HS. Probabilistic Design of Wind Turbines. Energies 2010; 3: 241-57.

[8] Ingraffea AR, Grigoriu M. Probabilistic Fracture Mechanics: A Validation of Predictive Capability. Report No. 90-8. Department of structural Engineering, Cornwell University. 1990.

[9] Dowling NE. Mechanical behaviour of materials. 4th ed. London: Springer; 2013.

[10] Ruiz-Muñoz GA. Method to Analyse Multiple Site Damage Fatigue before and after Crack Coalescence. 2017; (Under Review).

[11] Ditlevsen O, Madsen HO. Structural Reliability Methods. Internet edition 2.2.5: DTU; 2005.

Appendix D Probabilistic inspection planning of offshore welds subject to the transition from protected to corrosive environment (Manuscript D)

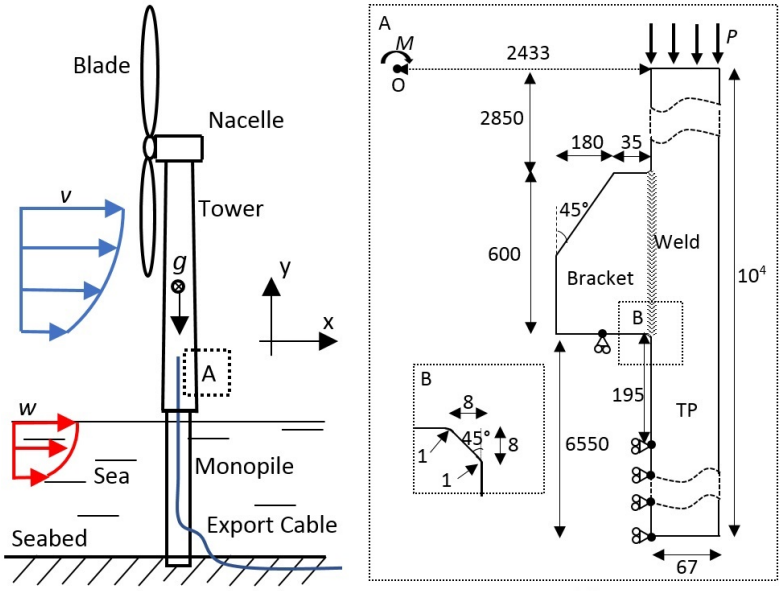

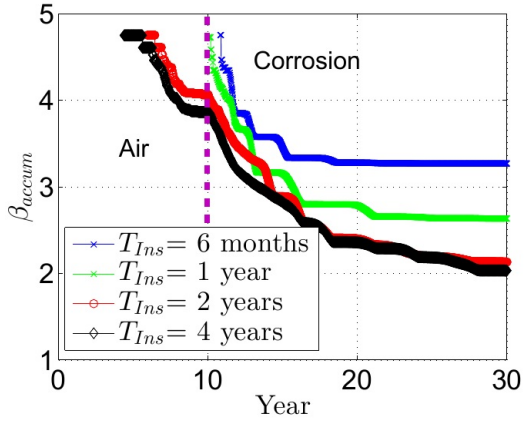

Probabilistic inspection planning of offshore welds subject to the transition from protected to corrosive environment

G.A. Ruiz Muñoz[a,b], J.D. Sørensen[b,c]

[a] *Ørsted, Nesa Allé 1 2820 Gentofte, Denmark*
[b] *Department of Wind Energy, DTU, 4000 Roskilde, Denmark*
[c] *Department of Civil Engineering, AAU, 9220 Aalborg Ø, Denmark*

Abstract

Welds commonly include high stress concentration locations that, under fatigue loading, may be responsible for a low life performance. Additionally, offshore welded components may face corrosive environments which are detrimental to the integrity of the structure. These structures are usually isolated or protected from the corrosive environment through e.g. dehumidifiers or coating. However, the protective systems may fail during the lifetime of a structure, a phenomenon denoted as the Transitional Environmental Protection (TEP) process. The present paper proposes a novel method to evaluate how the reliability of a structure is affected by corrosive, protected or TEP process conditions, as well as by different inspection/repair intervals. The algorithm included is based on Monte Carlo simulations from a probabilistic fracture mechanics approach. This method shows the effects of enlarging the environmental protection on the maintenance plan of an offshore weld in a

Email addresses: g_a.ruiz@hotmail.com & gusru@orsted.dk (G.A. Ruiz Muñoz), jds@civil.aau.dk (J.D. Sørensen)

given case.

Keywords: Inspection, Fatigue, Fracture Mechanics, Corrosion

Nomenclature

$a, \Delta a$	Crack length and crack growth.
a_{ini},a_f	Initial crack length and crack size limit before failure.
$\bar{a}_{SN}$	S-N curve parameter.
$a_{ini,air}$	Initial crack length for air conditions.
$a_{ini,cor}$	Initial crack length for corrosive conditions.
a_{repLim}	Maximum length a crack can be repaired.
b	Probability of detection parameter.
C	Paris Law parameter.
C_A, C_B	Parameters for the bilinear Paris Law.
D, D_{accum}, D_f	Damage, accumulated damage and damage limit to failure.
f, f_{lt}	Loading frequency and long term stress cycle frequency.
i, k	Integer indexes.
K_{eq}	Equivalent Stress Intensity Factor(SIF).
K_{max}	Maximum SIF for Paris Law analysis.
K_C	Maximum SIF before fatigue failure.
ΔK_{th}	Stress Intensity Factor threshold.
ΔK_{TP}	Transition point in between the two linear stages of the Paris Law.
L	Unit load in the order of magnitude of the load signal.
ΔL	Load range of the load signal.
m	Paris Law parameter.

Nomenclature

m_A, m_B	Parameters for the bilinear Paris Law.
m_{SN}	S-N curve parameter.
n	Number of nodes.
N, N_f	Number of cycles and number of cycles to failure.
N_I, N_P	Number of cycles to crack initiation and crack propagation.
p, q	Material crack growth parameters.
$P(F)$	Probability that event F occurs.
Q	Proportionality loading factor.
r_0	Notch radius.
t, t_{lim}, T	Time, limit of time and number of years.
T_{Ins}	Inspection interval.
t_{TEP}	Period of time a system is environmentally protected.
U_L, U_{FM}, U_{ENS}	Uncertainty parameters.
x, y	Cartesian axis.
X_0	Probability of detection parameter.
v, w	Wind and wave velocity.
β	Reliability index.
β_{accum}	Accumulated reliability index.
β_t	Annual reliability index.
σ_A,σ_B	Tensional stresses.
$\sigma_{pr,max}$	Maximum principal stress.
$\sigma_{pr,max,L}$	Maximum principal stress calculated for a load L.
Φ	Acceleration factor.

1. Introduction

Offshore structures such as ships or wind turbines [[1],[2]] are subject to dynamic loading and corrosive conditions that may generate fatigue crack propagation [3]. The offshore industry commonly demands inspection/repair programs to detect and avoid possible failures. In the early 1970's, Yang and Trapp [4] started to design deterioration models and optimized inspection plans. During the next decade, Skjong [5] and Madsen et al. [6], among others, generated optimized inspection plans for offshore structures.

Nowadays, multiple researchers are involved in inspection plan simulations. The two main inspection planning categories are the qualitative approach, based on subjective judgement, and the quantitative approach, based on statistical data [7]. The Fracture Mechanics (FM) approach to probabilistic inspection planning is a quantitative approach that is becoming very popular. This field deals with crack propagation and repair simulations. Eltaif et al. [8] performed a dynamic optimal inspection planning where they generated cost effective solutions by using FM models. Eltaif et al. evaluated multiple scenarios and updated their model over time from previous inspection results. Doshi et al. [9] included FM models in order to measure the reliability of ship components with different inspection techniques. Maljaars et al. [10] modelled 3D crack propagation and calculated the reliability curves for visual inspection techniques on multiple critical locations.

Among the different parts of offshore structures, a welded component may include stress riser locations where fatigue problems are likely to occur [[11],[12],[13]]. Lotsberg et al. [14] proposed new methods for inspection planning of offshore welds, where the FM models are calibrated with another

well established methods for fatigue life estimation in industry, known as the Stress Based (SB) or the S-N curve approach.

These recent studies, together with standards [15], suggest to implement Probabilistic Fracture Mechanics (PFM) approaches in the offshore industry in order to optimize inspection intervals of offshore welded steel details. However, some offshore components face an environmental condition, denoted in this work as the Transitional Environmental Protection (TEP) process. The TEP process occurs when a component is protected or isolated from a corrosive environment for a limited period of time. Examples of the TEP can be seen e.g. when the coating of a weld is damaged after a certain period of time, or when there are high moisture levels inside a wind turbine after a leak, Fig. 1. Despite the multiple cases in industry, this research has not found previous studies of the TEP process from a FM and inspection planning perspective.

Figure 1: Welded component inside a wind turbine foundation under the Transitional Environmental Protection (TEP) process. The weld was protected against corrosion for a certain operational time. Afterwards, a leakage generated a corrosive environment. Photograph from Ørsted®.

The current paper presents an innovative inspection/repair simulation algorithm for offshore welded components under the TEP process. The algorithm performs probabilistic fatigue analysis for two different types of methods: the Probabilistic Effective Notch Stress (PENS) approach and the Probabilistic Fracture Mechanics (PFM) approach. The reliability curves obtained in the PFM approach are calibrated against the PENS reliability curves. The calibrated PFM model is finally used to perform different inspection/repair simulations and determine their corresponding reliability curves. The algorithm is extremely versatile and applicable for offshore welded components.

2. Theoretical background

The offshore industry commonly calculates the fatigue life of structures through the Stress Based (SB) approach, where Finite Element (FE) models are designed in order to retrieve stress distributions. The SB approaches rely on S-N curves to estimate the fatigue life. The three main SB approaches are the Nominal Stress (NS) approach, the Hot Spot (HS) approach and the Effective Notch Stress (ENS) approach [15]. The NS approach is the simplest method but it is limited to a certain number of geometries and load distributions. On the other hand, the HS approach is versatile but may not be accurate when two Stress Concentration (SC) locations are nearby. Finally, the ENS approach is the most flexible method and, therefore, it is the one covered in this publication. However, it is complex since it requires a detailed geometrical model of the weld. [15]

2.1. The effective notch stress (ENS) approach

The ENS approach is described in DNVGL-RP-C203 [15] where e.g. fillet weld geometries are defined as Fig. 2. The weld is described using a flank angle of 45^o and a toe radius $r_0 = 1$ mm.

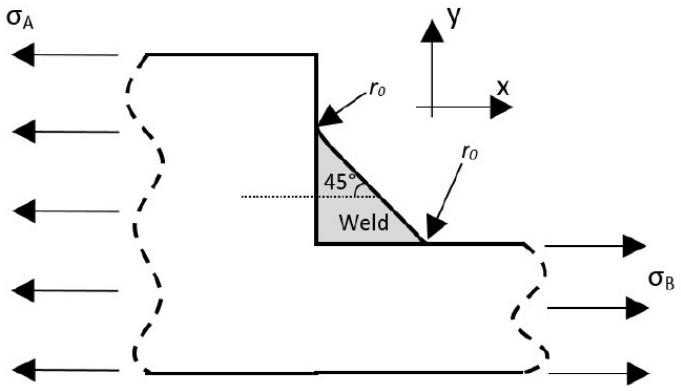

Figure 2: Fillet weld model for the ENS approach. Flank angle of 45^o and toe radius $r_0 = 1$ mm, measurements defined in[15]. The paremeters σ_A and σ_B are tensional stresses.

The geometry, loads and constraints are included in a Finite Element (FE) model. The results give a maximum principal stress, generally located in a notch toe or root. For constant amplitude loading, the stress range at that location $\Delta\sigma_{pr,max}$ is used to calculate the fatigue life as

$$\log N_f = \log \bar{a}_{SN} - m_{SN} \log \Delta\sigma_{pr,max} \tag{1}$$

where N_f is the number of cycles to failure, and $\bar{a}_{SN}$ and m_{SN} are parameters retrieved from the S-N curves. Different environmental conditions, e.g. air or free corrosion, are associated with different types of S-N curves. [15]

In cases of variable amplitude loading, damage accumulation models are often required in order to estimate the fatigue life. Among these models, the

Palmgren-Miners rule [16] is generally used in standards

$$D = \sum_{i=1}^{k} \frac{N_i}{N_{f,i}}, \tag{2}$$

where D is the damage accumulation parameter, i is an index associated with a stress range, k is the number of stress ranges in a load signal, N_i is the number of cycles that correspond to stress range $\Delta\sigma_i$, and $N_{f,i}$ is the number of cycles to failure calculated in Eq. 1 and associated with i. As the loading cycles increase over time, the values of each N_i may increase or new load ranges are incorporated in Eq. 2. The limit state equation for the damage accumulation model is [17]

$$g(D_f, D) = D_f - D, \tag{3}$$

where $g(D_f, D) \leq 0$ indicates failure and the mean of D_f is usually 1.

Despite the fact that SB approaches are widely used for fatigue life estimations, these methods do not contain information about the crack size, which is an important parameter needed for inspection planning [17].

2.2. The Fracture Mechanics (FM) approach

The FM approach for fatigue analysis describes the shape of the crack development. The associated limit state is usually described as [10]

$$g(a_f, a) = a_f - a(N). \tag{4}$$

where a_f is the crack length limit to failure and $a(N)$ is the crack length a for N loading cycles. Whenever the number of cycles is large enough, i.e. $g(a_f, a) \leq 0$, failure of the structure is assumed.

According to Schijve [18], the number of cycles to failure N_f is divided into two phases $N_f = N_I + N_P$, where N_I is the number of cycles for crack initiation and N_P is the number of cycles for crack propagation.

2.2.1. Crack Initiation

The crack initiation phase is a fatigue period where cracks are generated through different mechanisms, e.g. slip-band cracking or voids, and start to propagate with a rate according to a curve for short/small cracks as shown in [[17],[19]]. During this period, the crack length is normally small enough, $a < 0.1$ mm, so LEFM is not applicable [[11],[17]].

Bai-Mao et al. [20] and Maierhofer et al. [21] present different studies that explain the crack initiation. However, the formulations proposed are limited to certain cases and further research is required for universal crack initiation formulations. Additionally, the crack initiation studies of offshore welds need to consider corrosive factors e.g. pitting corrosion [3] or weld characteristics such as occlusions that may result in negligible initiation periods compared to the crack propagation period [11].

The crack initiation simulation from a fracture mechanics approach may be cumbersome and computationally demanding. A detailed computational model of this phase may be inefficient in terms of industrial applicability when compared with the crack propagation phase.

2.2.2. Crack Propagation

The Crack propagation phase is generally divided into three stages: the Stage I, the Paris Law regime, Stage II, and the Stage III, Fig. 3a [17]. The

crack growth in the Paris Law phase for mixed mode-I,-II is calculated as

$$da/dN = C(\Delta K_{eq})^m, \tag{5}$$

where a is the crack length, N is the number of cycles, K_{eq} is the Equivalent Stress Intensity Factor (SIF) and C, m are material parameters [22].

A more advanced formulation, which includes the crack propagation rate of the three stages, Fig. 3a, is described as [3]

$$da/dN = C(\Delta K_{eq})^m \frac{\left(1 - \frac{\Delta K_{th}}{\Delta K_{eq}}\right)^p}{\left(1 - \frac{K_{max}}{K_C}\right)^q}, \tag{6}$$

where p and q are material parameters, K_C is the maximum SIF a crack can propagate without an immediate failure, K_{max} is the maximum SIF a crack propagates according to the Paris Law and ΔK_{th} is the SIF threshold, i.e. the minimum SIF range for fatigue crack propagation.

Finally, corrosive effects can be accounted for fatigue calculations as [3]

$$\frac{da}{dN}_{corrosive} = \bar{\Phi}\frac{da}{dN}_{Air} + \left(\frac{1}{f}\frac{d\bar{a}}{dt}\right)_{EAC}, \tag{7}$$

where the term $\bar{\Phi}\frac{da}{dN}_{Air}$ is the cycle-dependent corrosion fatigue and the term $\left(\frac{1}{f}\frac{d\bar{a}}{dt}\right)_{EAC}$ is the time-dependent corrosion fatigue. The parameter $\bar{\Phi}$ is an acceleration factor, $\frac{da}{dN}_{air}$ is calculated in Eq. 6, f is the loading frequency and $\left(\frac{d\bar{a}}{dt}\right)_{EAC}$ is the average environmental crack growth over a loading cycle.

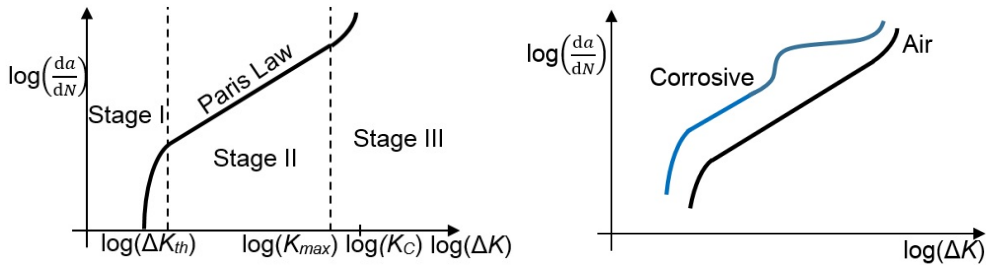

(a) (b)

Figure 3: Crack growth rate as a function of the SIF range for: (a) Air environment. (b) Air or corrosive environment.[3]

Fig. 3b shows the difference between applying Eq. 6 and 7. These equations present a higher degree of complexity than Eq. 5 and they include further parameters required for the FM study. The BS7910 [23] suggests to simplify the FM analysis by dividing the fatigue crack growth into two linear stages of the Paris Law regime, Fig. 4,

$$\frac{da}{dN} = \begin{cases} \Delta C_A (\Delta K_{eq})^{m_A} & \Delta K_{eq} \geq \Delta K_{TP} \\ \Delta C_B (\Delta K_{eq})^{m_B} & \Delta K_{eq} < \Delta K_{TP}, \end{cases} \tag{8}$$

where K_{TP} C_A, m_A, C_B and m_B are material parameters that depend on the environmental conditions and are defined in [23].

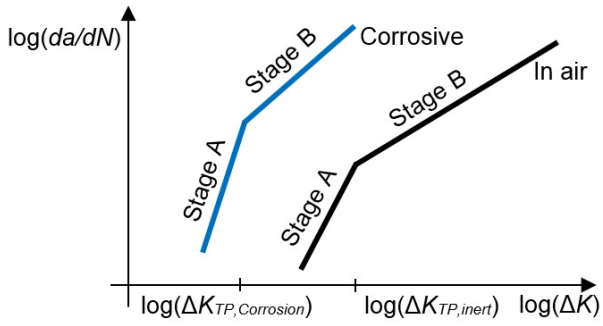

Figure 4: Bristish Standard approach [23]. Eq. 6 and 7 are simplified to Eq. 8, where two crack growth linear stages are defined in a logarithmic scale.

BS7910 [23] also includes a threshold value for fatigue calculations in air. However, authors such as Dowling [19] explain that there is fatigue crack growth below the threshold and, therefore, a more conservative approach is to assume $\Delta K_{th} = 0$

The Residual Stresses (RS) also influence fatigue crack propagation in a weld [[24],[25],[26]]. Ruiz et al. [27] state that the study of RS is complex because these stresses vary during the lifetime of a structure. If the RS variation is not simulated over time, fatigue life predictions can be overestimated. Moreover, the RS simulation may involve computationally time consuming simulations. Ruiz et al. [27] propose to circumvent the RS calculations by applying the *Residual Stress Intensity Factors Proportionality Conjecture*. This conjecture proposes a conservative approach to fatigue crack propagation by assuming no RS distribution and Paris Law parameters for high stress ratios. [27]

Under variable amplitude loading, different values of $K_{Eq,i}$ are achieved for different loading amplitudes. Therefore, each load cycle N_i may result in a different crack growth rate $(da/dN)_i$. However, if for a number of cy-

cles N_{total} there is no significant crack growth, the crack growth rate can be calculated as a weighted average [3]

$$\frac{da}{dN} = \frac{\sum_{i=1}^{k} N_i \left(da/dN\right)_i}{N_{total}}, \tag{9}$$

where i is an index that refers to a certain load range, k is the number of different load ranges in a load signal and N_i is the number of cycles in a load signal of N_{total} cycles that corresponds to load i.

2.2.3. Drawbacks of the Fracture Mechanics approach

The main inconvenience of the FM method is the lack of universal formulations for the crack initiation phase. Additionally, including geometrical defects of welds in FM models can be cumbersome. Finally, highly complex calculations are involved in simulating crack initiation and propagation in welds under different environmental conditions. The crack propagation phase can be simplified through standards suggestions and conservative approaches. However, according to DNVGL-RP-C203 [15], FM methods are not accurate enough to predict the full fatigue life of a complex welded structure and, therefore, a calibration with well stablished industrial approaches, e.g. the ENS approach, is required.

2.3. Probabilistic fatigue: The reliability-based approach

Fatigue calculations for real structural cases often include different uncertainties that are incorporated in probabilistic models. This type of analysis focuses on the reliability and probability of failure. Ditlevsen et al. [28] propose several methods to estimate the reliability as a function of time, e.g. First Order Reliability Methods, Second Order Reliability Methods or

Monte Carlo simulations. The Monte Carlo techniques are very popular for probabilistic fatigue simulations as they are simple and well established in literature [[17],[10]].

The reliability as function of time can be calculated using different fatigue methods, e.g. Probabilistic Fracture Mechanics (PFM) or Probabilistic Stress Based (PSB) approaches. Chen et al. [16], Doshi et al. [9] and Sørensen [29], among others, suggest to calibrate the reliability curve from the PFM approach against the PSB analysis. The result is a similar probabilistic fatigue performance in between the SB and the FM approach. Sørensen [29] proposes to calibrate the annual reliability index. On the other hand, Lotsberg et al. [14] suggest to work with the accumulated reliability index β_{accum} in the cases of inspection plan simulations.

2.4. The inspection/repair procedure.

A calibrated PFM model is suitable for inspection/repair simulations. Standard DNVGL-RP-0001 [30] suggests multiple methods for crack inspections. Each method includes a corresponding Probability of Detection (PoD) curve. The PoD for e.g. ultrasonic inspections is calculated as

$$P(a) = 1 - \frac{1}{1 + (a/X_0)^b} \tag{10}$$

where a is the crack size, $X_0 = 0.41$mm and $b = 0.642$ [30]

If a crack is detected, there is the option to repair it through e.g. grinding or TIG dressing [[31],[32]]. Straub [17] suggests two types of repair: the repair component is perfectly repaired and will not fail for the rest of the fatigue analysis; or the repair component behaves as new.

3. The algorithms for constant environmental and TEP conditions.

The current research focuses on the analysis of reliability of offshore welds under fatigue loading, different environmental conditions and inspection/repair simulations. First, an algorithm for constant environmental conditions is designed. Then, the algorithm is extended to cover the TEP process.

3.1. The algorithm for constant environmental conditions

The algorithm for constant environmental conditions is illustrated in Fig. 5, and it is divided into three main parts:

- The structural analyses: The geometries and constraints are implemented in two structural models, a FM model and an ENS model. A unit load L with the order of magnitude of the load signal is submitted to both models. The geometry of the weld is coherent with the DNV standards for the ENS approach [15]. The FM approach includes an initial crack located in the highest stress concentration spot with an initial size $a_{ini} = 0.1$ mm. The FM approach is used to calculate the equivalent SIF as a function of the crack length $\mathbf{K}_{eq,L}(\mathbf{a})$. The ENS model proportionates the maximum principal stress $\sigma_{pr,max,L}$. The parameters $\mathbf{K}_{eq,L}(\mathbf{a})$ and $\sigma_{pr,max,L}$ will be multiplied by different load ranges in order to retrieve the values of $\Delta\mathbf{K}_{eq}(\mathbf{a})$ and $\Delta\sigma_{pr,max}$ necessary for Eq. 1 and Eq. 4.

- Calibration: The results from the structural analyses are combined with input parameters to calculate reliability curves through the PFM and the PENS. The initial crack size a_{ini} and the uncertainty of the

PFM model U_{FM} are modified until both reliability curves are similar, where U_{FM} is directly applied to SIF values retrieved from the FM model.

- Inspection/repair analysis: Probabilistic Inspection/Repair Simulations are executed generating reliability curves for different inspection intervals.

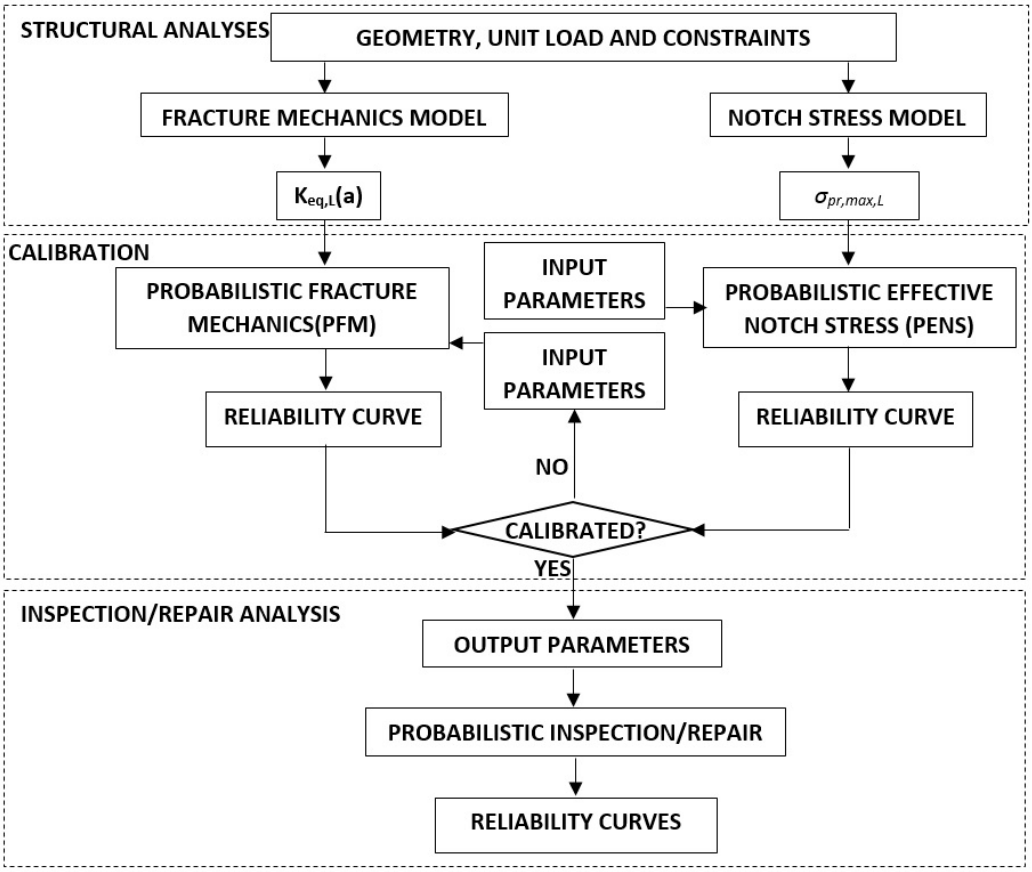

Figure 5: Algorithm to calculate reliability curves for different inspection/repair intervals under constant environmental conditions. The algorithm is divided into the structural analyses, the calibration and the inspection repair analysis.

3.1.1. Input Parameters

The Input Parameters, Fig. 5, are stochastic variables that follow different statistical distributions. These parameters are divided into three categories. The first category includes common parameters for both approaches. The load signal, the mean frequency of long term stress cycles f_{lt} and the limit of years a structure is under fatigue loading t_{lim} are these parameters. The load signal includes the different loading ranges and periodicity inside a signal and it is assumed to periodically repeat over time.

The second category is the input parameters associated with the PFM approach, i.e. Paris-Law Parameters for Eq. 8, initial crack size, the crack length associated with failure a_f and the uncertainty of the FM approach U_{FM}. The uncertainty U_{FM} is directly applied to the value $K_{eq,L}(a)$ retrieved from the FM model.

The third category is the input parameters associated with the PENS approach, i.e. S-N curve parameters for Eq. 1, the Palmgren-Miner limit to failure D and uncertainty of the ENS, U_{ENS}. The uncertainty U_{ENS} is directly applied to the value $\sigma_{pr,max,L}$ retrieved from the ENS model.

3.1.2. Probabilistic Fracture Mechanics (PFM)

The PFM of Algorithm Fig. 5 is further described in Fig. 6. The PFM simulation generates through a Monte Carlo technique multiple pseudo-random samples that follow distributions set in the Input Parameters. The vector $\mathbf{K}_{eq,L}(\mathbf{a})$, is interpolated to a polynomial function for each sample, with $\mathbf{K}_{eq,L}(0) = 0$.

All cracked specimens are simultaneously evaluated at each cycle increment ΔN. The results of each sample are included in the crack growth

analysis, Fig. 5: For each load range i, the equivalent SIF is calculated as $\Delta\mathbf{K}_{eq,i}(\mathbf{a}) = Q_i\mathbf{K}_{eq,L}(\mathbf{a})$, where Q_i is a scale factor between the load range ΔL_i and the unit load L, obtained from $\Delta L_i = Q_i L$. All crack growth rates for each sample are calculated using each $\Delta K_{eq,i}$ in Eq. 8. the average crack growth rate is the result from Eq. 9. Finally, the crack growth for each sample is calculated as $\Delta a \approx \Delta N\, da/dN$ [19].

The crack lengths are updated and the number of failures associated with the period of time t is obtained in order to calculate the probabilities of failure and reliability index. If all samples have failed or the period of time reaches the limit of years, the PFM analysis finishes. Note that the cycle increment ΔN and number of samples is calculated through a convergence analysis of these parameters and the resulting reliability curve.

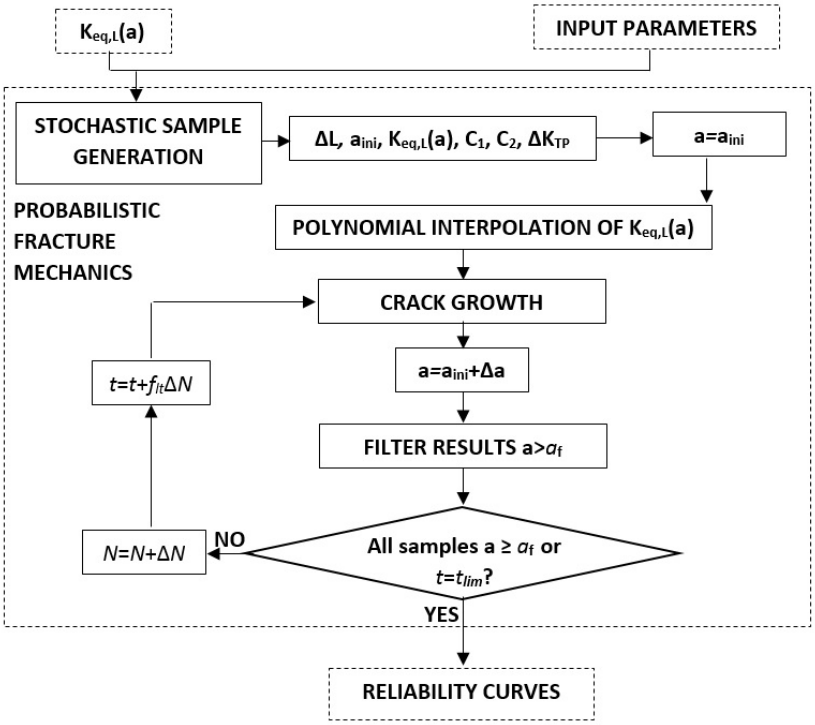

Figure 6: Probabilistic Fracture Mechanics Approach. Random variables are calculated for each sample in a Monte Carlo simulation. The crack growth of all specimens is simulatenously calculated for each cycle increment ΔN. The samples that fail are filtered in each ΔN.

3.1.3. Probabilistic Effective Notch Stress (PENS)

The algorithm in Fig. 7 explains the procedure to perform PENS calculations. The maximum principal stress for the load L, $\bar{\sigma}_{pr,max,L}$, is computed together with the Input Parameters in a Monte Carlo simulation that generates pseudo-random variables. The accumulated damage is initialized for each sample, $D_{accum}(0)$=0. Every load range ΔL_i is used to calculate its corresponding maximum principal stress range in a similar procedure as in the PFM, $\Delta\sigma_{pr,max,i} = Q_i\sigma_{pr,max,L}$. The number of cycles to failure for each

stress range is calculated using Eq. 1. At this point, the damage for a given cycle period ΔN is the result from Eq. 2. The damage is accumulated as $D_{accum} = D_{accum} + D$. The number of samples that fail in each period is used to calculate the reliability index. The time t and load cycle N are updated, and the algorithm continues until all samples fail or a limit of years is reached. The number of samples and ΔN necessary for the study is reached by a convergence analysis of these parameters and the resulting reliability curve.

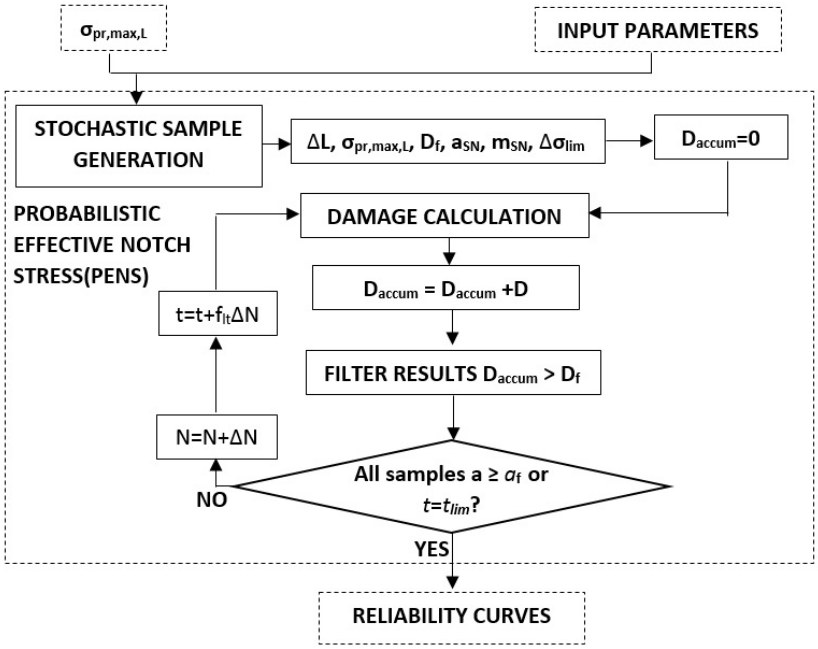

Figure 7: Probabilistic Effective Notch Stress approach. The damage is calculated for each time iteration. Samples which include damage above the limit D_f are filtered from the damage accumulation model and used to calculate the reliability curves.

3.1.4. Probabilistic Inspection/Repair simulation

The Probabilistic Inspection/Repair simulation depicted in Fig. 8 follows a similar procedure to the PFM simulation, Fig. 6. However, sample generation is not required since the data is retrieved from the calibrated PFM model. Additionally, the user sets the inspection interval, the inspection technique and the repair technique, and the algorithm in Fig. 8 performs a crack inspection/repair procedure.

The Inspection/Repair mechanism, Fig. 8, generates pseudo-random values equally distributed from 0 to 1 for each sample. This value is evaluated with respect to the PoD curve associated with the method of inspections. Whenever a crack is detected, the crack is repaired as long as it is short enough, i.e. $a < a_{repLim}$, where a_{repLim} is the maximum size at which a crack can be repaired. The value of a_{repLim} depends on the technique, and repairs are assumed to be perfect.

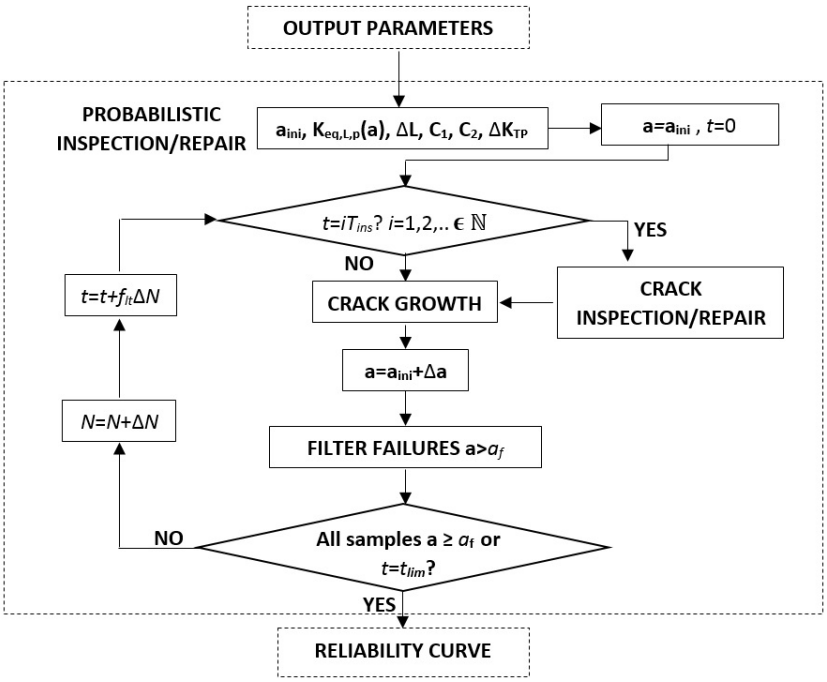

Figure 8: Probabilistic inspection/repair simulation. The method is similar to the PFM approach, Fig. 6. However, initial values of the samples from the PFM are directly used in this approach. The crack of every sample is inspected after every time interval, T_{ins}. Detected cracks are repaired if $a < a_{repLim}$.

3.2. The algorithm for the Transitional Environmental Protection(TEP) Process

The algorithm in Fig. 5 stands for constant environmental conditions. However, the analysis of the Transitional Environmental Protection (TEP) process contains two phases. A phase where the component is protected from a corrosive environment by either isolation or other mechanism such as e.g. cathodic protection, and a phase where free corrosion affects the structure.

The TEP process can be directly accounted in PENS by shifting the S-N curves parameters from protected to corrosive environment whenever the en-

vironmental conditions change, i.e. at $t = t_{TEP}$. This change could be done assuming full correlation between parameters to assure that corrosion always has a detrimental effect on the structure. After the shift, the method would continue to accumulate damage.

However, the analysis of the TEP for the FM approach is more complex because the calibrated parameter a_{ini} might not be the same for corrosive and for protected conditions. The current research proposes to evaluate the TEP as a combination of the stochastic samples from protected and corrosive conditions, Fig. 9. Firstly, structural calculations are performed following the same scheme as in Fig. 5. Afterwards, two calibrations are incorporated: one calibration for corrosive and another for environmentally protected conditions. The stochastic parameters resulting from the calibrations are included in Inspection/Repair simulations with the TEP process. The simulations are similar to Fig. 8, but with a slight modification shown in Fig. 10.

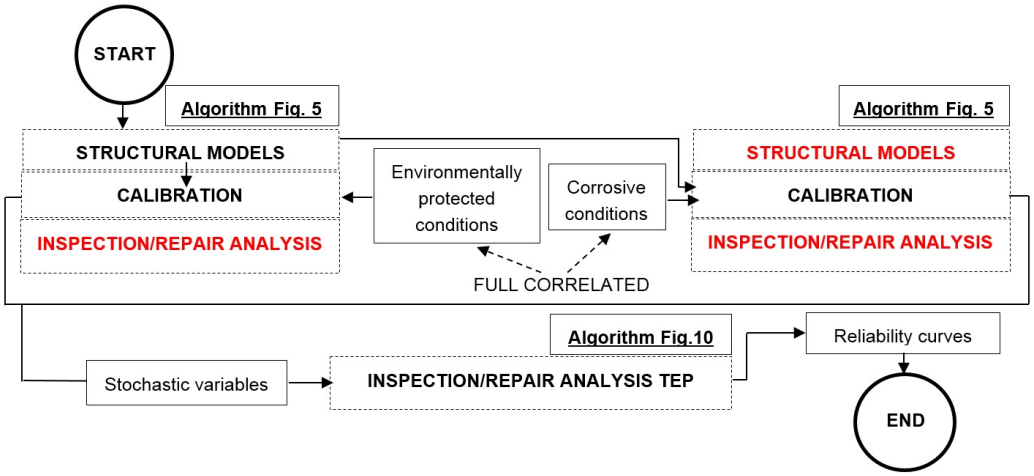

Figure 9: Global algorithm for the Transitional Environmental Protection process. The method executes the algorithm in Fig. 5 for for envionmentally protected conditions and for corrosive conditions, except some parts denoted in red. Finally, the inspection/repair procedure is executed as explained in Fig. 10.

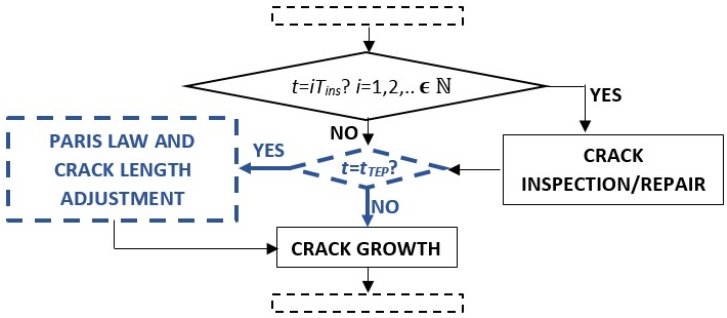

Figure 10: Inspection repair analysis for the TEP process. The algorithm is the same as in Fig. 8, but it includes a slight modification denoted in blue.

Fig. 11 illustrates the crack growth of different samples when the algorithm in Fig. 9 is executed. Fig. 11a shows the crack growth of different samples in a Monte Carlo simulation for air conditions. The initial crack of each sample follows a statistical distribution found during the calibration

process, $a_{ini,air}$. In every inspection interval T_{ins}, the crack of some samples, i.e $\mathcal{A}$ or $\mathcal{C}$, are detected and repaired. The sample $\mathcal{B}$ results in failure.

Fig. 11b presents how the cracks grow under the TEP process. When the environmental conditions shift $t = t_{TEP}$, the samples with $a < a_{ini,cor}$, $\mathcal{A}$, $\mathcal{C}$, $\mathcal{D}$, are adjusted $a = a_{ini,cor}$. The parameter $a_{ini,cor}$ is the initial crack size of the structure under corrosion, which is obtained through the calibration process. The repaired sample $\mathcal{A}$ keeps growing from $t = t_{TEP}$. A final inspection detects and repairs the crack of sample $\mathcal{C}$, whereas samples $\mathcal{B}$ and $\mathcal{A}$ result in failure.

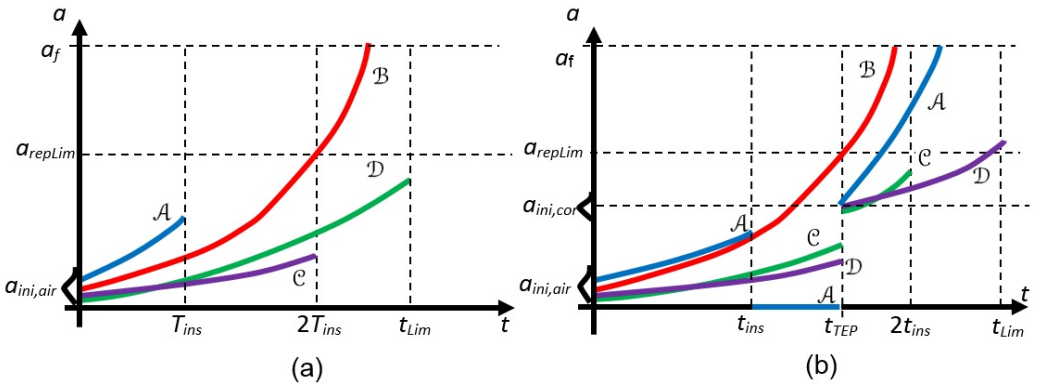

Figure 11: Simulation of the crack growth for multiple cracked samples: (a) Inspection/repair simulation for constant environmental conditions. The illustration shows some samples are detected and repaired after an inspection interval. Repaired samples vanish from the crack growth calculations. During the second inspection the crack $\mathcal{B}$ will not be repaired since $a > a_{repLim}$; (b)Inspection/repair simulation under the Transitional Environmental Protection (TEP) process. Cracks grow according to protection system conditions before $t = t_{TEP}$. When $t = t_{TEP}$, the crack size is readjusted for those cracks smaller than the initial crack size for corrosive conditions, including repaired samples. The crack growth parameters change to corrosive conditions.

4. Example

The reliability analysis of a welded component from an offshore wind turbine, Fig. 12, is studied for different TEP process and inspection/repair periods. The case is a 2D simplification of a 3D offshore bracket component. Plane strain conditions are assumed and the material is structural steel, with Young's modulus $E = 210$ GPa and Poisson's ratio $v = 0.3$

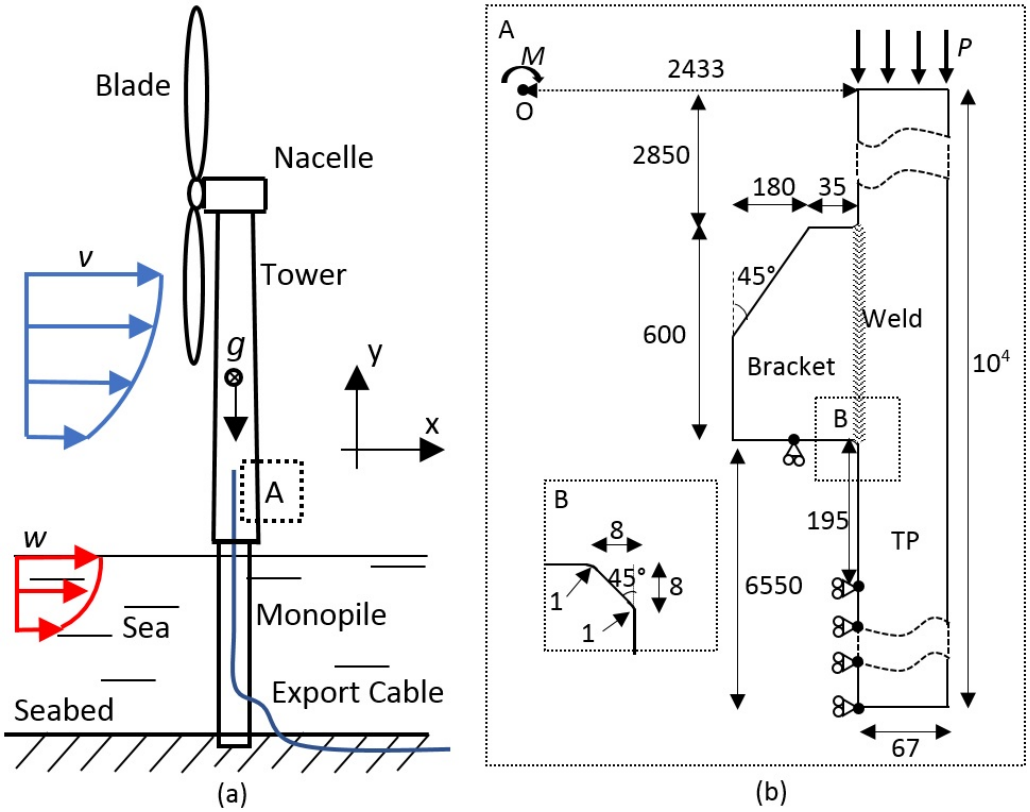

Figure 12: Offhosore weld analysis: (a) 2D representation of an offshore wind turbine subject to wind with velocity v and waves with velocity w; (b) Geometry, constraints and load set-up of the offshore welded component with dimensions in mm.

The Transition Piece (TP) is subject to two fatigue loading, a moment M

and a homogeneous pressure P during 30 years. Both loads are distributed along the top surface of the TP, Fig. 12b, where the moments origin is at O point. The magnitude of both loads is proportional during the fatigue analysis in a relation $P/M = 1/10^5$ mm^{-1}. The mean load values are $P = 4$ MPa and $M = 4 \times 10^5$ Nmm, where a unit load L is considered as $P = 1$ MPa and $M = 10^5$ Nmm. Table 1 presents the features of the loading signal, which includes three main loading ranges. The value N_{MP} describes the average number of cycles for each load range in every 131 cycles. The load signal does not correspond to realistic data and it is assumed to be the result after a signal analysis through conventional methods, e.g. rain-flow counting [19] and Markov matrix [33]. The mean frequency of long term stress cycles is $f_{lt} = 10^6$ cycles/year.

Table 1: Different load ranges ΔL_i of the load signal. Q_i correspond to $\Delta L_i = Q_i L$.

ΔL_i	ΔM (Nmm)	ΔP (MPa)	N_{MP} (cycles)	Q_i
ΔL_1	8×10^5	0.8	1	8
ΔL_2	4×10^5	0.4	30	4
ΔL_3	0.8×10^5	0.08	100	0.8

The ultrasonic technique, with PoD Eq. 10, is selected to perform inspections. The repair technique proposed is grinding, which is capable to repair cracks with size $a \leq 3$mm [32] once they are detected. The question posed is: what is the maximum inspection interval in order to keep a reliability level of e.g. $\beta_{accum} \geq 3.1$ [8] for air conditions, corrosive conditions, TEP process $t_{TEP} = 10$ years and TEP process $t_{TEP} = 20$ years?

In order to answer the question the Algorithm Fig. 9 is executed. The

load L is submitted to the structural models and the ENS approach is performed through the commercial software ANSYS® [34]. The element type used is PLANE183, a quadratic 8-node element which requires less element size refinement than linear elements to proportionate similar results [3]. A mesh convergence analysis was performed by increasing the number of nodes. The results converged at 177582 nodes with a maximum principal stress is $\bar{\sigma}_{pr,max,L} = 23.63$ MPa , Fig. 12b.

The FM analysis is performed by using a method described by Ruiz in [22], which consists of a Matlab®-ANSYS® [35] [34] system that calculates crack propagation. No RS are imposed on the model by assuming the *Residual Stress Intensity Factors Proportionality Conjecture* [27]. The FEM model includes an initial crack in the location where the highest stress concentration is in the weld, Fig. 12. The initial crack size for the FM structural model is $\bar{a}_{ini} = 0.1$ mm and the parameter $K_{eq}(a)$ is calculated through two convergence analyses: reducing the mesh size and reducing the crack growth step Δa in between the calculation of $K_{eq}(a)$. The result is a mesh with 1085298 nodes, crack step $\Delta a = 0.075$ mm for crack lengths $a < 4$ mm and crack step $\Delta a = 1.5$ mm for crack lengths $a \geq 4$ mm. The FM analysis is run until the crack length is half of the width $a_f = 67$ mm/2=33.5 mm, where failure is considered [11].

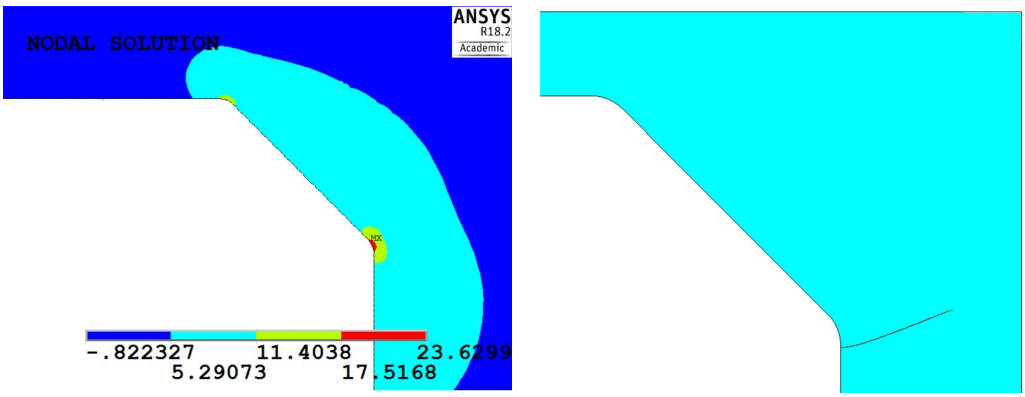

(a) (b)

Figure 13: Illustration of the two structural analyses for section A, Fig. 12b: (a) Maximum principal stress after the ENS approach; (b) Shape of the crack after a certain growth during the FM approach.

A non-linear geometrical analysis is performed for both structural models, presenting very similar results as for linear geometrical deformations. Once the evaluation of the structural models is finished, the calibration in Fig 9 is run. The parameters and their stochastic distribution are described in Table 2 and Table 3, where the initials SD stand for Standard Deviation.

Table 2: Parameters for PENS. D:Deterministic, LN:Lognormal, N:Normal

Parameter	Mean	SD	Unit	Distribution	Reference
$\log \overline{a_1}$(In-air)	13.758	0.2	log(cycles)	N	[15]
m_1(In-air)	3	———	$\frac{\log(\text{cycles})}{\log(\text{MPa})}$	D	[15]
$\log \overline{a_2}$(In-air)	17.996	0.2	log(cycles)	N	[15]
m_2(In-air)	5	———	$\frac{\log(\text{cycles})}{\log(\text{MPa})}$	D	[15]
$\log \overline{a_1}$(Corrosion)	13.28	0.2	log(cycles)	N	[15]
m_1(Corrosion)	3	———	$\frac{\log(\text{cycles})}{\log(\text{MPa})}$	D	[15]
U_{ENS}	1	0.1	———	N	[15]
U_L	1	0.2	———	LN	[15]
D_f	1	0.3	———	LN	[15]

Table 3: Parameters for PFM. D: Deterministic, LN: Lognormal, N: Normal, *: Calibration

Parameter	Mean	SD	Unit	Distribution	Ref.
C_A(Air)	4.8×10^{-18}	8.1×10^{-18}	$\frac{\text{mm/cycle}}{(\text{MPa}\sqrt{\text{mm}})^{m_A}}$	LN	[23]
m_A(Air)	5.1	———	———	D	[23]
C_B(Air)	5.86×10^{-13}	3.52×10^{-13}	$\frac{\text{mm/cycle}}{(\text{MPa}\sqrt{\text{mm}})^{m_B}}$	LN	[23]
m_B(Air)	2.88	———	———	D	[23]
C_A(Corrosion)	5.37×10^{-14}	5.915×10^{-14}	$\frac{\text{mm/cycle}}{(\text{MPa}\sqrt{\text{mm}})^{m_A}}$	LN	[23]
m_A(Corrosion)	3.42	———	———	D	[23]
C_B(Corrosion)	5.67×10^{-7}	9.05×10^{-7}	$\frac{\text{mm/cycle}}{(\text{MPa}\sqrt{\text{mm}})^{m_B}}$	LN	[23]
m_B(Corrosion)	1.11	———	———	D	[23]
U_{FM}	*	*	———	N	
U_L	1	0.2	———	LN	[15]
a_{ini}	*	*	mm	LN	

The parameter U_L represents the uncertainty of the loads described in Table 1, where all load ranges are fully correlated. The parameters U_{ENS} and U_{FM} represents the uncertainty of the ENS model and the FM model. The uncertainty of the geometrical dimensions are assumed to be included in U_{NS} and U_{FM}. The reliability curve for PFM and PENS is calculated using the algorithms in Fig. 6 and Fig. 7. The polynomial interpolation in Fig. 6 is evaluated for each sample through the Matlab function *Polyfit* [35], where 8th order polynomials present curves that fits very well with the resulting $\mathbf{K}_{eq,L}(\mathbf{a})$ from the structural calculations, with a maximum deviation of around 0.3%.

The calibration of the PFM approach is performed, where results are shown in Fig. 14a and Table 4 present good results. The convergence of reliability results is found at 10^6 samples and $\Delta N = 10^4$ cycles.

Table 4: Parameters calibrated. D: Deterministic, LN:Lognormal and N: Normal

Parameter	Mean	COV	Unit	Distribution
$U_{FM,Air}$	1	0.05	————	N
$a_{ini,Air}$	0.15	0.66	mm	LN
$U_{FM,corrosive}$	1	0.05	————	N
$a_{ini,corrosive}$	1	0.05	mm	LN

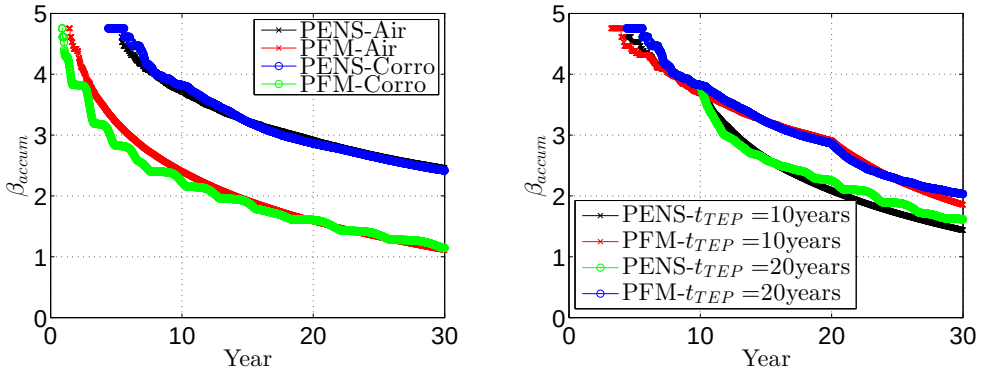

(a) (b)

Figure 14: Comparisson between the PENS and PFM reliability curves: (a) Results after calibration for air and corrosive conditions; (b) Result for the TEP process for different times when corrosion starts t_{TEP}.

Once the calibration is finished, the TEP is evaluated for different cases in Algorithm Fig. 9. Fig. 14b shows a comparison between the PENS and PFM for different TEP periods. The results show a slight deviation at the

end of the fatigue period t=30 years.

The accumulative reliability index β_{accum} is calculated for different inspection intervals, Fig. [15a-15d]. The results show a striking difference in reliability curves for different inspection plans, Fig 15d. Finally, Table 5 includes the maximum inspection interval to keep a reliability $\beta_{accum} \gtrsim 3.1$ [8] for different environmental conditions. If corrosion affects the structure, the optimum inspection interval drops from 3 years to 6 months.

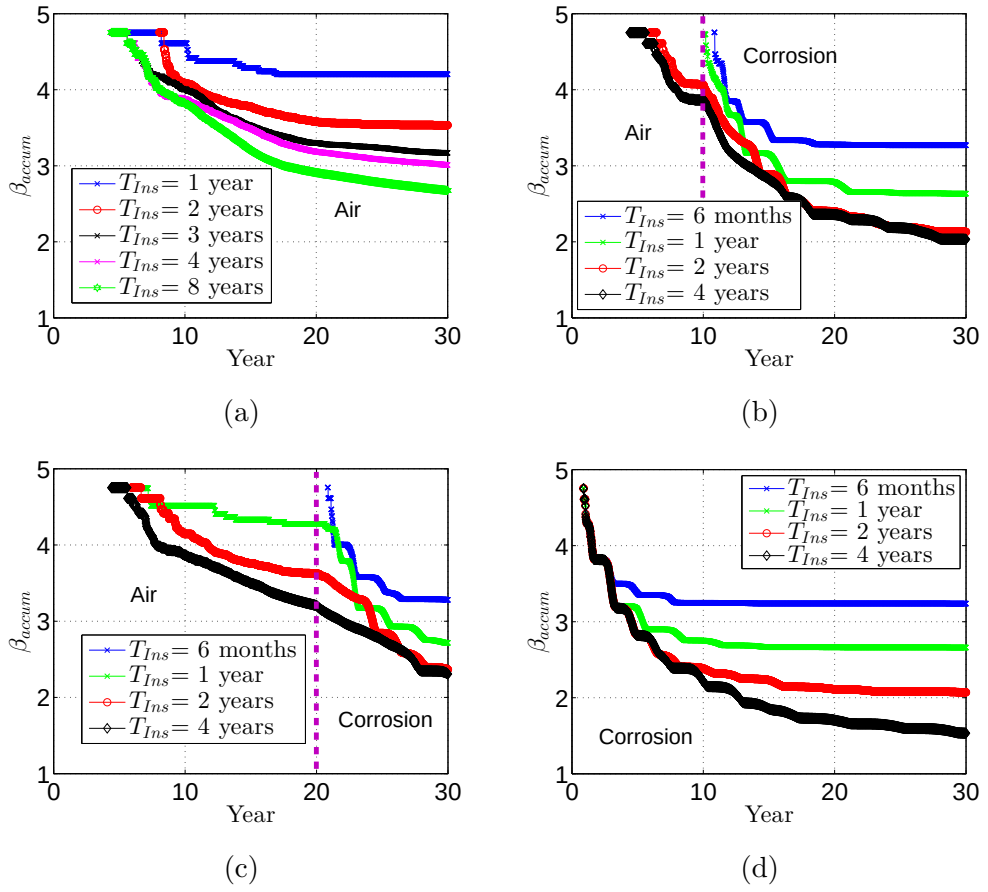

Figure 15: Reliability curves for different inspection interval T_{Ins}: (a) Results for permanent air conditions; (b) Results for the TEP process from air to corrosive at $t_{TEP} = 10$ years; (c) Results for TEP process from air to corrosive at $t_{TEP} = 20$ years; (d) Results for permanent corrosive conditions.

Table 5: Inspection period in years in order to keep $\beta_{accum} \gtrsim 3.1$. The analyises only accounts constant inspection intervals during the 30 years of maintenance.

Air ($t_{TEP} > 30$ years)	$t_{TEP} = 20$ years	$t_{TEP} = 10$ years	Corrosion ($t_{TEP} = 0$ years)
3	1/2	1/2	1/2

5. Discussion about the results and method

The current research introduces an algorithm, Fig. 9, able to calculate the reliability index for multiple environmental conditions and for different inspection/repair intervals. The algorithm has been used in the example in Fig. 12a, where the calibration results of the initial crack size in air are coherent with literature [36]. Under corrosive conditions, the calibration results involve a considerably higher initial crack size, Table 4. Additionally, the algorithm has shown similar results between PFM and PENS for different t_{TEP} imposed in the example. Finally, the results show that each inspection interval involves a different reliability curve.

The algorithm is based on a number of assumptions. Firstly, it relies on stress based methods and the Palngrem-Miner rule to calibrate the FM method, something not necessary realistic with the lifetime performance of the structure.

Another issue is found when evaluating the initial size of some cracks, which present values lower than the LEFM limit, i.e. 0.1mm. Despite the fact that the initial growth of those cracks does not follow the crack propagation Eq. 8, this equation has been used to evaluate the fatigue crack growth of all the cracks because of two reasons. The first reason is that a(N) is coherent with literature once $a \geq 0.1$mm due to the calibration process. The second reason, is that for $a < 0.1$ mm the crack length is generally too low to be detected, and therefore a more realistic crack length as a function of the number of cycles $a(N)$ becomes irrelevant for those sizes.

The inspection strategy is arguable. Further improvements could introduce variable inspection intervals. Additionally, the grinding repair strategy

conducted in the wind turbine example could be replaced by other techniques in order to increase a_{repLim}.

It is suggested that future research could be conducting assuming imperfect repairs, as described by Straub [17], or incorporating advanced crack propagation formulations. Finally, the assumption of full correlation between stochastic parameters for air and corrosive conditions should be reviewed.

6. Conclusion

The following conclusions can be drawn:

(i) A novel algorithm to assess reliability results for different inspection/repair intervals is presented. The method incorporates the Transitional Environmental Protection process, i.e. a situation where the corrosion protection system fails after a period of time.

(ii) The analysis of an example shows coherent results between the Probabilistic Fracture Mechanics approach and the Probabilistic Effective Notch Stress approach for different environmental conditions.

(iii) The algorithm is suitable for industrial applications where inspections of offshore welded structures are common. This publication describes the effects of different TEP processes on the inspection intervals necessary to keep a high reliability level.

Acknowledgement

The authors are grateful for the support and scientific advice of Christian Frithiof Niordson, Thomas Østergaard, Martin Alexander Eder, Mathias Stolpe and Rachel Meyer.

Funding

The research is supported by the research project Advancing BeYond Shallow waterS (ABYSS), funded by Innovation Fund Denmark, Grant no. 1305-00020B, and in collaboration with Ørsted. The funding source had no influence in the outcome or in the decision to publish the manuscript.

References

[1] Zhang C, Gao W, Guo S, Li Y, Yang T. Opportunistic maintenance for wind turbines considering imperfect, reliability-based maintenance. Renew Energ 2017; 103: 606-12.

[2] Adedipe O, Brennan F, Kolios A. Review of corrosion fatigue in offshore structures: Present status. Renew Sust Energ Rev 2016; 61: 141-54.

[3] Anderson TL. Fracture Mechanics: Fundamentals and Applications. 3th ed. Boca Raton: CRC Press Taylor & Francis Group; 2005.

[4] Yang JN, Trapp WJ. Inspection frequency optimization for aircraft structures based on reliability analysis. J Aircraft 1975; 12(5): 494-6.

[5] Skjong R. Reliability Based Optimization of Inspection Strategies. Proceedings ICOSSAR'85; International Conference on Structural Safety and Reliability; 1985 May 27-29; Kobe (Japan); p. 614-8.

[6] Madsen HO, Sørensen JD, Olesen R. Optimal Inspection Planning for Fatigue Damage of Offshore Structures. Proceedings ICOSSAR'89; International Conference on Structural Safety and Reliability; 1989 Aug 7-11; San Francisco (USA); p. 2099-106.

[7] Mohamed K. Optimal Risk-Based Inspection and Maintenance (RBIM) Planning for Process Assets [PhD dissertation]. St John's: Memorial University of Newfoundland; 2012.

[8] Eltaief M, Chateauneuf A, Boraoui C, Hassine T. Dynamic approach for optimal inspection planning of fatigue cracked component. J Constr Steel Res 2015; 115: 263-75.

[9] Doshi K, Roy T, Parihar YS. Reliability based inspection planning using fracture mechanics base fatigue evaluations for ship structural details. Mar Struct 2017; 54: 1-22.

[10] Maljaars J, Vrouwenvelder ACWM. Probabilistic fatigue life updating accounting for inspections of multiple critical locations. Int J Fatigue 2014; 68: 24-37.

[11] Al-Mukhtar AM. The safety analysis concept of welded components under cyclic loads using fracture mechanics method [PhD dissertation]. Freiberg: Technische Universität Bergakademie Freiberg; 2010.

[12] Bertini L, Cera A, Frendo F. Experimental investigation of the fatigue resistance of pipe-to-plate welded connections under bending, torsion and mixed mode loading. Int J Fatigue 2014; 68: 178-85.

[13] Lautrou N, Thevenet D, Cognard JY. Fatigue crack initiation life estimation in a steel welded joint by the use of a two-scale damage model. Fatigue Fract Engng Mater Struct 2009; 32: 403-17.

[14] Lotsberg I, Sigurdsson G, Fjeldstad A, Moan T. Probabilistic methods

for panning of inspection for fatigue cracks in offshore structures. Mar Struct 2016; 46: 167-92.

[15] DNVGL-RP-C203:2016: Fatigue design of offshore steel structures. 2016.

[16] Chen NZ, Wang G, Soares CG. Palmgren-Miner's rule and fracture mechanics-based inspection planning. Eng Fract Mech 2011; 78: 3166-82.

[17] Straub D. Generic Approaches to Risk Based Inspection Planning for Steel Structures [PhD dissertation]. Zürich: Swiss Federal Institute Of Technology ETH; 2004.

[18] Schijve J. Four lectures on fatigue crack growth. Eng Fract Mech 1979; 11(1): 167-221.

[19] Dowling NE. Mechanical behavior of materials. 4th ed. London: Springer; 2013.

[20] Lei B-M, Tran V-X, Taheri S, le Roux J-C, Curtit F, He M, Wan L, Zhou Y. Toward consistent fatigue crack initiation criteria for 304L austenitic stainless steel under multi-axial loads. Int J Fatigue 2015; 75: 57-68.

[21] Maierhofer J, Pippan R, Gänser H-P. Modified NASGRO equation for physically short cracks. Int J Fatigue 2014; 68: 200-7.

[22] Ruiz-Muñoz GA. Method to Analyse Multiple Site Damage Fatigue before and after Crack Coalescence. Eng Fract Mech 2017; In press. Available from: `https://doi.org/10.1016/j.engfracmech.2017.09.011`

[23] Committee reference WEE/37. British Standard BS 7910:2005: Guide to methods for assessing the acceptability of flaws in metallic structures. London: BSI; 2007.

[24] Bao R, Zhang X, Yahaya NA. Evaluating Stress Intensity Factors due to Weld Residual Stresses by the Weight Function and Finite Element Methods. Eng Fract Mech 2010; 77: 2550-66.

[25] Seifi R. Effect of Residual Stresses on Fracture Parameters of through Cracks in Welded Plates. Procedia Eng 2011; 10: 1895-900.

[26] Sumi Y, Yang C, Wang ZN. Morphological aspects of fatigue crack growth Part II-Effects of stress biaxiality and welding residual stress. Int J Fract 1996; 82: 221-35.

[27] Ruiz-Muñoz GA, Eder MA. A conservative approach for Mode I-II fatigue analysis under residual stresses: The RSIF proportionality Conjecture. 2018. Submitted.

[28] Ditlevsen O, Madsen HO. Structural Reliability Methods. Internet ed. 2.2.5. Lyngby: The Technical University of Denmark; 2005.

[29] Sørensen JD. Reliability-Based Calibration of Fatigue Safety Factors for Offshore Wind Turbines. J Offshore Polar Eng 2012; 22(3): 234-41.

[30] DNVGL-RP-0001:2015: Probabilistic methods for planning inspection for fatigue cracks in offshore structures. 2015.

[31] Marazani T, Madyira DM, Akinlabi ET. Repair of cracks in metals: A review. Procedia Manuf 2017; 8: 673-9.

[32] Haagensen PJ, Maddox SJ. IIW Recommendations on Post Weld Improvement of Steel and Aluminium Structures. Cambridge: The International Institute of Welding; 2001 Jul. Report No. XIII-1815-00.

[33] Krenk S, Gluver H. A Markov matrix for fatigue load simulation and rainflow range evaluation. Struct Saf 1989; 6(2-4): 247-58.

[34] ANSYS Documentation. Version 18.2.0; 2017.

[35] Matlab Documentation. Version R2013b; 2013.

[36] Joint Committee on Structural Safety. JCSS Probabilistic Model Code Part 3: Resistance Models. 2011 [Accessed 2017 Dec] Available from: URL: `http://www.jcss.byg.dtu.dk/`.